UNIVERSITY OF CALIFORNIA
RIVERSIDE

Reinforcement Learning Influences Widespread Changes in Cortical Representations in a Selective Whisker Detection Task in Mice

A Dissertation submitted in partial satisfaction
of the requirements for the degree of

Doctor of Philosophy

in

Psychology

by

Krithiga Aruljothi

March 2024

Dissertation Committee:
Dr. Edward Zagha, Chairperson
Dr. Anubhuti Goel
Dr. Aaron Seitz

The Dissertation of Krithiga Aruljothi is approved:

Committee Chairperson

University of California, Riverside

ACKNOWLEDGEMENTS

Included in this dissertation are Chapters 2 and 3, adaptations from previously published materials (Aruljothi et al., 2020; Marrero et al., 2022). Primary contributions, additions, or changes are noted at the beginning of their respective chapters.

I express my gratitude to my committee members, Dr. Eddie Zagha, Dr. Anu Goel, and Dr. Aaron Seitz, for their unwavering support and invaluable teachings throughout my research journey. My appreciation extends to all the faculty members in the Psychology department and the interdepartmental Ph.D. program in Neuroscience at UCR for their ceaseless inspiration and engaging interactions, including professional talks, conferences, casual discussions, and classes. A special acknowledgment goes to Dr. Khaleel Razak, Dr. Hongdian Yang, Dr. Martin Riccomagno, Dr. Peter Hickmott, Dr. Kalina Michalska, and Dr. Viji Santhakumar for significantly shaping my academic experience through their mentorship. I am also grateful to the Psychology department staff, including Renee Young, Jay Melashenko, Sarah Turnbull, and Kirsten Alonso, for their administrative efforts and contributions to routine graduate affairs.

Above all, my deepest gratitude goes to Dr. Eddie Zagha, my principal investigator, graduate mentor, and brother. I consider myself incredibly fortunate to have had the best mentor and the most intellectually gifted person I know to guide my

scientific journey through his exceptional mentorship. I owe much of my growth as a researcher to you, and I wouldn't be where I am today without your influence.

DEDICATIONS

To my beloved parents, Mammishka and Daddishka, as I affectionately call them: This entire life journey, encompassing education and, most importantly, my PhD, is dedicated to my father, Aruljothi R., my eternal teacher, and best friend. Dad, you guided me through this vision we shared, holding my hand through life's highs and lows. Initiating this journey without you was daunting, but even in your absence, your influence helped me reach the finish line. There were moments when I nearly gave up, but the determination to make you proud propelled me to the end. Thank you, Daddy; I wish you were here to witness me becoming Dr. Aruljothi. To my mom, Geetha Aruljothi: Navigating life and studies wouldn't have been possible without your unwavering support. You stood by me through thick and thin, especially during the challenging times. I hope I have made you proud, and my commitment to doing so will persist.

To my dear friends: Aditi, my best friend, confidante, and soul sister, has been my unwavering cheerleader throughout our decade-long friendship. Thank you for patiently listening to my ramblings for hours every single day. Your encouragement, whether in the form of a pat on the shoulder for my achievements or a smack on the head when I needed redirection, means the world to me.

To my REC and ASU buddies—Sujata, Deepika, Sneha, Yashwanth, Swarnima, and Ranjani—thank you for becoming my U.S. family and creating memories that will be cherished forever.

And to my UCR and Riverside buddies—Marissa, Krista, Sirajan, Zoe, Jamiela, Sam J, Sam P, Manas, Uma, Donna and Manish—thank you for being my pillars of moral and emotional support.

Lastly, to my lab family—the Zaghies, both longstanding members and newcomers, including Krista, Manas, Angelina, Joanne, Behzad, Sarah, Dominic, Christian, Emaan, Lovleen, Maham, Lourance, Raghad, and everyone else who has been part of the lab from the outset. Your constant presence and support have been invaluable. I've navigated the journey of growth, faced losses, and celebrated victories—all with your unwavering support and love. I eagerly anticipate witnessing the exceptional scientists and doctors you will undoubtedly become in the near future.

ABSTRACT OF THE DISSERTATION

Reinforcement Learning Influences Widespread Changes in Cortical Representations in a Selective Whisker Detection Task in Mice

by

Krithiga Aruljothi

Doctor of Philosophy, Graduate Program in Psychology
University of California, Riverside, March 2024
Dr. Edward Zagha, Chairperson

A fundamental aspect of goal-directed behavior involves the capacity to selectively respond to specific stimuli during the decision-making process. My dissertation project is dedicated to uncovering the associations between changes in behavioral outcomes and the broader patterns of cortical activity as mice acquire proficiency in the selective detection task. In our research, we aim to delve into the neural mechanisms that underlie sensory selection (sensory detection and impulse control), employing the Widefield Calcium imaging technique. To achieve this, we conducted a training regimen with mice, employing a whisker-based selective

detection paradigm where they learned to respond to preferred target stimuli while disregarding non-preferred distractor stimuli throughout the learning process. Notably, mice that achieved expertise in the task demonstrated a clear attenuation of sensory-to-motor signal propagation in distractor-aligned cortical regions. Additionally, we explored the impact of prestimulus activity in the neocortex on stimulus detection. We observed that reduced prestimulus activity in the dorsal cortex correlated with improved stimulus detection, predicting whether a response would occur or not, and resulting in faster reaction times. Finally, we investigated whether learning the selective detection task induces widespread changes across the cortex, examining whether alterations in specific behavioral measures can be linked to distinct cortical modulations. Our results showed that the learning process entails extensive neocortical adaptations as mice advance to expert-level performance in the task. This research offers valuable insights into the learning mechanisms involved in the selection process, with potential applications for understanding impairments in learning trajectories observed in certain mental health disorders.

TABLE OF CONTENTS

LIST OF ABBREVIATIONS

ADHD – Attention Deficit Hyperactive Disorder
ALM – Anterior Lateral (anterolateral) Motor Cortex
AUC – Area Under the Curve
Ca^{2+} – Calcium
CR – Correct Rejections
GFP – Green Fluorescent Protein
GCaMP6s – GFP Calmodulin M13 Protein 6 Slow
HR- Hit Rate
FA/ FAR – False Alarm/ False Alarm Rate
ITI – Intertrial Interval
ILI – Interlick Interval
LFP – Local Field Potential
Preme – Premature
Resp – Response
ROC – Receiver Operating Characteristic
ROI – Region of Interest
RSP – Retrosplenial Cortex
RT – Reaction Time
wS1 – Primary Whisker Somatosensory Cortex
Snap25 – Synaptosome Associated Protein
Spont – Spontaneous
tjMC- Tongue/Jaw Motor Cortex
wM1 – Primary Whisker Motor Cortex
WME – Whisker Motion Energy

LIST OF FIGURES

Chapter 1: Introduction

Each day, instrumental actions can fall into the categories of habit or goal-directed behavior. A “goal-directed” action is a behavior driven by an expectation that it is likely to bring about a desired outcome (Dickinson & Weiskrantz, 1985). An action is considered goal-directed if it meets two criteria. Firstly, the individual must demonstrate awareness of the causal impact of their actions and their outcomes in the present state or context (causal efficacy). Secondly, intentional actions are aimed at specific conditions in the external world, referred to as goals, driven by internal motivations and guided by representations of those goals (goal representations).

The capacity to adapt behavior based on desired outcomes in a given situation represents a fundamental aspect of flexible behavior, speculated to be compromised in various psychological disorders like obsessive-compulsive disorder (Gillan et al., 2011) and addiction (Everitt et al., 2008). Despite its behavioral significance, there remains a limited understanding of the neural mechanisms that empower individuals to dynamically modify their behavior in pursuit of desired outcomes.

Learning to become an expert

Gaining feedback from the results of decisions has the potential to enhance future decision-making and increase overall success. Both humans and other animals adeptly learn from past rewards, selecting actions that have recently resulted in

the most favorable outcomes (Daw et al., 2006; D. Lee et al., 2012; Samejima et al., 2005; Tai et al., 2012). Decision-making, besides assessing past rewards, typically requires the consideration of present perceptual signals. Therefore, effective decisions should encompass both the current sensory evidence and the prior history of successes and failures. Examining decisions influenced by past rewards falls under the purview of a reinforcement learning framework (Sutton & Barto, 2018). Learning can also occur even without reinforcement, such as in statistical learning, an unconscious cognitive process in which repeated patterns, or regularities, are extracted from the sensory environment (Fiser & Aslin, 2001; Turk-Browne, 2012; Turk-Browne et al., 2010).

Experience dependent performance

In perceptual decision-making paradigms, overt learning typically does not occur once the task is acquired. Nevertheless, numerous studies have demonstrated the significant impact of past rewards, actions, and stimuli on subsequent perceptual choices (Abrahamyan et al., 2016; Akaishi et al., 2014; Akrami et al., 2018; Braun et al., 2018; Busse et al., 2011; Cho et al., 2002; Fan et al., 2018; Fischer & Whitney, 2014; Fritsche et al., 2017; Fründ et al., 2014; Gold et al., 2008; Hwang et al., 2017; Lueckmann et al., 2018; Luu & Stocker, 2018; Marcos et al., 2013; Tsunada et al., 2019; Urai et al., 2017). Certain observations suggest that simple forms of reward-based learning contribute to asymptotic perceptual performance. For instance, subjects may tend to repeat a previously rewarded choice or avoid it after an unsuccessful trial (Abrahamyan et al., 2016; Busse et al., 2011; Tsunada

et al., 2019; Urai et al., 2017). However, these types of choice biases appear suboptimal and may reflect simple heuristics. Consequently, the extent to which normative considerations in reinforcement learning can explain choice biases in perceptual decisions has remained unclear.

Reinforcement in Operant Conditioning

Within operant conditioning, the term "reinforcement" denotes anything that enhances the probability of a response occurring. Psychologist B.F. Skinner introduced this concept in 1937 (Skinner, 1937). While the term 'operant behavior' wasn't inherently groundbreaking, Skinner's introduction of automated training with intermittent reinforcement and the exploration of reinforcement schedules it prompted represented a novel approach.

In operant conditioning, there exist two distinct forms of reinforcement. Both exert an influence on behavior, but their mechanisms differ. These two types are:

1. Positive reinforcement: This entails adding something to amplify a response.
2. Negative reinforcement: This involves removing something to augment a response.

While these terms include the words positive and negative, it's crucial to recognize that Skinner employed them without connotations of "good" or "bad." Instead, consider these terms in a mathematical context: positive functions like a plus sign, indicating the addition or application of something to the situation, while negative

functions like a minus sign, denoting the removal or subtraction of something from the situation.

A fundamental question in behavioral neuroscience is how subjects select actions in the face of reward and punishment and the neural mechanisms of the decision-making processes. In behavioral psychology, this question has been investigated in detail through the classical and operant conditioning paradigms and much evidence has accumulated regarding the associations that control different aspects of learned behavior (Bornstein & Daw, 2011; Dayan & Niv, 2008; Ito & Doya, 2011; van der Meer & Redish, 2011). While the psychological foundations are well established, the neuronal implementations are very poorly understood. One possible hypothesis could be that learning induces specific changes in distinct brain regions, like S1 for somatosensory detection. Alternatively, another hypothesis could be that learning leads to broad changes throughout the entire cortex and brain.

Goal-directed Behavior Paradigms

Goal-directed behavior has been investigated across various paradigms, animal models, and mental health disorders. Goal-directed sensory and motor paradigms encompass tasks such as detection (Huber et al., 2012), discrimination (Erlich et al., 2011; Pai et al., 2011; Rudebeck & Murray, 2008), categorization (Baunez & Robbins, 1997, 1999; Freedman et al., 2003; Reinert et al., 2021), and sequencing (Jin & Costa, 2010; Smits-Bandstra & De Nil, 2007), among other features. Our

investigations focus on the selective detection process, where subjects selectively respond to target stimuli while ignoring distractors.

Common measures such as detection (of stimulus) and discrimination (between stimuli) are typically employed in standard selection paradigms, particularly in primate studies, where standardized signal detection measures determine the selectivity of detection (Britten et al., 1992, 1996; Luck et al., 1997). To investigate the correlations between cortical neural modulation and behavioral changes across learning, we designed a simple go/no-go whisker-based selective detection task paradigm. This paradigm involves selectively responding to a target stimulus and refraining from responding to a distractor stimulus, with fixed assignments for target and distractor stimuli.

Rodent Whisker System

Sensory information plays a crucial role in action planning, and the execution of actions relies on sensory feedback. The whisker primary sensory cortex (wS1) is believed to facilitate the integration of sensory, motor, and top-down signals for specific computations in individual neurons and neuronal circuits. The complex neuronal circuits involved in cortical whisker-related sensorimotor processing are gradually being uncovered through advancements in labeling, recording, and manipulating specific cell types during behavior. In the mouse wS1, the somatotopic map reveals individual representations for each mystacial whisker, known as a 'barrel' (Figure 1.1 B) (Woolsey & Van der Loos, 1970). This barrel

map seems to develop through genetic programs and is refined through experience and activity (Fukuchi-Shimogori & Grove, 2001; Hannan et al., 2001; Iwasato et al., 2000; Van der Loos & Woolsey, 1973; Welker et al., 1996; Welker & Van der Loos, 1986).

Whisker deflection triggers sensory information through glutamatergic synapses in the brainstem and thalamus before reaching the cortex. This incoming sensory information is processed within neuronal microcircuits in wS1 and transmitted to various directly connected downstream cortical and subcortical brain regions (Aronoff et al., 2010; Ferezou et al., 2007; Yamashita et al., 2018). The sensory (S1) and motor (M1) cortical representations of the mouse whisker system are depicted in Figure 1.1 A derived from (Aronoff et al., 2010).

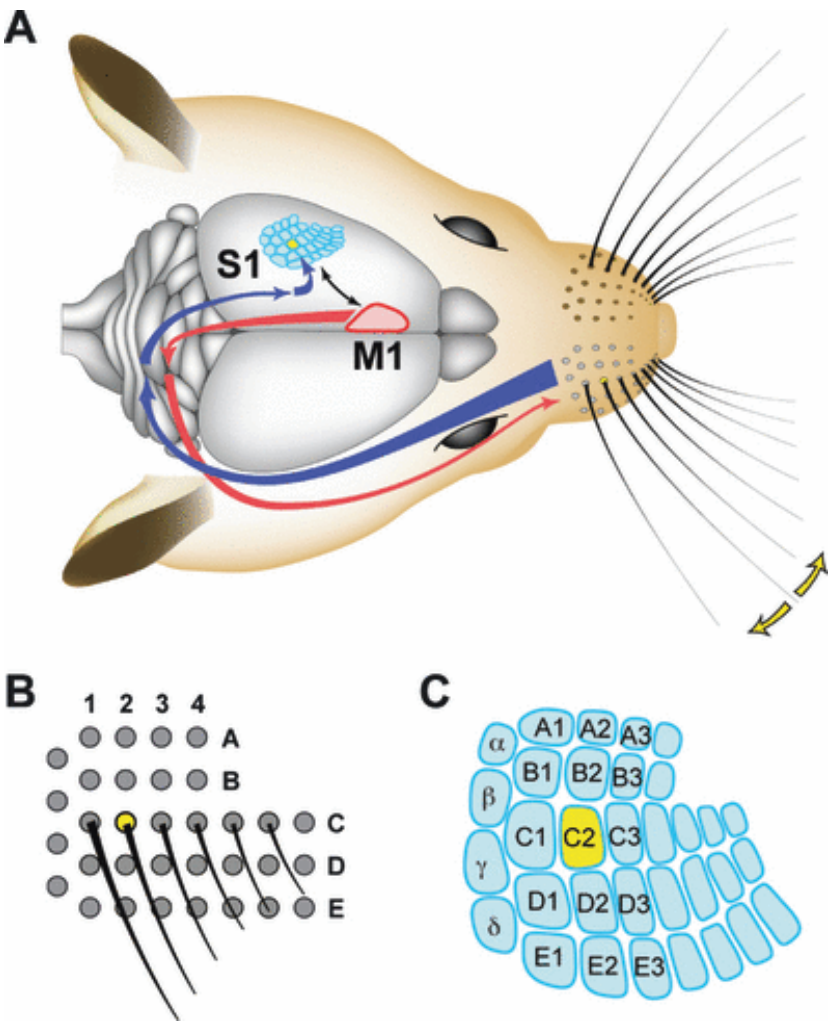

Figure 1.1 (derived from figure 1 of (Aronoff et al., 2010)) ***a)*** sensory (S1) and motor (M1) cortical representations of the mouse whisker system ***b) and c)*** The primary somatosensory cortex of rats and mice contains obvious anatomical units called 'barrels' in layer 4 of wS1, which represent individual whiskers on the snout and are somatotopically organized.

While selective detection has not been extensively explored in mice, the whisker barrel system in these animals provides an ideal framework for sensory stimuli due to its barrel-specificity and spatial laterality. The barrel cortex, with its precisely defined maps, offers a unique opportunity for a detailed analysis of causal mechanisms within well-defined cell-type-specific neuronal circuitry during sensory perception (Petersen, 2019). Despite wS1's direct involvement in whisker motor control (Matyas et al., 2010), its most significant contribution to behavior regulation is likely indirect. Through associative learning, whisker sensory information becomes crucial for goal-directed behavior. Context-, motivation-, and learning-dependent processing of whisker-related sensory information probably engages various brain regions, including wS1 and its downstream targets (Aruljothi et al., 2020; J. L. Chen et al., 2015; Eggermann et al., 2014; Marrero et al., 2022; Sachdev et al., 2004; Sofroniew et al., 2015; Zareian et al., 2021, 2023; Zhang & Zagha, 2023). Uncovering the neuronal circuits responsible for transforming whisker sensory information into goal-directed motor output is a key objective. Head-restrained mice can readily learn goal-directed tasks through trial-and-error, with neuronal recordings in wS1 revealing trial-by-trial correlates of task performance. Optogenetic and pharmacological inactivation of wS1 reduces hit rates in such tasks, indicating the involvement of wS1 neuronal activity in task execution (Sachidhanandam et al., 2013; H. Yang et al., 2016). Conversely, optogenetic stimulation of wS1 can substitute for whisker stimulation during both learning and execution (Sachidhanandam et al., 2013; Sofroniew et al., 2015).

Remarkably, in trained animals, even the stimulation of single wS1 neurons can drive licking responses (Houweling & Brecht, 2008; Tanke et al., 2018).

Widefield Calcium Imaging

Utilizing wide-field calcium imaging, particularly with genetically encoded calcium indicators like the GCaMP family, has emerged as a compelling method to observe neural activity across the entire dorsal cortex in live mice during diverse sensory and cognitive processes (Cardin et al., 2020; Ren & Komiyama, 2021). This approach offers excellent spatiotemporal resolution by illuminating large cortical areas simultaneously.

In recent years, the field of systems neuroscience has undergone a revolution in wide-field imaging, primarily driven by advancements in genetically encoded fluorescent indicators. Engineered proteins within this category exhibit changes in fluorescence intensity in response to various neuronal events, encompassing transmembrane voltage, intracellular calcium concentration, vesicle release, and alterations in neurotransmitter concentration (Lin & Schnitzer, 2016; Sabatini & Tian, 2020). Among these protein sensors, genetically encoded calcium indicators, notably the GCaMP family (Akerboom et al., 2012; Chen et al., 2013; Dana et al., 2019; Tian et al., 2009; Y. Yang et al., 2018), have become the standard choice for visualizing neural activity in both one-photon and multiphoton imaging.

GCaMP, a genetically encoded calcium indicator (GECI), is a synthetic fusion that includes green fluorescent protein (GFP), calmodulin (CaM), and M13, a peptide

sequence derived from myosin light-chain kinase (Chen et al., 2013). In the presence of Ca2+, GCaMP emits green fluorescence, with a peak excitation wavelength of 480 nm and a peak emission wavelength of 510 nm (Barnett et al., 2017). GCaMP fluorescence exhibits sensitivity to changes in intracellular calcium dynamics predominantly driven by action potentials, thereby reporting neuronal spiking activity with high signal-to-noise ratio (SNR). The genetic encoding of GCaMP also ensures stable expression over time, facilitating longitudinal recordings. These advantages position GCaMP as a powerful tool in wide-field calcium imaging, overcoming challenges often encountered with intrinsic signal imaging and voltage-sensitive dye imaging. As a result, it has become an attractive approach for characterizing large-scale cortical dynamics in behaving animals.

An increasing number of investigations utilize wide-field calcium imaging to characterize cortical activity on a macroscopic scale, covering a field of view (FOV) that spans most of the mouse dorsal cortex. These studies have significantly enhanced our comprehension of cortex-wide dynamics across various cognitive processes, ranging from relatively straightforward sensorimotor integration to more intricate decision-making tasks (Allen et al., 2017; Makino et al., 2017; Musall et al., 2019; Salkoff et al., 2020).

Dynamics of learning in dorsal cortical activity

Several studies have harnessed the stable expression of genetically encoded calcium indicators to conduct longitudinal wide-field calcium imaging, exploring

macroscopic dynamics associated with learning (Makino et al., 2017; Musall et al., 2019). A systematic characterization of cortex-wide activity reconfiguration during motor learning revealed that, with learning, the macroscopic sequence of activity during movement execution became more temporally compressed and reproducible across trials (Allen et al., 2019; Makino et al., 2017). This suggests that efficient and reliable signal transmission across cortical regions evolves as a function of learning. The observed cortex-wide dynamics in various learning tasks indicate that learning-induced plasticity extends beyond individual cortical regions and involves widespread changes in the interaction between regions (Makino et al., 2017).

As mice engage in the learning process of the goal-directed selective detection task, we expect the neocortex to undergo certain adaptations to meet the challenges posed by the cognitive functions related to sensory selection. Our objective is to assess this expectation by monitoring the progression of behavioral learning alongside changes in neocortical responses to sensory and motor events. In contrast to conventional learning studies that often concentrate on isolated behavioral measures and specific brain regions, our approach is designed to investigate two hypotheses: 1) that learning induces widespread alterations in sensory and motor responses throughout the cortex, and 2) that distinct cortical modulations are linked to the acquisition of specific behavioral processes. This exploration holds significance as it has the potential to generate multiple

hypotheses regarding the neuronal mechanisms that underlie the acquisition of various behavioral processes within the framework of a single task.

Attenuation of distractor signal in the brain

Selection serves as a cognitive filter, enabling us to sift through the overwhelming influx of sensory input and concentrate on what truly matters. Picture a scenario in your mind: you are at a bustling party with a myriad of conversations, booming music, and a cacophony of ambient sounds all vying for your attention. Yet, as you engage in a conversation with someone, you find yourself remarkably adept at tuning out the irrelevant noise and immersing yourself in the dialogue at hand. This intriguing phenomenon is known as **the cocktail party effect** and has been extensively explored within the realm of auditory psychology. Early theories on this form of selective attention, such as **Broadbent's filter model**, posited that our cognitive processing capacity is finite, leading to the early selection of information for processing while the rest gets blocked out (Broadbent, 1958). While this idea explained some behavioral data, it failed to explain our ability to process pertinent details within unattended messages. Here, Treisman proposed a different perspective: **selective attention operates through an attenuating filter rather than a blocking mechanism** (TREISMAN, 1964)**.**

Initially developed to understand the selection process within the auditory system, the attenuation theory has found applications in the study of sensory selection

across various sensory modalities and different species (Moran & Desimone, 1985; Sridharan et al., 2014; Wiederman & O'Carroll, 2013).

The precise processing stages at which motor learning incorporates selection have sparked substantial debate. According to early-selection theory, the initial selection of target information occurs at an early perceptual level (Broadbent, 1958; Cherry, 1953). Conversely, late-selection theory posits that both target and distractor information undergo similar encoding at the early perceptual stage, with the selection of the target happening only at a later, post-perceptual level of processing (Deutsch & Deutsch, 1963). In primate visual system, studies show that there is progressive distractor suppression along the cortical hierarchy (Moran & Desimone, 1985; Tootell et al., 1998; Treue, 2001). Our goal for our first study was to localize the attenuating filter for a simple sensorymotor task in the mouse whisker system.

References

Abrahamyan, A., Silva, L. L., Dakin, S. C., Carandini, M., & Gardner, J. L. (2016). Adaptable history biases in human perceptual decisions. *Proceedings of the National Academy of Sciences of the United States of America*, *113*(25), E3548-57. https://doi.org/10.1073/pnas.1518786113

Akaishi, R., Umeda, K., Nagase, A., & Sakai, K. (2014). Autonomous mechanism of internal choice estimate underlies decision inertia. *Neuron*, *81*(1), 195–206. https://doi.org/10.1016/j.neuron.2013.10.018

Akerboom, J., Chen, T.-W., Wardill, T. J., Tian, L., Marvin, J. S., Mutlu, S., Calderón, N. C., Esposti, F., Borghuis, B. G., Sun, X. R., Gordus, A., Orger, M. B., Portugues, R., Engert, F., Macklin, J. J., Filosa, A., Aggarwal, A., Kerr, R. A., Takagi, R., … Looger, L. L. (2012). Optimization of a GCaMP calcium indicator for neural activity imaging. *The Journal of Neuroscience : The Official Journal of the Society for Neuroscience*, *32*(40), 13819–13840. https://doi.org/10.1523/JNEUROSCI.2601-12.2012

Akrami, A., Kopec, C. D., Diamond, M. E., & Brody, C. D. (2018). Posterior parietal cortex represents sensory history and mediates its effects on behaviour. *Nature*, *554*(7692), 368–372. https://doi.org/10.1038/nature25510

Allen, W. E., Chen, M. Z., Pichamoorthy, N., Tien, R. H., Pachitariu, M., Luo, L., & Deisseroth, K. (2019). Thirst regulates motivated behavior through modulation of brainwide neural population dynamics. *Science (New York, N.Y.)*, *364*(6437), 253. https://doi.org/10.1126/science.aav3932

Allen, W. E., Kauvar, I. V, Chen, M. Z., Richman, E. B., Yang, S. J., Chan, K., Gradinaru, V., Deverman, B. E., Luo, L., & Deisseroth, K. (2017). Global Representations of Goal-Directed Behavior in Distinct Cell Types of Mouse Neocortex. *Neuron*, *94*(4), 891-907.e6. https://doi.org/10.1016/j.neuron.2017.04.017

Aronoff, R., Matyas, F., Mateo, C., Ciron, C., Schneider, B., & Petersen, C. C. H. (2010). Long-range connectivity of mouse primary somatosensory barrel cortex. *The European Journal of Neuroscience*, *31*(12), 2221–2233. https://doi.org/10.1111/j.1460-9568.2010.07264.x

Aruljothi, K., Marrero, K., Zhang, Z., Zareian, B., & Zagha, E. (2020). Functional Localization of an Attenuating Filter within Cortex for a Selective Detection Task in Mice. *Journal of Neuroscience*, *40*(28), 5443–5454. https://doi.org/10.1523/JNEUROSCI.2993-19.2020

Barnett, L. M., Hughes, T. E., & Drobizhev, M. (2017). Deciphering the molecular mechanism responsible for GCaMP6m's Ca2+-dependent change in fluorescence. *PloS One*, *12*(2), e0170934. https://doi.org/10.1371/journal.pone.0170934

Baunez, C., & Robbins, T. W. (1997). Bilateral Lesions of the Subthalamic Nucleus Induce Multiple Deficits in an Attentional Task in Rats. *European Journal of Neuroscience*, *9*(10), 2086–2099. https://doi.org/https://doi.org/10.1111/j.1460-9568.1997.tb01376.x

Baunez, C., & Robbins, T. W. (1999). Effects of transient inactivation of the subthalamic nucleus by local muscimol and APV infusions on performance on the five-choice serial reaction time task in rats. *Psychopharmacology*, *141*(1), 57–65. https://doi.org/10.1007/s002130050806

Bornstein, A. M., & Daw, N. D. (2011). Multiplicity of control in the basal ganglia: computational roles of striatal subregions. *Current Opinion in Neurobiology*, *21*(3), 374–380. https://doi.org/10.1016/j.conb.2011.02.009

Braun, A., Urai, A. E., & Donner, T. H. (2018). Adaptive History Biases Result from Confidence-Weighted Accumulation of past Choices. *The Journal of Neuroscience : The Official Journal of the Society for Neuroscience*, *38*(10), 2418–2429. https://doi.org/10.1523/JNEUROSCI.2189-17.2017

Britten, K. H., Newsome, W. T., Shadlen, M. N., Celebrini, S., & Movshon, J. A. (1996). A relationship between behavioral choice and the visual responses of neurons in macaque MT. *Visual Neuroscience*, *13*(1), 87–100. https://doi.org/10.1017/s095252380000715x

Britten, K. H., Shadlen, M. N., Newsome, W. T., & Movshon, J. A. (1992). The analysis of visual motion: a comparison of neuronal and psychophysical performance. *The Journal of Neuroscience*, *12*(12), 4745 LP – 4765. https://doi.org/10.1523/JNEUROSCI.12-12-04745.1992

Broadbent, D. E. (1958). Perception and communication. In *Perception and communication.* Pergamon Press. https://doi.org/10.1037/10037-000

Busse, L., Ayaz, A., Dhruv, N. T., Katzner, S., Saleem, A. B., Schölvinck, M. L., Zaharia, A. D., & Carandini, M. (2011). The detection of visual contrast in the behaving mouse. *The Journal of Neuroscience : The Official Journal of the Society for Neuroscience*, *31*(31), 11351–11361. https://doi.org/10.1523/JNEUROSCI.6689-10.2011

Cardin, J. A., Crair, M. C., & Higley, M. J. (2020). Mesoscopic Imaging: Shining a Wide Light on Large-Scale Neural Dynamics. *Neuron*, *108*(1), 33–43. https://doi.org/10.1016/J.NEURON.2020.09.031

Chen, J. L., Margolis, D. J., Stankov, A., Sumanovski, L. T., Schneider, B. L., & Helmchen, F. (2015). Pathway-specific reorganization of projection neurons in somatosensory cortex during learning. *Nature Neuroscience*, *18*(8), 1101–1108. https://doi.org/10.1038/nn.4046

Chen, T.-W., Wardill, T. J., Sun, Y., Pulver, S. R., Renninger, S. L., Baohan, A., Schreiter, E. R., Kerr, R. A., Orger, M. B., Jayaraman, V., Looger, L. L., Svoboda, K., & Kim, D. S. (2013). Ultrasensitive fluorescent proteins for imaging neuronal activity. *Nature*, *499*(7458), 295–300. https://doi.org/10.1038/nature12354

Cherry, E. C. (1953). Some Experiments on the Recognition of Speech, with One and with Two Ears. *The Journal of the Acoustical Society of America*, *25*(5), 975–979. https://doi.org/10.1121/1.1907229

Cho, R. Y., Nystrom, L. E., Brown, E. T., Jones, A. D., Braver, T. S., Holmes, P. J., & Cohen, J. D. (2002). Mechanisms underlying dependencies of performance on stimulus history in a two-alternative forced-choice task. *Cognitive, Affective & Behavioral Neuroscience*, *2*(4), 283–299. https://doi.org/10.3758/cabn.2.4.283

Dana, H., Sun, Y., Mohar, B., Hulse, B. K., Kerlin, A. M., Hasseman, J. P., Tsegaye, G., Tsang, A., Wong, A., Patel, R., Macklin, J. J., Chen, Y., Konnerth, A., Jayaraman, V., Looger, L. L., Schreiter, E. R., Svoboda, K., & Kim, D. S. (2019). High-performance calcium sensors for imaging activity in neuronal populations and microcompartments. *Nature Methods*, *16*(7), 649–657. https://doi.org/10.1038/s41592-019-0435-6

Daw, N. D., O'Doherty, J. P., Dayan, P., Seymour, B., & Dolan, R. J. (2006). Cortical substrates for exploratory decisions in humans. *Nature*, *441*(7095), 876–879. https://doi.org/10.1038/nature04766

Dayan, P., & Niv, Y. (2008). Reinforcement learning: the good, the bad and the ugly. *Current Opinion in Neurobiology*, *18*(2), 185–196. https://doi.org/10.1016/j.conb.2008.08.003

Deutsch, J. A., & Deutsch, D. (1963). Attention: Some theoretical considerations. *Psychological Review*, *70*(1), 80–90. https://doi.org/10.1037/h0039515

Dickinson, A., & Weiskrantz, L. (1985). Actions and habits: the development of behavioural autonomy. *Philosophical Transactions of the Royal Society of London. B, Biological Sciences*, *308*(1135), 67–78. https://doi.org/10.1098/rstb.1985.0010

Eggermann, E., Kremer, Y., Crochet, S., & Petersen, C. C. H. (2014). Cholinergic signals in mouse barrel cortex during active whisker sensing. *Cell Reports*, *9*(5), 1654–1660. https://doi.org/10.1016/j.celrep.2014.11.005

Erlich, J. C., Bialek, M., & Brody, C. D. (2011). A Cortical Substrate for Memory-Guided Orienting in the Rat. *Neuron*, *72*(2), 330–343. https://doi.org/10.1016/j.neuron.2011.07.010

Everitt, B. J., Belin, D., Economidou, D., Pelloux, Y., Dalley, J. W., & Robbins, T. W. (2008). Review. Neural mechanisms underlying the vulnerability to develop compulsive drug-seeking habits and addiction. *Philosophical Transactions of the Royal Society of London. Series B, Biological Sciences*, *363*(1507), 3125–3135. https://doi.org/10.1098/rstb.2008.0089

Fan, Y., Gold, J. I., & Ding, L. (2018). Ongoing, rational calibration of reward-driven perceptual biases. *ELife*, *7*. https://doi.org/10.7554/eLife.36018

Ferezou, I., Haiss, F., Gentet, L. J., Aronoff, R., Weber, B., & Petersen, C. C. H. (2007). Spatiotemporal Dynamics of Cortical Sensorimotor Integration in Behaving Mice. *Neuron*, *56*(5), 907–923. https://doi.org/10.1016/j.neuron.2007.10.007

Fischer, J., & Whitney, D. (2014). Serial dependence in visual perception. *Nature Neuroscience*, *17*(5), 738–743. https://doi.org/10.1038/nn.3689

Fiser, J., & Aslin, R. N. (2001). Unsupervised Statistical Learning of Higher-Order Spatial Structures from Visual Scenes. *Psychological Science*, *12*(6), 499–504. https://doi.org/10.1111/1467-9280.00392

Freedman, D. J., Riesenhuber, M., Poggio, T., & Miller, E. K. (2003). A Comparison of Primate Prefrontal and Inferior Temporal Cortices during Visual Categorization. *The Journal of Neuroscience*, *23*(12), 5235. https://doi.org/10.1523/JNEUROSCI.23-12-05235.2003

Fritsche, M., Mostert, P., & de Lange, F. P. (2017). Opposite Effects of Recent History on Perception and Decision. *Current Biology : CB*, *27*(4), 590–595. https://doi.org/10.1016/j.cub.2017.01.006

Fründ, I., Wichmann, F. A., & Macke, J. H. (2014). Quantifying the effect of intertrial dependence on perceptual decisions. *Journal of Vision*, *14*(7). https://doi.org/10.1167/14.7.9

Fukuchi-Shimogori, T., & Grove, E. A. (2001). Neocortex patterning by the secreted signaling molecule FGF8. *Science (New York, N.Y.)*, *294*(5544), 1071–1074. https://doi.org/10.1126/science.1064252

Gillan, C. M., Papmeyer, M., Morein-Zamir, S., Sahakian, B. J., Fineberg, N. A., Robbins, T. W., & de Wit, S. (2011). Disruption in the balance between goal-directed behavior and habit learning in obsessive-compulsive disorder. *The American Journal of Psychiatry*, *168*(7), 718–726. https://doi.org/10.1176/appi.ajp.2011.10071062

Gold, J. I., Law, C.-T., Connolly, P., & Bennur, S. (2008). The relative influences of priors and sensory evidence on an oculomotor decision variable during perceptual learning. *Journal of Neurophysiology*, *100*(5), 2653–2668. https://doi.org/10.1152/jn.90629.2008

Hannan, A. J., Blakemore, C., Katsnelson, A., Vitalis, T., Huber, K. M., Bear, M., Roder, J., Kim, D., Shin, H. S., & Kind, P. C. (2001). PLC-beta1, activated via mGluRs, mediates activity-dependent differentiation in cerebral cortex. *Nature Neuroscience*, *4*(3), 282–288. https://doi.org/10.1038/85132

Houweling, A. R., & Brecht, M. (2008). Behavioural report of single neuron stimulation in somatosensory cortex. *Nature*, *451*(7174), 65–68. https://doi.org/10.1038/nature06447

Huber, D., Gutnisky, D. A., Peron, S., O'Connor, D. H., Wiegert, J. S., Tian, L., Oertner, T. G., Looger, L. L., & Svoboda, K. (2012). Multiple dynamic representations in the motor cortex during sensorimotor learning. *Nature*, *484*(7395), 473–478. https://doi.org/10.1038/nature11039

Hwang, E. J., Dahlen, J. E., Mukundan, M., & Komiyama, T. (2017). History-based action selection bias in posterior parietal cortex. *Nature Communications*, *8*(1), 1242. https://doi.org/10.1038/s41467-017-01356-z

Ito, M., & Doya, K. (2011). Multiple representations and algorithms for reinforcement learning in the cortico-basal ganglia circuit. *Current Opinion in Neurobiology*, *21*(3), 368–373. https://doi.org/10.1016/j.conb.2011.04.001

Iwasato, T., Datwani, A., Wolf, A. M., Nishiyama, H., Taguchi, Y., Tonegawa, S., Knöpfel, T., Erzurumlu, R. S., & Itohara, S. (2000). Cortex-restricted disruption of NMDAR1 impairs neuronal patterns in the barrel cortex. *Nature*, *406*(6797), 726–731. https://doi.org/10.1038/35021059

Jin, X., & Costa, R. M. (2010). Start/stop signals emerge in nigrostriatal circuits during sequence learning. *Nature*, *466*(7305), 457–462. https://doi.org/10.1038/nature09263

Lee, D., Seo, H., & Jung, M. W. (2012). Neural basis of reinforcement learning and decision making. *Annual Review of Neuroscience*, *35*, 287–308. https://doi.org/10.1146/annurev-neuro-062111-150512

Lin, M. Z., & Schnitzer, M. J. (2016). Genetically encoded indicators of neuronal activity. *Nature Neuroscience*, *19*(9), 1142–1153. https://doi.org/10.1038/nn.4359

Luck, S. J., Chelazzi, L., Hillyard, S. A., & Desimone, R. (1997). Neural Mechanisms of Spatial Selective Attention in Areas V1, V2, and V4 of Macaque Visual Cortex. *Journal of Neurophysiology*, *77*(1), 24–42. https://doi.org/10.1152/jn.1997.77.1.24

Lueckmann, J.-M., Macke, J. H., & Nienborg, H. (2018). Can Serial Dependencies in Choices and Neural Activity Explain Choice Probabilities? *The Journal of Neuroscience : The Official Journal of the Society for Neuroscience*, *38*(14), 3495–3506. https://doi.org/10.1523/JNEUROSCI.2225-17.2018

Luu, L., & Stocker, A. A. (2018). Post-decision biases reveal a self-consistency principle in perceptual inference. *ELife*, *7*. https://doi.org/10.7554/eLife.33334

Makino, H., Ren, C., Liu, H., Kim, A. N., Kondapaneni, N., Liu, X., Kuzum, D., & Komiyama, T. (2017). Transformation of Cortex-wide Emergent Properties during Motor Learning. *Neuron*, *94*(4), 880-890.e8. https://doi.org/10.1016/j.neuron.2017.04.015

Marcos, E., Pani, P., Brunamonti, E., Deco, G., Ferraina, S., & Verschure, P. (2013). Neural variability in premotor cortex is modulated by trial history and predicts behavioral performance. *Neuron*, *78*(2), 249–255. https://doi.org/10.1016/j.neuron.2013.02.006

Marrero, K., Aruljothi, K., Zareian, B., Gao, C., Zhang, Z., & Zagha, E. (2022). Global, Low-Amplitude Cortical State Predicts Response Outcomes in a Selective Detection Task in Mice. *Cerebral Cortex*, *32*(9), 2037–2053. https://doi.org/10.1093/cercor/bhab339

Matyas, F., Sreenivasan, V., Marbach, F., Wacongne, C., Barsy, B., Mateo, C., Aronoff, R., & Petersen, C. C. H. (2010). Motor control by sensory cortex. *Science (New York, N.Y.)*, *330*(6008), 1240–1243. https://doi.org/10.1126/science.1195797

Moran, J., & Desimone, R. (1985). Selective attention gates visual processing in the extrastriate cortex. *Science (New York, N.Y.)*, *229*(4715), 782–784. https://doi.org/10.1126/science.4023713

Musall, S., Kaufman, M. T., Juavinett, A. L., Gluf, S., & Churchland, A. K. (2019). Single-trial neural dynamics are dominated by richly varied movements. *Nature Neuroscience*, *22*(10), 1677–1686. https://doi.org/10.1038/s41593-019-0502-4

Pai, S., Erlich, J., Kopec, C., & Brody, C. (2011). Minimal Impairment in a Rat Model of Duration Discrimination Following Excitotoxic Lesions of Primary Auditory and Prefrontal Cortices. *Frontiers in Systems Neuroscience*, *5*. https://doi.org/10.3389/fnsys.2011.00074

Reinert, S., Hübener, M., Bonhoeffer, T., & Goltstein, P. M. (2021). Mouse prefrontal cortex represents learned rules for categorization. *Nature*, *593*(7859), 411–417. https://doi.org/10.1038/s41586-021-03452-z

Ren, C., & Komiyama, T. (2021). Characterizing Cortex-Wide Dynamics with Wide-Field Calcium Imaging. *The Journal of Neuroscience*, *41*(19), 4160. https://doi.org/10.1523/JNEUROSCI.3003-20.2021

Rudebeck, P. H., & Murray, E. A. (2008). Amygdala and Orbitofrontal Cortex Lesions Differentially Influence Choices during Object Reversal Learning. *The Journal of Neuroscience*, *28*(33), 8338. https://doi.org/10.1523/JNEUROSCI.2272-08.2008

Sabatini, B. L., & Tian, L. (2020). Imaging Neurotransmitter and Neuromodulator Dynamics In Vivo with Genetically Encoded Indicators. *Neuron*, *108*(1), 17–32. https://doi.org/10.1016/j.neuron.2020.09.036

Sachdev, R. N. S., Ebner, F. F., & Wilson, C. J. (2004). Effect of Subthreshold Up and Down States on the Whisker-Evoked Response in Somatosensory Cortex. *Journal of Neurophysiology*, *92*(6), 3511–3521. https://doi.org/10.1152/jn.00347.2004

Sachidhanandam, S., Sreenivasan, V., Kyriakatos, A., Kremer, Y., & Petersen, C. C. H. (2013). Membrane potential correlates of sensory perception in mouse barrel cortex. *Nature Neuroscience*, *16*(11), 1671–1677. https://doi.org/10.1038/nn.3532

Salkoff, D. B., Zagha, E., McCarthy, E., & McCormick, D. A. (2020). Movement and Performance Explain Widespread Cortical Activity in a Visual Detection Task. *Cerebral Cortex*, *30*(1), 421–437. https://doi.org/10.1093/cercor/bhz206

Samejima, K., Ueda, Y., Doya, K., & Kimura, M. (2005). Representation of action-specific reward values in the striatum. *Science (New York, N.Y.)*, *310*(5752), 1337–1340. https://doi.org/10.1126/science.1115270

Skinner, B. F. (1937). Two types of conditioned reflex: a reply to Miller and Konorski. *Journal of General Psychology*, *16*, 272–279. https://doi.org/10.1080/00221309.1937.9917951

Smits-Bandstra, S., & De Nil, L. F. (2007). Sequence skill learning in persons who stutter: Implications for cortico-striato-thalamo-cortical dysfunction. *Journal of Fluency Disorders*, *32*(4), 251–278. https://doi.org/https://doi.org/10.1016/j.jfludis.2007.06.001

Sofroniew, N. J., Vlasov, Y. A., Hires, S. A., Freeman, J., & Svoboda, K. (2015). Neural coding in barrel cortex during whisker-guided locomotion. *ELife*, *4*. https://doi.org/10.7554/eLife.12559

Sridharan, D., Schwarz, J. S., & Knudsen, E. I. (2014). Selective attention in birds. *Current Biology : CB*, *24*(11), R510-3. https://doi.org/10.1016/j.cub.2013.12.046

Sutton, R. S., & Barto, A. G. (2018). *Reinforcement learning: An introduction*. MIT press.

Tai, L.-H., Lee, A. M., Benavidez, N., Bonci, A., & Wilbrecht, L. (2012). Transient stimulation of distinct subpopulations of striatal neurons mimics changes in action value. *Nature Neuroscience*, *15*(9), 1281–1289. https://doi.org/10.1038/nn.3188

Tanke, N., Borst, J. G. G., & Houweling, A. R. (2018). Single-Cell Stimulation in Barrel Cortex Influences Psychophysical Detection Performance. *The Journal of Neuroscience : The Official Journal of the Society for Neuroscience*, *38*(8), 2057–2068. https://doi.org/10.1523/JNEUROSCI.2155-17.2018

Tian, L., Hires, S. A., Mao, T., Huber, D., Chiappe, M. E., Chalasani, S. H., Petreanu, L., Akerboom, J., McKinney, S. A., Schreiter, E. R., Bargmann, C. I., Jayaraman, V., Svoboda, K., & Looger, L. L. (2009). Imaging neural activity in worms, flies and mice with improved GCaMP calcium indicators. *Nature Methods*, *6*(12), 875–881. https://doi.org/10.1038/nmeth.1398

Tootell, R. B., Hadjikhani, N., Hall, E. K., Marrett, S., Vanduffel, W., Vaughan, J. T., & Dale, A. M. (1998). The retinotopy of visual spatial attention. *Neuron*, *21*(6), 1409–1422. https://doi.org/10.1016/s0896-6273(00)80659-5

TREISMAN, A. M. (1964). SELECTIVE ATTENTION IN MAN. *British Medical Bulletin*, *20*, 12–16. https://doi.org/10.1093/oxfordjournals.bmb.a070274

Treue, S. (2001). Neural correlates of attention in primate visual cortex. *Trends in Neurosciences*, *24*(5), 295–300. https://doi.org/10.1016/s0166-2236(00)01814-2

Tsunada, J., Cohen, Y., & Gold, J. I. (2019). Post-decision processing in primate prefrontal cortex influences subsequent choices on an auditory decision-making task. *ELife*, *8*. https://doi.org/10.7554/eLife.46770

Turk-Browne, N. B. (2012a). Statistical learning and its consequences. In *The influence of attention, learning, and motivation on visual search.* (pp. 117–146). Springer Science + Business Media. https://doi.org/10.1007/978-1-4614-4794-8_6

Turk-Browne, N. B. (2012b). Statistical Learning in Perception. In N. M. Seel (Ed.), *Encyclopedia of the Sciences of Learning* (pp. 3182–3185). Springer US. https://doi.org/10.1007/978-1-4419-1428-6_1707

Turk-Browne, N. B., Scholl, B. J., Johnson, M. K., & Chun, M. M. (2010). Implicit Perceptual Anticipation Triggered by Statistical Learning. *The Journal of Neuroscience*, *30*(33), 11177. https://doi.org/10.1523/JNEUROSCI.0858-10.2010

Urai, A. E., Braun, A., & Donner, T. H. (2017). Pupil-linked arousal is driven by decision uncertainty and alters serial choice bias. *Nature Communications*, *8*, 14637. https://doi.org/10.1038/ncomms14637

Van der Loos, H., & Woolsey, T. A. (1973). Somatosensory cortex: structural alterations following early injury to sense organs. *Science (New York, N.Y.)*, *179*(4071), 395–398. https://doi.org/10.1126/science.179.4071.395

van der Meer, M. A. A., & Redish, A. D. (2011). Ventral striatum: a critical look at models of learning and evaluation. *Current Opinion in Neurobiology*, *21*(3), 387–392. https://doi.org/10.1016/j.conb.2011.02.011

Welker, E., Armstrong-James, M., Bronchti, G., Ourednik, W., Gheorghita-Baechler, F., Dubois, R., Guernsey, D. L., Van der Loos, H., & Neumann, P. E. (1996). Altered sensory processing in the somatosensory cortex of the mouse mutant barrelless. *Science (New York, N.Y.)*, *271*(5257), 1864–1867. https://doi.org/10.1126/science.271.5257.1864

Welker, E., & Van der Loos, H. (1986). Quantitative correlation between barrel-field size and the sensory innervation of the whiskerpad: a comparative study in six strains of mice bred for different patterns of mystacial vibrissae. *The Journal of Neuroscience : The Official Journal of the Society for Neuroscience*, *6*(11), 3355–3373. https://doi.org/10.1523/JNEUROSCI.06-11-03355.1986

Wiederman, S. D., & O'Carroll, D. C. (2013). Selective Attention in an Insect Visual Neuron. *Current Biology*, *23*(2), 156–161. https://doi.org/https://doi.org/10.1016/j.cub.2012.11.048

Woolsey, T. A., & Van der Loos, H. (1970). The structural organization of layer IV in the somatosensory region (SI) of mouse cerebral cortex. The description of a cortical field composed of discrete cytoarchitectonic units. *Brain Research*, *17*(2), 205–242. https://doi.org/10.1016/0006-8993(70)90079-x

Yamashita, T., Vavladeli, A., Pala, A., Galan, K., Crochet, S., Petersen, S. S. A., & Petersen, C. C. H. (2018). Diverse Long-Range Axonal Projections of Excitatory Layer 2/3 Neurons in Mouse Barrel Cortex. *Frontiers in Neuroanatomy*, *12*, 33. https://doi.org/10.3389/fnana.2018.00033

Yang, H., Kwon, S. E., Severson, K. S., & O'Connor, D. H. (2016). Origins of choice-related activity in mouse somatosensory cortex. *Nature Neuroscience*, *19*(1), 127–134. https://doi.org/10.1038/nn.4183

Yang, Y., Liu, N., He, Y., Liu, Y., Ge, L., Zou, L., Song, S., Xiong, W., & Liu, X. (2018). Improved calcium sensor GCaMP-X overcomes the calcium channel perturbations induced by the calmodulin in GCaMP. *Nature Communications*, *9*(1), 1504. https://doi.org/10.1038/s41467-018-03719-6

Zareian, B., Lam, A., & Zagha, E. (2023). Dorsolateral Striatum is a Bottleneck for Responding to Task-Relevant Stimuli in a Learned Whisker Detection Task in Mice. *The Journal of Neuroscience*, *43*(12), 2126–2139. https://doi.org/10.1523/JNEUROSCI.1506-22.2023

Zareian, B., Zhang, Z., & Zagha, E. (2021). Cortical localization of the sensory-motor transformation in a whisker detection task in mice. *ENeuro*, *8*(1), 1–14. https://doi.org/10.1523/ENEURO.0004-21.2021

Zhang, Z., & Zagha, E. (2023). Motor cortex gates distractor stimulus encoding in sensory cortex. *Nature Communications*, *14*(1), 2097. https://doi.org/10.1038/s41467-023-37848-4

Chapter 2: Functional Localization of an attenuating filter

This first study introduced both our new whisker-based selective detection task and the use of widefield imaging to study sensory selection in mice. Employing the signal detection theory framework, we determined key behavioral measures, including stimulus detection, discrimination between stimuli, and response rates, crucial for characterizing expert behavior in mice. We used widefield calcium imaging technique to record the spatio-temporal flow of activity across dorsal cortex of expert mice. Our selective detection paradigm provided compelling and consistent evidence of the presence of an attenuation filter localized within the cortex for the selective detection task in mice. The findings of our study support Treisman's framework over Broadbent's, observing sensory encoding for both target and distractor stimulus propagation, as evidenced by the reduction in distractor compared to target responses beyond primary somatosensory cortex.

My contributions to this work included establishing the behavioral paradigm, animal surgeries, behavioral training of mice used in imaging analyses, collection of widefield imaging data, and data analyses for fluorescence activity and stimulus encoding (as shown in Figures 1, 2, 3, 5 and 6).

Title: Functional Localization of an Attenuating Filter within Cortex for a Selective Detection Task in Mice

Abbreviated title: Cortical attenuation during selective detection

Authors: Krithiga Aruljothi[1*], Krista Marrero[2*], Zhaoran Zhang[2], Behzad Zareian[1], Edward Zagha[1,2]

[1] Department of Psychology, [2] Neuroscience Graduate Program, University of California Riverside, 900 University Avenue, Riverside CA 92521 USA

* equal contributors

Correspondence to: edward.zagha@ucr.edu

Number of pages: 51

Number of figures: 11

Number of words in abstract (190), introduction (649), discussion (987)

Conflict of interest statement: The authors declare no competing financial interests.

Acknowledgements: This work was supported by the Whitehall Foundation (Research Grant 2017-05-71 to E.Z.) and the National Institutes of Health (R01NS107599 to E.Z.). We thank Trevor Stavropoulos for assistance with Arduino programming. We thank Shaida Abachi for collecting whisker imaging data. We thank Hongdian Yang, Martin Riccomagno, Aaron Seitz and Megan Peters for many helpful discussions throughout the project.

Abstract

An essential feature of goal-directed behavior is the ability to selectively respond to the diverse stimuli in one's environment. However, the neural mechanisms that enable us to respond to target stimuli while ignoring distractor stimuli are poorly understood. To study this sensory selection process, we trained male and female mice in a selective detection task in which mice learn to respond to rapid stimuli in the target whisker field and ignore identical stimuli in the opposite, distractor whisker field. In expert mice, we used widefield Ca^{2+} imaging to analyze target-related and distractor-related neural responses throughout dorsal cortex. For target stimuli, we observed strong signal activation in primary somatosensory cortex (S1) and frontal cortices, including both the whisker region of primary motor cortex (wMC) and anterior lateral motor cortex (ALM). For distractor stimuli, we observed strong signal activation in S1, with minimal propagation to frontal cortex. Our data support only modest subcortical filtering, with robust, step-like attenuation in distractor processing between mono-synaptically coupled regions of S1 and wMC. This study establishes a highly robust model system for studying the neural mechanisms of sensory selection and places important constraints on its implementation.

Significance Statement

Responding to task-relevant stimuli while ignoring task-irrelevant stimuli is critical for goal-directed behavior. Yet, the neural mechanisms involved in this selection process are poorly understood. We trained mice in a detection task with both target and distractor stimuli. During expert performance, we measured neural activity throughout cortex using widefield imaging. We observed responses to target stimuli in multiple sensory and motor cortical regions. In contrast, responses to distractor stimuli were abruptly suppressed beyond sensory cortex. Our findings localize the sites of attenuation when successfully ignoring a distractor stimulus, and provide essential foundations for further revealing the neural mechanism of sensory selection and distractor suppression.

Introduction

We are constantly bombarded by sensory stimuli. To complete a given task, we must selectively respond to task-relevant stimuli while ignoring task-irrelevant stimuli. A framework for understanding stimulus selection is provided by the Treisman attenuation theory (Figure 1). According to this theory, both attended and unattended signals enter short-term storage. Responses to attended stimuli propagate forward for higher-order processing. Responses to unattended stimuli, however, are suppressed by an attenuating filter at some point along the processing stream (TREISMAN, 1964). The attenuation theory was originally developed to understand selection amongst conflicting speech patterns, yet has since been adapted to study sensory selection across multiple sensory modalities and species (Moran & Desimone, 1985; Sridharan et al., 2014; Wiederman & O'Carroll, 2013).

Where in the brain does attenuation occur and what are the neural mechanisms involved? Extensive studies in the primate visual system have identified stimulus filtering throughout multiple brain regions. Sensory selection was initially proposed to occur in the thalamus, mediated by the modulation of thalamic relay neuron activation by the reticular thalamus (Crick, 1984). Recordings in behaving primates have demonstrated early-onset attentional modulations in thalamus (McAlonan et al., 2008), consistent with stimulus filtering prior to reaching cortex. However, earlier physiological studies demonstrated robust attentional filtering within cortex, between primary visual cortex and visual

area V4 (Moran & Desimone, 1985). Alternatively, other studies argue for filtering occurring primarily within prefrontal cortex (Mante et al., 2013). Potential 'top-down' pathways establishing an attenuating filter include cortical feedback and ascending neuromodulation (Miller & Cohen, 2001; Noudoost & Moore, 2011). Yet, these mechanisms are poorly understood, in part due to the apparent highly distributed filtering processes of the primate visual system.

Our goal in this study is to localize the attenuating filter for a simple sensory-motor task in the mouse whisker system. This model system benefits from extensive characterization of the sensory and motor regions and pathways involved, with significantly fewer hierarchical levels than the primate visual system (Guo et al., 2014; Kleinfeld et al., 1999; Petersen, 2019). Whisker deflection activates brainstem pathways which travel predominantly through the ventral posteromedial (VPM) thalamus and onto primary somatosensory (barrel) cortex (S1). From S1, there are robust, mono-synaptic connections to the whisker region of primary motor cortex (wMC) (Mao et al., 2011; Miyashita et al., 1994; Porter & White, 1983). Sensory responses in S1 rapidly propagate to wMC, under both anesthetized and awake conditions (Chakrabarti et al., 2008; Farkas et al., 1999; Ferezou et al., 2007; Kleinfeld et al., 2002; Zagha et al., 2015). Moreover, this pathway may be particularly important for input detection; S1-wMC projection neurons were found to be preferentially responsive to touch in an object detection task (Chen et al., 2013), which enhanced during task training (J. L. Chen et al., 2015). Recent studies in the rodent whisker system have reported sensory filtering

within the thalamus (Rodenkirch et al., 2019) and brainstem (Chakrabarti & Schwarz, 2018). However, it remains unknown to what extent these subcortical or cortical pathways contribute to filtering during a sensory selection task.

We designed a selective detection task with spatially and temporally distinct processing streams. Mice respond to rapid deflections of one whisker field (target) and ignore identical stimuli in the opposite, contralateral whisker field (distractor). Rather than presenting target and distractor stimuli together, as in the original studies on sensory selection (Moran & Desimone, 1985; TREISMAN, 1964), we present each stimulus individually on different trials. Thus, we can evaluate target and distractor processing separately across space (different hemispheres) and time (different trials). The motor response in our task is a straight-forward lick. As the sensory and motor content of our task is symmetric, the only asymmetry is the selection process. In expert performing mice, we used widefield Ca^{2+} population imaging (Wekselblatt et al., 2016) to simultaneously monitor neural activity bilaterally in sensory and motor regions. We then quantified the asymmetry in target-aligned versus distractor-aligned sensory processing streams to localize sites of attenuation.

Materials and Methods

Animal Subjects and Surgery

All experiments performed in this study were approved by the IACUC of University of California, Riverside. Mice were purchased from Jackson Laboratories (JAX). Task-related neural imaging data were obtained from GCaMP6s expressing Snap25-2A-GCaMP6s-D mice (JAX #025111). The SNAP25-2A-GCaMP6s mouse line expresses GCaMP6s pan-neuronally, in both excitatory and inhibitory neurons throughout the brain (Madisen et al., 2015). Transgenic mice were backcrossed into the BALB/cByJ (JAX 000651) background. Both male and female mice were used in these experiments. Recording sessions from male and female mice were similar according to behavioral performance (imaging experiments: 4 male mice, 32 sessions, 1 female mouse, 7 sessions; discriminability d': male 2.0 ± 0.1, female 1.9 ± 0.2, two sample t-test, p= 0.36, t(37)= 0.92; target stimulus reaction time (s): male 0.30 ± 0.01, female 0.32 ± 0.02 , two sample t-test, p= 0.70, t(37)= -0.38) and neural responses (data not shown), and therefore data were combined for grand average analyses. Mice were housed on a light cycle of 12 hours light/ 12 hours dark. All trainings and recordings were conducted on mice head-fixed in the behavioral apparatus. For headpost implantation, 2 to 5 months-old mice were placed under a combination of isoflurane (1-2%), ketamine (100 mg/kg), and xylazine (10 mg/kg) anesthesia. A 10 mm x 10 mm piece of scalp was resected to expose the skull. The exposed skull was cleared of connective tissue and a custom-built headpost was implanted onto the skull with cyanoacrylate glue. The

lightweight titanium or stainless steel headpost (3 cm in length and 1.5 grams in weight) had an 8 mm x 8 mm central window for imaging and recording. For in vivo widefield Ca^{2+} imaging, a thin layer of cyanoacrylate gap-filling medium (Insta-Cure, Bob Smith Industries) was applied to the window, to both seal the exposed skull and enhance skull transparency. Silicone elastomer (Reynolds Advanced Materials) was additionally applied above the imaging window. After surgery, mice were placed onto a heating pad to recover and administered meloxicam (0.3 mg/kg) and enrofloxacin (5 mg/kg) for three days post-op. Mice were given a minimum of three days to recover from surgery before water-restriction and behavioral training. Recordings under anesthesia were conducted immediately after headpost implantation.

Animal Behavior

Mice were trained in a Go/NoGo passive whisker selective detection task. During behavioral training mice were given food ad libitum but were water-restricted to a minimum of 1 mL per day. Weights were monitored daily to maintain over 85% of their initial post-surgery weights, and additional water was given as needed to maintain this level. The behavioral apparatus was controlled by Arduino and custom MATLAB (MathWorks) code. Piezo-controlled paddles (Physik Instrumente and Piezo.com) were placed bilaterally in the whisker fields, with each paddle contacting 2 to 4 whiskers. Paddle deflections of a triangle waveform had rising

phases that ranged from 0.1 s (for large deflections) to 0.01 s (for small deflections), followed by an immediate falling phase. Deflection velocity was constant, therefore increased duration correlated with increased deflection amplitude. The maximum amplitude, for 0.1 s deflections, was 1 mm. Stimulus duration and amplitude were varied with training with the goal of maintaining a 75% hit rate. This target hit rate was selected to maintain high reward rates while still operating within the dynamic range of each mouse's psychometric curve. Within every session, target and distractor stimulus strengths were identical. Directly below the mouse's snout was a central lick port. Each 'hit' trial was rewarded with ~5 mL of water delivered through the lick port.

Behavioral training consisted of three stages. Inter-trial intervals for all stages varied from 5 to 9 s with a negative exponential distribution to minimize potential timing strategies. Additionally, in all stages a 'lockout' period of 200 ms separated stimulus onset and the earliest opportunity for reward. Target and distractor whisker fields were assigned at Stage 1 and remained constant throughout training. Target/distractor assignment was varied across the population and analyzed separately (Figure 7A-C) before combining for grand average analyses. Each session lasted approximately 60 minutes and consisted of ~200 trials. (Stage 1) Classical conditioning: Unilateral (target) whisker deflection was paired with fluid reward; distractor whisker deflection was neither rewarded nor punished. Mice were trained on this stage for 1 to 3 days, 1 to 2 sessions per day. (Stage 2) Operant conditioning: Following unilateral (target) whisker deflection,

mice were required to contact the lick port within a lick detection window of 1.5 s in order to initiate the fluid reward. Mice were trained on this stage for 2 to 3 days, 1 session per day. (Stage 3) Impulse control: Similar task structure as above, except all incorrect responses (licking during the ITI, during the lockout period, or following distractor deflections) were punished by re-setting the ITI, effectively acting as a time-out. The response detection window was shortened to 1 s. Following full-length ITIs, trial types were selected randomly from a distribution of 80% distractor and 20% target. For distractor trials, not responding (*correct rejection*) was rewarded with a shortened ITI (2 to 4 s, negative exponential distribution) and a subsequent target trial. Licking to the distractor (*false alarm*) or not responding to the target (*miss*) initiated a subsequent full-length ITI. Responding to the target stimulus (*hit*) triggered a fluid reward, followed by a full-length ITI. Behavioral and neural imaging data for hit trials with and without preceding correct rejections were compared (Figure 7D, E) before combining for grand average analyses. For approximately half of the mice in this study, following full-length ITIs, catch trials without a whisker stimulus were interspersed at a rate of 10% of all stimulus trials.

A single, contiguous behavioral window was considered for analyses, from session onset until 120 s of no responding, which we interpreted as task disengagement. Hit rate, false alarm rate, spontaneous lick rate, and reaction times were all used to assess task performance. Foremost, we used the sensitivity or d-prime (d') framework from signal detection theory. Traditionally, d' is used as

a measure of detection between stimulus present and stimulus absent conditions. Here, we implemented a discriminability d' between target detection and distractor detection [$d' = Z_{\text{hit rate}} - Z_{\text{false alarm rate}}$] where Z is the inverse of the normal cumulative distribution function. Mice were considered expert in our task once they achieved a d'>1 for three consecutive days. Spontaneous lick rate was calculated as the response rate during the last 1 s of the full-length ITI.

Widefield Imaging

Widefield imaging was performed through-skull in head-fixed mice while they performed the selective detection task. Imaging was conducted through a Macroscope IIa (RedShirtImaging), beam diverter removed, 75 mm inverted lens with 0.7x magnification and 16 mm working distance. The lens (NA 0.4) was positioned directly over the cranial window, providing a 7 mm x 5.8 mm field of view, including most of dorsal parietal and frontal cortex bilaterally. Illumination was provided by a mounted 470 nm LED (Thorlabs M470L3), dispersed with a collimating lens (Thorlabs ACL2520-A), band-pass filtered (Chroma ET480/40x) and directed through the macroscope using a dichroic mirror (Chroma T510lpxrxt). Fluorescent light returning to the brain was band-pass filtered (Chroma ET535/50m) prior to reaching an RT sCMOS camera (SPOT Imaging). On camera 2x2 binning and post-processing image size reduction gave a final resolution of 142 x 170 pixels at 41 μm per pixel and 12-bit depth. Images were acquired at a temporal resolution of 10 Hz, aligned to the trial structure. TIF image sequences were imported to MATLAB for preprocessing and analysis.

Local field potential (LFP) recordings

LFP recordings were conducted through small (<0.5 mm diameter) craniotomies and durotomies positioned above S1 (from bregma: posterior 1.5 mm, lateral 3.5 mm), wMC (anterior 1 mm, lateral 1 mm) and ALM (anterior 2.5 mm, lateral 1.5 mm), in target-aligned and distractor-aligned cortices. Recording sites were positioned 750 mm below the pial surface, targeting layer 5. Recordings were acquired with silicon probes (Neuronexus, A1x16-Poly2-5mm-50s-177), bandpass filtered from 0.1 Hz to 8 kHz and digitized at 32 kHz (Neuralynx). Further analyses were conducted in MATLAB.

Imaging of whisker movements

A CMOS camera (Thorlabs DCC3240M camera with Edmund Optics lens 33-301) was positioned directly above the mouse while performing the detection task. Field of view included both whisker fields and stimulus paddles. Images were captured at 8-bit depth continuously at 60 Hz (ThorCam) and imported to MATLAB for analyses.

Data Analysis

All data analyses were performed in MATLAB using custom scripts.

Fluorescence Preprocessing and Trial-Based Neural Activity

Peri-stimulus trial imaging time windows included 1 s before stimulus onset and 1.2 s after stimulus onset, which included the lockout and response windows. The

first step of image processing was to concatenate fluorescence activity from consecutive trials to create a raw movie F, where $F_n(i,j,f)$ shows the fluorescence of each pixel (i^{th} row, j^{th} column) in the f^{th} frame for each individual trial n. The pre-stimulus baseline fluorescence $F_o(i,j,n)$ was calculated by averaging pixelwise activity across the first 10 frames preceding the stimulus onset per trial n (1 s pre-stimulus). Finally, relative fluorescent signal normalized to pre-stimulus baseline (dF/F) was calculated as

$$dF/F_0(i,j,n) = [F_n(i,j,f) - F_0(i,j,n)]/F_0(i,j,n)$$

Average trial movies were created by indexing trials according to trial outcome (*hit*, *miss*, *false alarm*, *correct rejection*, *spontaneous*) and averaging activities at each pixel across the corresponding frame of each corresponding trial. Frame alignments were conducted both with reference to stimulus onset (stimulus-aligned) and with reference to the first frame containing the response (response-aligned) (see Figure 4). Spontaneous trials were those in which a response occurred during the 1 s pre-stimulus imaging period. Trials with responses during the lockout period were excluded from all further analyses.

Data were analyzed per session (n=39), per mouse (n=5), per target-distractor assignment (n=2) and across all experiments (grand average). For a session to be included in our analyses, our inclusion criteria were d'>1 for at least 10 minutes of continuous engagement. Only one engagement period per session was included. For qualitative analyses, trial movies from recording sessions were

spatially aligned to bregma and averaged per mouse. These data were then averaged per target-distractor assignment (see Figure 7 for whisker deflection assignments). One target-distractor assignment dataset was then flipped horizontally (rostro-caudal axis) at bregma before the grand average dF/F. For quantitative analyses, the subsequent datasets were first flipped at bregma according to target-distractor assignment (as before) and then averaged across all sessions.

Quantification of Stimulus Encoding

To quantify stimulus response magnitude, we calculated the neurometric d' (Britten et al., 1992) comparing activity pre-stimulus (stimulus absent) and post-stimulus (stimulus present), specifically during the lockout period. Neurometric d' was calculated separately for target and distractor trials, and included all trials regardless of outcome (hit and miss trials for target, false alarm and correct rejection for distractor). Pre-stimulus (10 frames preceding stimulus onset) and post-stimulus activities were binned and plotted in an ROC (receiver operating characteristic) curve. The area under the curve (AUC) was converted to d' using the equation:

$$\text{neurometric d'} = \sqrt{2} * Z_{AUC}$$

In the context of this study, neurometric d' is the performance measurement of a pixel where d'>0 denotes more post-stimulus pixel activity and d'<0 denotes more pre-stimulus pixel activity. For each region of interest, we report the peak

neurometric d' within the spatially-defined region of interest (ROI). Subsequent analyses compared target stimulus encoding in target-aligned cortices to distractor stimulus encoding in distractor-aligned cortices.

Quantification of Choice Probability

To quantify choice-related neural activity, we calculated choice probability d' (Britten et al., 1996) comparing activity on hit trials (response present) and miss trials (response absent), specifically during the lockout phase. Sessions were included in this analysis if they had 5 or more trials of each type. Trials with stimuli of different amplitudes were combined only if response rates for each amplitude-specific trial type were comparable (within 15%). Overall, 9 sessions were excluded from this analysis, due to too few miss trials (n=30, instead of n=39). Choice probability was calculated for activity within the pre-response frame (100 to 200 ms during the lockout) and for activity between the pre-response frames (change in activity, subtraction of activity in the 0 to 100 ms frame window from the 100 to 200 ms frame window during the lockout). In the context of this study, choice probability d' is the performance measurement of a pixel where d'>0 denotes more response-related pixel activity and d'<0 denotes more no response-related pixel activity. Response present and response absent activities were binned and plotted in a ROC curve. The area under the curve was converted to d' as described above.

Seed Correlation Analysis

Correlation maps were generated separately for target and distractor hemispheres and for S1, wMC and ALM seed regions (generating six correlation maps per session). Baseline averaged fluorescence activity trajectories from all trial types (excluding spontaneous) were concatenated into a single time series. The following trial structures were analyzed separately: 1) full trial, including 10 frames pre-stimulus and 12 frames post-stimulus including the lockout and response windows, 2) pre-stimulus only, including 10 frames pre-stimulus, 3) peri-stimulus and lockout, including 1 frame pre-stimulus and 2 frames post-stimulus during the lockout, and 4) response, including 10 frames after the lockout and during the response window. The seed was the average time series from all pixels in the indicated region of interest. Pairwise correlation coefficients were calculated between the seed and all other pixels. To reduce computation time, all trial movies were spatially down sampled 4-fold across both axes for a resolution of 36 x 43 pixels at 164 um per pixel prior to running the correlation analyses. We report r^2 values, as the square of the correlation coefficient. For each region of interest, we report the average correlation r^2 within the spatially defined region. Subsequent analyses compared target-aligned intracortical correlations to distractor-aligned intracortical correlations.

Evoked-potential analyses

Single-trial LFP recordings were aligned to target and distractor stimulus onset. To isolate the LFP signal, single-trial data were bandpass filtered from 0.2 Hz to 100 Hz using a second order Butterworth filter, then downsampled to a sampling frequency of 400 Hz. Following filtering and downsampling, single-trial data were averaged according to trial type. In figure 9, stimulus artifacts at 0-10 ms post-stimulus were truncated when present.

Whisker movement analyses

Movies were parsed into regions of interest containing target or distractor whisker fields. Whisker motion energy (WME) within each region was calculated for each frame as the temporal derivative for each pixel of the mean gray value from the previous frame. Values per pixel were normalized (squared) and summed across pixels, providing a single WME value. WME data from the movies were aligned to target and distractor stimulus onset and averaged across trial type.

Statistical Analyses

For neurometric d' and choice probability d', statistical analyses were performed to determine whether each pixel value was significantly different than zero across sessions (one sample t-test). Data were spatially aligned across sessions as described above. Threshold for statistical significance was corrected for multiple comparisons using the Bonferroni correction [$0.05/(142 \times 170) = 2.1 \times 10^{-6}$ for a single imaging session and $0.05/(156 \times 194) = 1.7 \times 10^{-6}$ across aligned imaging

sessions]. For neurometric d' and seed correlation, we additionally conducted region of interest (ROI) analyses. For neurometric d', reduction in distractor encoding was calculated as: (target d' – distractor d') / target d', calculated separately for S1, wMC and ALM. Statistical analyses were performed to determine whether reduction in distractor encoding was significantly different than zero within each region across sessions (one sample t-test, significance threshold corrected for multiple comparisons 0.05/3 = 0.017). Additionally, comparison of reduction in distractor encoding between the three ROIs across sessions was conducted using ANOVA and post-hoc Tukey test. For seed correlation, comparison between the three ROIs across sessions and comparisons between different trial phases across sessions were conducted using ANOVA and post-hoc Tukey test. To quantify changes in whisker motion energy (WME), post-stimulus values (each frame) were compared to average pre-stimulus (1 s baseline) values. Comparisons were conducted using paired t-test for each post-stimulus window, with a p-value threshold of 0.01 for significance. Average data are reported as mean ± standard error of the mean.

Results

Training mice in a selective detection task

To study the neural mechanisms of sensory selection, we developed a Go/NoGo passive whisker detection task in head-fixed mice (Figure 2). In this task, target stimuli are rapid deflections of multiple whiskers in one whisker field and distractor stimuli are identical deflections in the opposite whisker field (Figure 2A). Throughout training we quantified task performance as the separation (d') between hit rate and false alarm rate (Figure 2C). We considered mice 'expert' once they achieved a discriminability d'>1 on three consecutive sessions. Average time to expert performance was 11 days in the full task (see Methods) (Figures 2D and 2E) (number of sessions to expert performance: 11.2 ± 0.9, n=43 mice). Performance measures for the imaging sessions used in subsequent analyses are shown in Figure 2F (n=39 sessions across n=5 mice, hit rate (%), 80.4 ± 2.2; false alarm rate, 13.6 ± 1.1; spontaneous lick rate, 8.1 ± 0.5; d' comparing hit vs false alarm rates, 2.0 ± 0.1).

Two key features of this task facilitate the study of sensory selection. First, target and distractor stimuli are presented to contralateral whisker fields. Given the highly lateralized somatosensory whisker representation, we expect the target-aligned and distractor-aligned processing streams to be well separated across hemispheres. Second, we imposed a short (200 ms) lockout period after stimulus onset and before the response window. Responding during the lockout is punished

with a time-out, and mice learn to withhold their licking responses through this period (e.g., Figure 2G). All analyses of stimulus selection are conducted within this lockout period, which is post-stimulus onset and pre-reward, thereby isolating the selection process from reward-associated behavior.

Propagation of cortical activity during task performance

We used widefield calcium imaging (GCaMP6s Ca^{2+} sensor) to monitor neural activity broadly across dorsal cortex during task performance. We used a combination of anatomic landmarks and functional mapping to identify various cortical regions (Figures 3A and 3B). Whisker deflection in anesthetized mice was used to localize the primary somatosensory barrel field (S1) and the whisker region of primary motor cortex (wMC) (n=13, example session shown in Figure 3B, left). Reward-triggered licking in water-restricted yet task naïve mice was used to localize anterior lateral motor cortex (ALM), which has recently been identified as a pre-motor licking-related region (T.-W. Chen et al., 2017; Guo et al., 2014) (n=6, example session shown in Figure 3B, right). Thus, our anatomic and functional mapping confirms that we can simultaneously monitor licking-related and whisker sensory and motor cortical regions bilaterally.

We imaged expert mice while they were performing the whisker detection task. Here, we show stimulus evoked cortical activity on target and distractor trials across all mice and all sessions (grand average: n=5 mice, n=39 sessions) (Figures 3C and 3D). The two sequential imaging frames both occurred within the

lockout period, which is after stimulus onset and before the earliest allowed response time. As expected, for both trial types we observed activity initiation in S1 contralateral to the deflected whisker field. By the end of the lockout period we observed strong S1 activity following both target and distractor stimuli. On target trials we observed propagation of activity to wMC, ALM, and retrosplenial cortex (RSP). Note that the activity does not spread uniformly from the site of initiation, but rather emerges in discrete cortical regions. In contrast, on distractor trials the activity was largely contained within S1, with only mild activation of wMC.

In Figure 4, we show the grand average fluorescence signals across all trial types and outcomes, aligned to both stimulus onset and response onset. Notice that during the response (post-response onset for hit, false alarm and spontaneous licking trials) we observed strong signals that are widespread throughout dorsal cortex. However, in this study we are most interested in the activity initiating, and therefore preceding, the response. On hit trials (Figure 4A), we observed the propagation of activity from S1 to frontal and parietal regions post-stimulus (aligned to stimulus) and pre-response (aligned to response). On correct rejection trials (Figure 4E), we also saw strong activity in S1, but with very little propagation to other cortical regions. Propagation is not simply delayed on these trials, as we can track the resolution of distractor-evoked activity into the response window.

The incorrect trial types also showed distinct activation patterns. On both false alarm trials (Figure 4B) and miss trials (Figure 4D), in addition to lateralized S1 responses, we also observed prominent bilateral activity in the somatosensory

limb regions. We interpret these neural signals as reflecting self-motion of the mouse. Prior studies have shown that during passive whisker detection tasks, self-motion (quantified by whisking behavior) reduces detection probability (Ollerenshaw et al., 2012). Thus, limb region activation observed here is consistent with self-motion contributing to incorrect, both miss and false alarm, trial outcomes. On spontaneous trials (responses not preceded by a whisker stimulus) we observed minimal pre-response cortical activity (Figure 4C).

Quantification of stimulus encoding and attenuation across cortex

The above analyses demonstrate, qualitatively, the differential propagation of cortical signals for target and distractor stimuli. Next, we sought to quantify these responses. To do this, we calculated the neurometric sensitivity index (d') (Britten et al., 1992) for each pixel in our imaging window (Figure 5). Across each session we compared the pre-stimulus activity (stimulus absent) to activity during the lockout period (stimulus present). Importantly, for this analysis we included all target trials and all distractor trials regardless of trial outcome (although excluding trials with responses during the lockout). We use d' rather than dF/F, as the former accounts for trial-by-trial variability and reflects the ability of an ideal observer to distinguish signal from noise on single trials. The d' maps from target and distractor stimuli largely match dF/F patterns described above; for target stimuli high d' values are observed in S1, wMC, ALM and RSP (Figure 5A, right) whereas for distractor stimuli, high d' values are only observed in S1 (Figure 5B, right). These regions show neurometric d' values significantly above zero (Figure 5C and 5D).

We do observe a focal increase in d' for distractor wMC (Figure 5B, right), but this does not reach statistical significance after correction for multiple comparisons (Figure 5D).

Next, we quantified the propagation of stimulus responses for target versus distractor stimuli. We describe this analysis first for S1. For each session, we determined the peak neurometric d' for the target stimulus in target-aligned S1 versus the peak neurometric d' for the distractor stimulus in distractor-aligned S1. We plotted these data in Figure 6A. Data along the unity line indicate equal neurometric d' values for target and distractor stimuli for that session. For S1, the data are widely distributed, yet with a nonsignificant trend towards larger responses for target stimuli (n=39 sessions, 8.8 ± 7.9% reduction in distractor d', one sample t-test, p=0.27, t(38)= 1.12) (Figure 6D). We repeated these analyses for wMC and ALM. For these regions we find that neurometric d' values are consistently larger for target stimuli (Figures 6B and 6C). Reduction in distractor d' is 61.0±7.1% in wMC (one sample t-test, $p=1.76e^{-10}$, t(38)= 8.62) and 72.1 ± 6.9 % in ALM (one sample t-test, $p=8.83e^{-13}$, t(38)= 10.49) (Figure 6D). Additionally, reduction in distractor encoding is greater for wMC and ALM compared to S1 (ANOVA, $p=7.97e^{-9}$, F(1,38) = 54.2, with post-hoc Tukey comparison). Overall, these data demonstrate robust attenuation of distractor responses between the mono-synaptically connected regions of S1 and wMC.

Analyses of intrinsic lateralization, trial history, electrical activity, whisker movements and choice probability

We performed a series of analyses to determine whether the neural activity described above reflects the selection process or can be accounted for by task or behavioral confounds. First, widespread cortical propagation in our task could reflect target selection or an intrinsic lateralization of cortical activity (e.g., left-sided whisker deflections always evoke more widespread cortical activation). To distinguish between these possibilities, two cohorts of mice were trained with opposite target-distractor assignments. In previous analyses we aligned all data with respect to target-distractor orientation. Here, we show behavioral performance (Figure 7A) and neural activity separately according to target assignment (Figure 7B target-aligned right hemisphere, n=3 mice and n=25 sessions; Figure 7C target-aligned left hemisphere, n=2 mice, n=14 sessions). Note that propagation from S1 to frontal and other parietal cortices occurs selectively on target trials, irrespective of the side of target assignment. Therefore, these differential patterns of cortical activation reflect learned adaptations to our task, rather than intrinsic lateralization.

In our task, most target trials followed a correct rejection and shortened inter-trial interval (80%), while a minority of target trials was not preceded by a correct rejection and followed a long inter-trial interval (20%). It is possible that the mice in our task implemented a strategy of using the distractor stimulus to orient attention to the target whisker field rather than solely attending the target stimulus.

To determine the likelihood of this strategy, we compared behavioral performance on target trials (Figure 7D) and hit-related neural activity (Figure 7E) separately according to the presence of a preceding correction rejection. The similar behavioral performance (hit rate, paired t-test, p=0.63, t(38)=-0.49; reaction time, paired t-test, p=0.77, t(38)=0.29) and neural activity suggest that the distractor stimulus was not utilized to enhance target detection.

Next, we sought to confirm our Ca^{2+} imaging findings with local field potential (LFP) recordings, which have much higher temporal resolution. We recorded LFP signals from layer 5 of S1, wMC and ALM, in target-aligned and distractor-aligned hemispheres (not simultaneously recorded). We compared target-evoked responses in target-aligned cortices (Figure 8 A-C) to distractor-evoked responses in distractor-aligned cortices (Figure 8 D-F). We find that early post-stimulus activity, likely reflecting the initial feedforward sensory sweep, is similar in target-aligned and distractor-aligned S1 and wMC (Figure 8 G, H; peak 1, occurring within 50 ms post-stimulus). Late activity does diverge in S1 and wMC between target and distractor recordings. In ALM, notably, the large post-stimulus activity in target recordings is nearly absent in distractor recordings. These LFP data support our Ca^{2+} imaging findings of minimal subcortical filtering of the sensory response followed by robust attenuation across cortex.

To further understand how neural activity relates to movements during the task, in four additional sessions we imaged whisker movements during task performance and analyzed task-aligned whisker motion energy. We present two

example sessions in Figure 9, in which we plot whisker motion energy for target and distractor whiskers aligned to target and distractor stimulus trials. We find that whisker movements increase on target trials in both target and distractor whiskers approximately 100 ms after stimulus onset (Figure 9 A, B, E, F) (latency, n=4; target whiskers: 100 +/- 10 ms; distractor whiskers: 129 +/- 4 ms). This increase in bilateral whisker movements is before the onset of licking (>200 ms, due to lockout window), and therefore appears to be part of a response motor sequence (Musall et al., 2019). Whisker motion energy on distractor trials remained at pre-stimulus levels or increased late in the trial (Figure 9G, H), for target and distractor whiskers. In comparing the onset of neural signals (LFP) to the onset of behavior (whisking and licking) we find that the cortical signals precede overt behavior. Our data are therefore consistent with activation of wMC and ALM triggering a whisking and licking response sequence.

We conducted additional analyses of the widefield imaging data to determine whether the observed propagation to frontal cortex for target stimuli is predictive of response initiation. The alternative hypothesis is that propagation reflects a learned stimulus association that may be independent of responding. To distinguish between these hypotheses, we calculated choice probability (Britten et al., 1996) for each pixel (Figure 10), comparing activity on hit trials (response present) versus miss trials (response absent). The average spatial map of target stimulus choice probability is shown in Figure 10A (left). This analysis revealed pixels with modest positive (increased on hit trials) and negative (increased on

miss trials) values of choice probability. However, none of the pixel values were significantly different than zero after correction for multiple comparisons (Figure 10A, right).

We reasoned that hit versus miss outcomes may depend on both the state of the mouse as well as the strength of the stimulus-evoked responses. In order to isolate the latter component, we recalculated choice probability based on the difference in activity between early and late lockout period activity (see Methods). With this method, we observed large and significant choice probability values in target-aligned wMC and bilateral ALM (Figure 10B). We also observed focal increases in choice probability in target-aligned S1 and RSP, but these regions did not reach statistical significance after correction for multiple comparisons (Figure 10B). Thus, cortical activation of frontal cortex on target trials is predictive of response initiation.

Quantification of functional connectivity across cortex

Finally, we sought to determine whether the differences in propagation for target versus distractor stimuli are reflected in the correlation patterns, or 'functional connectivity', between sensory and motor cortices. To do this, we created pixel-by-pixel correlation maps for S1, wMC, and ALM in target-aligned or distractor-aligned hemispheres as seed regions of interest (ROIs). We show the correlation maps for the full trial data, which include the pre-stimulus, peri-stimulus, and response windows for all stimulus trial types (Figures 11A-F). The most striking findings are

regional structure and symmetry. The spatial correlation patterns are highly similar for wMC and ALM seeds, which are quite different from S1 seeds (compare Figures 11A/D with 11B/E, C/F). This regional structure illustrates that the correlation values reflect local neural activity rather than global imaging artifacts. Regarding symmetry, for all three cortical regions, the target-aligned and distractor-aligned seed maps are qualitatively extremely similar (compare Figure 11A-C with 11D-F).

Despite these similarities, we do find significant differences in correlations between S1 and wMC (r^2, target 0.84±0.01, distractor 0.76±0.01, paired t-test, $p=2.9e^{-7}$, $t(38)=6.2$, $n=39$) and between S1 and ALM (r^2, target 0.80±0.01, distractor 0.68±0.02, paired t-test, $p=8.6e^{-10}$, $t(38)=8.1$, $n=39$). (Figure 11G). The largest differences in target-aligned and distractor-aligned correlations were between S1 and ALM (ANOVA, $p=1.6e^{-8}$, $F(2,37)=30.3$, with post-hoc Tukey comparison) (Figure 11G). To determine whether these differences are persistent or related to specific phases of the task, we ran the correlation analyses separately for the pre-stimulus, peri-stimulus, and response windows. We found that differences in correlations for target-aligned versus distractor-aligned S1 to wMC (Figure 11H) and S1 to ALM (Figure 11I) were significantly larger in the response phase compared to the pre-stimulus phase (ANOVA with post-hoc Tukey comparison, S1-wMC, p=0.0004; S1-ALM, p=0.0005). However, even in the pre-stimulus phase, there was a small yet significant increase in S1 to ALM correlation in target-aligned compared to distractor-aligned hemispheres (paired t-test, p=0.0018, t(38)=3.4) (Figure 11I). Overall, these data are inconsistent with large,

global changes in synaptic plasticity or functional connectivity driving task performance, but rather implicate more focal, possibly pathway-specific, adaptations.

Discussion

We developed a Go/NoGo selective detection task to study the neural processes of sensory selection in the mouse somatosensory whisker system. Mice learned to respond to target whisker deflections and ignore contralateral, distractor whisker deflections, achieving expert performance within 2 to 3 weeks of training (Figure 2). The main finding of this study is robust attenuation of distractor compared to target stimulus processing between mono-synaptically coupled cortical regions S1 and wMC (Figures 3-6). We interpret this observation as reflecting the presence of an intra-cortical attenuating filter, suppressing higher order processing of unattended stimuli (TREISMAN, 1964).

We note important differences between our study and previous studies of the neural correlates of sensory selection. In our task, target and distractor receptive fields were assigned at the onset of training and remained constant throughout the learning process. This contrasts with previous studies in primates, in which target and distractor assignments are cued each block or trial. Moreover, our target and distractor stimuli were always across hemispheres, rather than varying in proximity. Yet, despite differences in training, species, sensory modality, stimulus details, and recording technique, we do note remarkable similarities with previous studies. As in the primate visual system, we observe progressive

distractor suppression along the cortical hierarchy (Figure 6D) (Moran & Desimone, 1985; Tootell et al., 1998; Treue, 2001). Comparing modulation amplitudes between studies is problematic, because they vary widely depending on task and stimulus details. However, generally, within thalamus and primary visual cortex, attentional modulations of approximately 10% have been reported (McAlonan et al., 2008; Motter, 1993; Tootell et al., 1998), which is similar to the 8.8% average modulation we observed in primary somatosensory cortex. Within higher order sensory cortices, attentional modulations of 50 to 65% have been reported (Moran & Desimone, 1985; Tootell et al., 1998), which is similar to the 61.0% and 72.1% average modulations we observed in wMC and ALM, respectively.

What is the nature of distractor suppression? One possibility is that suppression is reactive, that once a distractor is detected, another brain region initiates an inhibitory brake to prevent further processing. This type of transient activation is observed, for example, in prefrontal cortex during stop-signal reaction time tasks at the detection of a 'stop' signal (Aron & Poldrack, 2006; Hanes et al., 1998). A second possibility is that suppression is proactive, already deployed in the initial conditions of the brain regions receiving the distractor stimulus. Insofar as we do not observe additional transient activations for distractor stimuli, our data support the second explanation of proactive suppression.

Given our localization of an attenuating filter between S1 and wMC, there are multiple possible mechanisms for implementing this filter. The most direct

mechanism would be bidirectional modulation of the S1-wMC intra-cortical projection pathway. Previous studies of whisker detection have identified increased sensory processing with learning in wMC and in specific S1-wMC projection neurons (J. L. Chen et al., 2015; Le Merre et al., 2018). Whether this pathway decreases in strength when aligned with a distractor has not been studied. However, such a finding of bidirectional modulation would provide strong evidence for involvement of this pathway in specific stimulus selection, rather than general task engagement. Additionally, regulated propagation between S1 and wMC may involve subcortical loops through the striatum (Alloway et al., 2006) or posterior medial thalamus (Kleinfeld et al., 1999), or cortical feedback projections from PFC to wMC or from wMC to S1 (Xu et al., 2012; Zagha et al., 2013). For example, wMC to S1 feedback may strengthen (target-aligned) or weaken (distractor-aligned) the reciprocal S1 to wMC feedforward pathway. Strengthening or weakening may occur through feedback targeting of excitatory, inhibitory or disinhibitory S1 neurons (Kinnischtzke et al., 2014; S. Lee et al., 2013; Petreanu et al., 2009; Rocco & Brumberg, 2007; Zagha et al., 2013). Our task provides an excellent platform for studying the plasticity and cellular/circuit contributions of each of these mechanisms towards target enhancement and/or distractor suppression. Alternatively, our findings are inconsistent with strong reductions in ascending sensory drives to distractor-aligned S1 (Figures 3-6 and 8) or large, global reductions in the structural or functional connectivity between distractor-aligned S1 and the rest of cortex (Figure 11).

While our study identifies a sensory filtering process distal to S1, other studies have identified sensory gating in S1 and earlier subcortical structures. Previous studies of the rodent whisker system have examined differences in sensory processing during periods of whisking versus non-whisking. In general, these studies find reductions in sensory responses during whisking (Chakrabarti & Schwarz, 2018; Crochet & Petersen, 2006; Fanselow & Nicolelis, 1999; Ferezou et al., 2007; S. Lee et al., 2008), which is already present in the first sensory brainstem relay (Chakrabarti & Schwarz, 2018). This sensory gating process is likely mediated by both top-down cortical (Chakrabarti et al., 2008; S. Lee et al., 2008) and neuromodulatory (Eggermann et al., 2014) inputs. Thus, modulations of sensory processing may occur all along the ascending sensory pathway, including brainstem, thalamus and cortex. Why different behavioral contexts engage different mechanisms of sensory gating is currently unknown.

Finally, we currently do not know how wMC contributes to the sensory selection process. This cortical region has been studied extensively with respect to whisking, specifically in establishing its set-point, initiation, and amplitude modulation (Carvell et al., 1996; Hill et al., 2011). Consistent with this, we find that wMC activation on target trials correlates with bilateral increases in whisking (Figure 9). Alternatively, more recent studies have demonstrated roles for this same region in orienting behaviors and action suppression (Ebbesen et al., 2017; Pai et al., 2011; Zagha et al., 2015). Our study demonstrates, at the representational level, a possible additional function of regulating the propagation

of sensory processing for sensory selection. And yet, wMC is only one of the many routes by which a whisker stimulus can initiate a motor output (Kleinfeld et al., 1999). Defining how wMC contributes to sensory-motor processing in this task and in other behavioral contexts will be a major focus of future investigations.

References

Alloway, K. D., Lou, L., Nwabueze-Ogbo, F., & Chakrabarti, S. (2006). Topography of cortical projections to the dorsolateral neostriatum in rats: Multiple overlapping sensorimotor pathways. *Journal of Comparative Neurology*, *499*(1), 33–48. https://doi.org/https://doi.org/10.1002/cne.21039

Aron, A. R., & Poldrack, R. A. (2006). Cortical and Subcortical Contributions to Stop Signal Response Inhibition: Role of the Subthalamic Nucleus. *The Journal of Neuroscience*, *26*(9), 2424 LP – 2433. https://doi.org/10.1523/JNEUROSCI.4682-05.2006

Britten, K. H., Newsome, W. T., Shadlen, M. N., Celebrini, S., & Movshon, J. A. (1996). A relationship between behavioral choice and the visual responses of neurons in macaque MT. *Visual Neuroscience*, *13*(1), 87–100. https://doi.org/10.1017/s095252380000715x

Britten, K. H., Shadlen, M. N., Newsome, W. T., & Movshon, J. A. (1992). The analysis of visual motion: a comparison of neuronal and psychophysical performance. *The Journal of Neuroscience*, *12*(12), 4745 LP – 4765. https://doi.org/10.1523/JNEUROSCI.12-12-04745.1992

Carvell, G. E., Miller, S. A., & Simons, D. J. (1996). The relationship of vibrissal motor cortex unit activity to whisking in the awake rat. *Somatosensory & Motor Research*, *13*(2), 115–127. https://doi.org/10.3109/08990229609051399

Chakrabarti, S., & Schwarz, C. (2018). Cortical modulation of sensory flow during active touch in the rat whisker system. *Nature Communications*, *9*(1), 3907. https://doi.org/10.1038/s41467-018-06200-6

Chakrabarti, S., Zhang, M., & Alloway, K. D. (2008). MI neuronal responses to peripheral whisker stimulation: relationship to neuronal activity in si barrels and septa. *Journal of Neurophysiology*, *100*(1), 50–63. https://doi.org/10.1152/jn.90327.2008

Chen, J. L., Margolis, D. J., Stankov, A., Sumanovski, L. T., Schneider, B. L., & Helmchen, F. (2015). Pathway-specific reorganization of projection neurons in somatosensory cortex during learning. *Nature Neuroscience*, *18*(8), 1101–1108. https://doi.org/10.1038/nn.4046

Chen, T.-W., Li, N., Daie, K., & Svoboda, K. (2017). A Map of Anticipatory Activity in Mouse Motor Cortex. *Neuron*, *94*(4), 866-879.e4. https://doi.org/10.1016/j.neuron.2017.05.005

Chen, T.-W., Wardill, T. J., Sun, Y., Pulver, S. R., Renninger, S. L., Baohan, A., Schreiter, E. R., Kerr, R. A., Orger, M. B., Jayaraman, V., Looger, L. L., Svoboda, K., & Kim, D. S. (2013). Ultrasensitive fluorescent proteins for imaging neuronal activity. *Nature*, *499*(7458), 295–300. https://doi.org/10.1038/nature12354

Crick, F. (1984). Function of the thalamic reticular complex: the searchlight hypothesis. *Proceedings of the National Academy of Sciences of the United States of America*, *81*(14), 4586–4590. https://doi.org/10.1073/pnas.81.14.4586

Crochet, S., & Petersen, C. C. H. (2006). Correlating whisker behavior with membrane potential in barrel cortex of awake mice. *Nature Neuroscience*, *9*(5), 608–610. https://doi.org/10.1038/nn1690

Ebbesen, C. L., Doron, G., Lenschow, C., & Brecht, M. (2017). Vibrissa motor cortex activity suppresses contralateral whisking behavior. *Nature Neuroscience*, *20*(1), 82–89. https://doi.org/10.1038/nn.4437

Eggermann, E., Kremer, Y., Crochet, S., & Petersen, C. C. H. (2014). Cholinergic signals in mouse barrel cortex during active whisker sensing. *Cell Reports*, *9*(5), 1654–1660. https://doi.org/10.1016/j.celrep.2014.11.005

Fanselow, E. E., & Nicolelis, M. A. L. (1999). Behavioral Modulation of Tactile Responses in the Rat Somatosensory System. *The Journal of Neuroscience*, *19*(17), 7603 LP – 7616. https://doi.org/10.1523/JNEUROSCI.19-17-07603.1999

Farkas, T., Kis, Z., Toldi, J., & Wolff, J. R. (1999). Activation of the primary motor cortex by somatosensory stimulation in adult rats is mediated mainly by associational connections from the somatosensory cortex. *Neuroscience*, *90*(2), 353–361. https://doi.org/10.1016/s0306-4522(98)00451-5

Ferezou, I., Haiss, F., Gentet, L. J., Aronoff, R., Weber, B., & Petersen, C. C. H. (2007). Spatiotemporal Dynamics of Cortical Sensorimotor Integration in Behaving Mice. *Neuron*, *56*(5), 907–923. https://doi.org/10.1016/j.neuron.2007.10.007

Guo, Z. V, Li, N., Huber, D., Ophir, E., Gutnisky, D., Ting, J. T., Feng, G., & Svoboda, K. (2014). Flow of cortical activity underlying a tactile decision in mice. *Neuron*, *81*(1), 179–194. https://doi.org/10.1016/j.neuron.2013.10.020

Hanes, D. P., Patterson, W. F. 2nd, & Schall, J. D. (1998). Role of frontal eye fields in countermanding saccades: visual, movement, and fixation activity. *Journal of Neurophysiology*, *79*(2), 817–834. https://doi.org/10.1152/jn.1998.79.2.817

Hill, D. N., Curtis, J. C., Moore, J. D., & Kleinfeld, D. (2011). Primary motor cortex reports efferent control of vibrissa motion on multiple timescales. *Neuron*, *72*(2), 344–356. https://doi.org/10.1016/j.neuron.2011.09.020

Kinnischtzke, A. K., Simons, D. J., & Fanselow, E. E. (2014). Motor cortex broadly engages excitatory and inhibitory neurons in somatosensory barrel cortex. *Cerebral Cortex (New York, N.Y. : 1991)*, *24*(8), 2237–2248. https://doi.org/10.1093/cercor/bht085

Kleinfeld, D., Berg, R. W., & O'Connor, S. M. (1999). Anatomical loops and their electrical dynamics in relation to whisking by rat. *Somatosensory & Motor Research*, *16*(2), 69–88. https://doi.org/10.1080/08990229970528

Kleinfeld, D., Sachdev, R. N. S., Merchant, L. M., Jarvis, M. R., & Ebner, F. F. (2002). Adaptive filtering of vibrissa input in motor cortex of rat. *Neuron*, *34*(6), 1021–1034. https://doi.org/10.1016/s0896-6273(02)00732-8

Le Merre, P., Esmaeili, V., Charrière, E., Galan, K., Salin, P.-A., Petersen, C. C. H., & Crochet, S. (2018). Reward-Based Learning Drives Rapid Sensory Signals in Medial Prefrontal Cortex and Dorsal Hippocampus Necessary for Goal-Directed Behavior. *Neuron*, *97*(1), 83-91.e5. https://doi.org/10.1016/j.neuron.2017.11.031

Lee, S., Carvell, G. E., & Simons, D. J. (2008). Motor modulation of afferent somatosensory circuits. *Nature Neuroscience*, *11*(12), 1430–1438. https://doi.org/10.1038/nn.2227

Lee, S., Kruglikov, I., Huang, Z. J., Fishell, G., & Rudy, B. (2013). A disinhibitory circuit mediates motor integration in the somatosensory cortex. *Nature Neuroscience*, *16*(11), 1662–1670. https://doi.org/10.1038/nn.3544

Madisen, L., Garner, A. R., Shimaoka, D., Chuong, A. S., Klapoetke, N. C., Li, L., van der Bourg, A., Niino, Y., Egolf, L., Monetti, C., Gu, H., Mills, M., Cheng, A., Tasic, B., Nguyen, T. N., Sunkin, S. M., Benucci, A., Nagy, A., Miyawaki, A., … Zeng, H. (2015). Transgenic mice for intersectional targeting of neural sensors and effectors with high specificity and performance. *Neuron*, *85*(5), 942–958. https://doi.org/10.1016/j.neuron.2015.02.022

Mante, V., Sussillo, D., Shenoy, K. V., & Newsome, W. T. (2013). Context-dependent computation by recurrent dynamics in prefrontal cortex. *Nature*, *503*(7474), 78–84. https://doi.org/10.1038/nature12742

Mao, T., Kusefoglu, D., Hooks, B. M., Huber, D., Petreanu, L., & Svoboda, K. (2011). Long-range neuronal circuits underlying the interaction between sensory

and motor cortex. *Neuron*, *72*(1), 111–123. https://doi.org/10.1016/j.neuron.2011.07.029

McAlonan, K., Cavanaugh, J., & Wurtz, R. H. (2008). Guarding the gateway to cortex with attention in visual thalamus. *Nature*, *456*(7220), 391–394. https://doi.org/10.1038/nature07382

Miller, E. K., & Cohen, J. D. (2001). An integrative theory of prefrontal cortex function. *Annual Review of Neuroscience*, *24*(February 2001), 167–202. https://doi.org/10.1146/annurev.neuro.24.1.167

Miyashita, E., Keller, A., & Asanuma, H. (1994). Input-output organization of the rat vibrissal motor cortex. *Experimental Brain Research*, *99*(2), 223–232. https://doi.org/10.1007/BF00239589

Moran, J., & Desimone, R. (1985). Selective attention gates visual processing in the extrastriate cortex. *Science (New York, N.Y.)*, *229*(4715), 782–784. https://doi.org/10.1126/science.4023713

Motter, B. C. (1993). Focal attention produces spatially selective processing in visual cortical areas V1, V2, and V4 in the presence of competing stimuli. *Journal of Neurophysiology*, *70*(3), 909–919. https://doi.org/10.1152/jn.1993.70.3.909

Musall, S., Kaufman, M. T., Juavinett, A. L., Gluf, S., & Churchland, A. K. (2019). Single-trial neural dynamics are dominated by richly varied movements. *Nature Neuroscience*, *22*(10), 1677–1686. https://doi.org/10.1038/s41593-019-0502-4

Noudoost, B., & Moore, T. (2011). The role of neuromodulators in selective attention. *Trends in Cognitive Sciences*, *15*(12), 585–591. https://doi.org/10.1016/j.tics.2011.10.006

Ollerenshaw, D. R., Bari, B. A., Millard, D. C., Orr, L. E., Wang, Q., & Stanley, G. B. (2012). Detection of tactile inputs in the rat vibrissa pathway. *Journal of Neurophysiology*, *108*(2), 479–490. https://doi.org/10.1152/jn.00004.2012

Pai, S., Erlich, J., Kopec, C., & Brody, C. (2011). Minimal Impairment in a Rat Model of Duration Discrimination Following Excitotoxic Lesions of Primary Auditory and Prefrontal Cortices. *Frontiers in Systems Neuroscience*, *5*. https://doi.org/10.3389/fnsys.2011.00074

Petersen, C. C. H. (2019). Sensorimotor processing in the rodent barrel cortex. *Nature Reviews Neuroscience*, *20*(9), 533–546. https://doi.org/10.1038/s41583-019-0200-y

Petreanu, L., Mao, T., Sternson, S. M., & Svoboda, K. (2009). The subcellular organization of neocortical excitatory connections. *Nature*, *457*(7233), 1142–1145. https://doi.org/10.1038/nature07709

Porter, L. L., & White, E. L. (1983). Afferent and efferent pathways of the vibrissal region of primary motor cortex in the mouse. *The Journal of Comparative Neurology*, *214*(3), 279–289. https://doi.org/10.1002/cne.902140306

Rocco, M. M., & Brumberg, J. C. (2007). The sensorimotor slice. *Journal of Neuroscience Methods*, *162*(1–2), 139–147. https://doi.org/10.1016/j.jneumeth.2007.01.002

Rodenkirch, C., Liu, Y., Schriver, B. J., & Wang, Q. (2019). Locus coeruleus activation enhances thalamic feature selectivity via norepinephrine regulation of intrathalamic circuit dynamics. *Nature Neuroscience*, *22*(1), 120–133. https://doi.org/10.1038/s41593-018-0283-1

Sridharan, D., Schwarz, J. S., & Knudsen, E. I. (2014). Selective attention in birds. *Current Biology : CB*, *24*(11), R510-3. https://doi.org/10.1016/j.cub.2013.12.046

Tootell, R. B., Hadjikhani, N., Hall, E. K., Marrett, S., Vanduffel, W., Vaughan, J. T., & Dale, A. M. (1998). The retinotopy of visual spatial attention. *Neuron*, *21*(6), 1409–1422. https://doi.org/10.1016/s0896-6273(00)80659-5

TREISMAN, A. M. (1964). SELECTIVE ATTENTION IN MAN. *British Medical Bulletin*, *20*, 12–16. https://doi.org/10.1093/oxfordjournals.bmb.a070274

Treue, S. (2001). Neural correlates of attention in primate visual cortex. *Trends in Neurosciences*, *24*(5), 295–300. https://doi.org/10.1016/s0166-2236(00)01814-2

Wekselblatt, J. B., Flister, E. D., Piscopo, D. M., & Niell, C. M. (2016). Large-scale imaging of cortical dynamics during sensory perception and behavior. *Journal of Neurophysiology*, *115*(6), 2852–2866. https://doi.org/10.1152/jn.01056.2015

Wiederman, S. D., & O'Carroll, D. C. (2013). Selective Attention in an Insect Visual Neuron. *Current Biology*, *23*(2), 156–161. https://doi.org/https://doi.org/10.1016/j.cub.2012.11.048

Xu, N., Harnett, M. T., Williams, S. R., Huber, D., O'Connor, D. H., Svoboda, K., & Magee, J. C. (2012). Nonlinear dendritic integration of sensory and motor input during an active sensing task. *Nature*, *492*(7428), 247–251. https://doi.org/10.1038/nature11601

Zagha, E., Casale, A. E., Sachdev, R. N. S., McGinley, M. J., & McCormick, D. A. (2013). Motor cortex feedback influences sensory processing by modulating network state. *Neuron*, *79*(3), 567–578. https://doi.org/10.1016/j.neuron.2013.06.008

Zagha, E., Ge, X., & McCormick, D. A. (2015). Competing Neural Ensembles in Motor Cortex Gate Goal-Directed Motor Output. *Neuron*, *88*(3), 565–577. https://doi.org/10.1016/j.neuron.2015.09.044

Figures and Legends

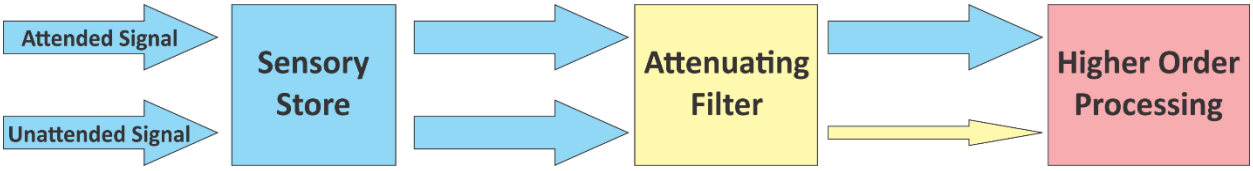

Figure 1: Treisman Attenuation Model

This model of selective attention proposes that both attended and unattended signals enter an early sensory store. At some point in the processing stream, however, an attenuating filter suppresses unattended signals while allowing attended signals to propagate forward for higher order processing.

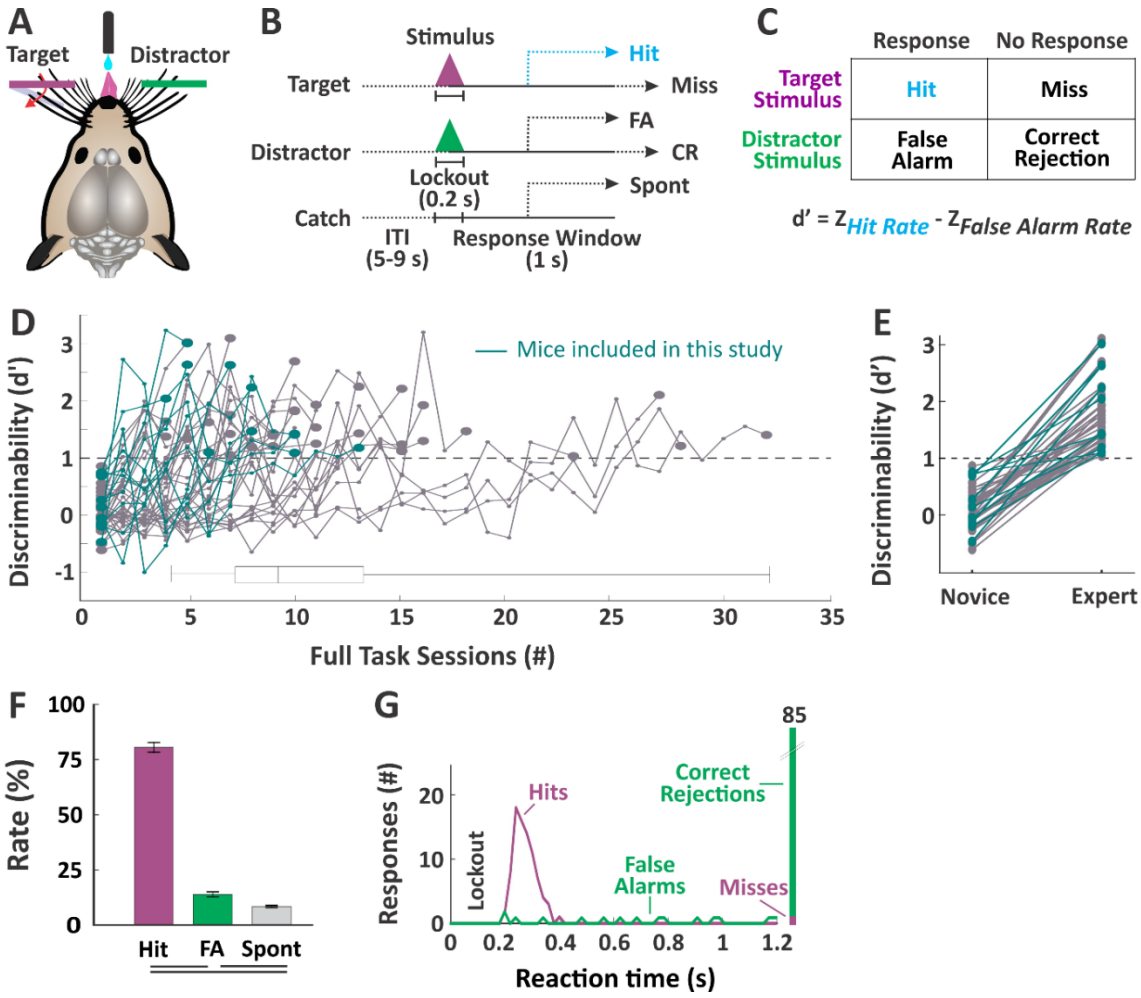

Figure 2: Behavior Paradigm and Measures of Selective Detection
(A) Illustration of the behavioral setup. Mice are head-fixed in the behavioral rig with piezo-controlled paddles within their whisker fields bilaterally. Each paddle is assigned as target (purple) or distractor (green) at the start of training. Mice report stimulus detection and receive rewards from a central lickport. **(B)** Task structure. Each trial consists of an inter-trial interval, a stimulus and 200ms lockout, and a 1 s response window. Trial type as determined by the stimulus could be target, distractor or catch (no stimulus). **(C)** Calculation of discriminability d', as the separation between hit rate and false alarm rate. **(D)** Performance trajectories for all mice (n=43 mice) and box and whiskers summary plot. Those used for imaging studies (n=5 mice) are indicated in blue. Mice were considered expert once they achieved a d'>1 for three consecutive days. **(E)** Comparison of d' for novice mice (first day of training on impulse control) and expert mice (n=43 mice, paired sample t-test, $p=3.7e^{-20}$, $t(42)=16.71$). **(F)** Performance measures for the imaging sessions (n=39 sessions). Lines below plot denote statistical significance. **(G)** Example session data showing reaction time distributions for target and distractor trials.

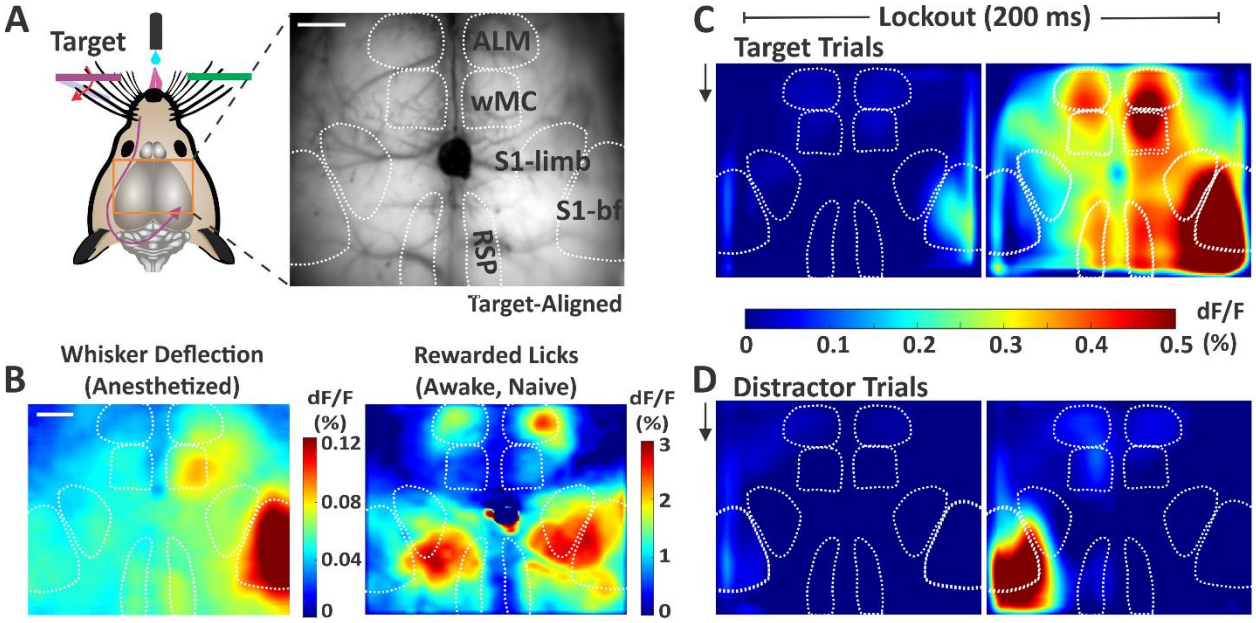

Figure 3: Sensory and Motor Cortical Representations Using Widefield Ca^{2+} Imaging

(A) Illustration of the imaging setup (left) and example frame from the through-skull GCaMP6s imaging (right). Surface vessels appear as dark striations overlaying the brain parenchyma. Bregma is indicated by the central ink blot. ALM, anterior lateral motor cortex; wMC, whisker region of primary motor cortex; S1, primary somatosensory cortex; bf, barrel field; RSP, retrosplenial cortex. **(B)** Cortical activity (dF/F) following whisker deflections in an anesthetized mouse (left), to localize of the sensory and motor whisker representations. Cortical activity following reward-triggered licking in a naïve mouse (right), to localize licking-related activity. **(C)** Cortical activity on target trials during the two sequential imaging frames of the lockout period in expert mice performing the detection task (grand average, n=39 sessions). Black arrow indicates whisker stimulus onset, which is coincident with the start of the first imaging frame. **(D)** Same as [C], but for distractor trials. Note the differential propagation of cortical activity depending on trial type. Scale bars in [A] and [B] are 1mm.

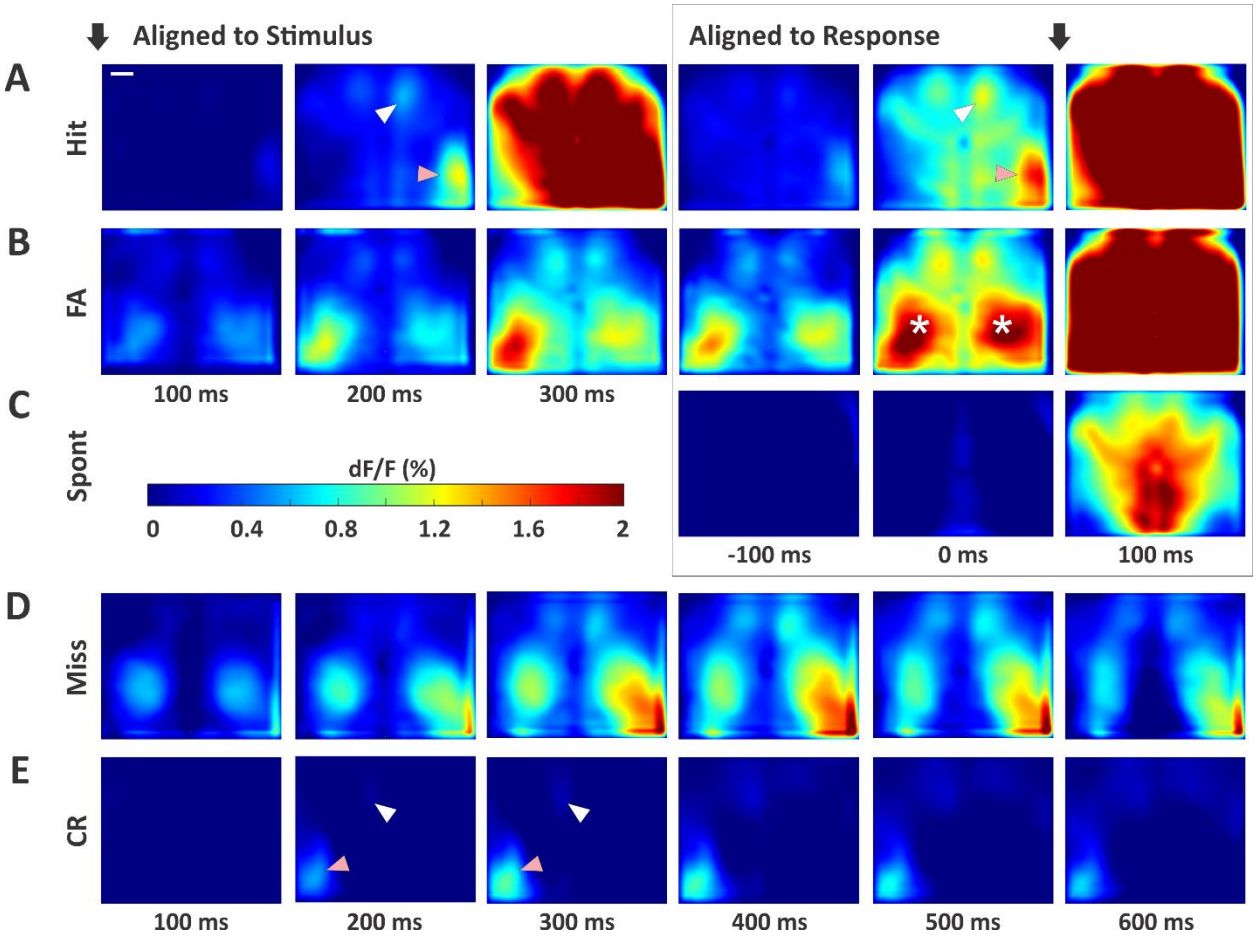

Figure 4: Cortical Activity Patterns Across All Trial Types
(A) Hit trials. Black arrows indicate alignment to stimulus onset (left three panels) or response onset (right three panels). The third frame aligned to stimulus (300 ms) is the first frame after the lockout and within the response window. Note the strong activity in contralateral S1 (pink arrows) with propagation to wMC (white arrows) and ALM, prior to response generation. **(B)** False alarm trials, with the same plot structure as in [A]. Asterisks mark elevated activity in the S1-limb regions, bilaterally. **(C)** Spontaneous trials (no stimulus alignment). **(D)** Miss trials. As there is no response on these trial types, we plot an extended series of post-stimulus activity. **(E)** Correct rejection trials, with the same plot structure as in [D]. Note the strong activity in S1 (pink arrow), yet lack of propagation to wMC (white arrow) and ALM. Scale bar in [A] is 1 mm.

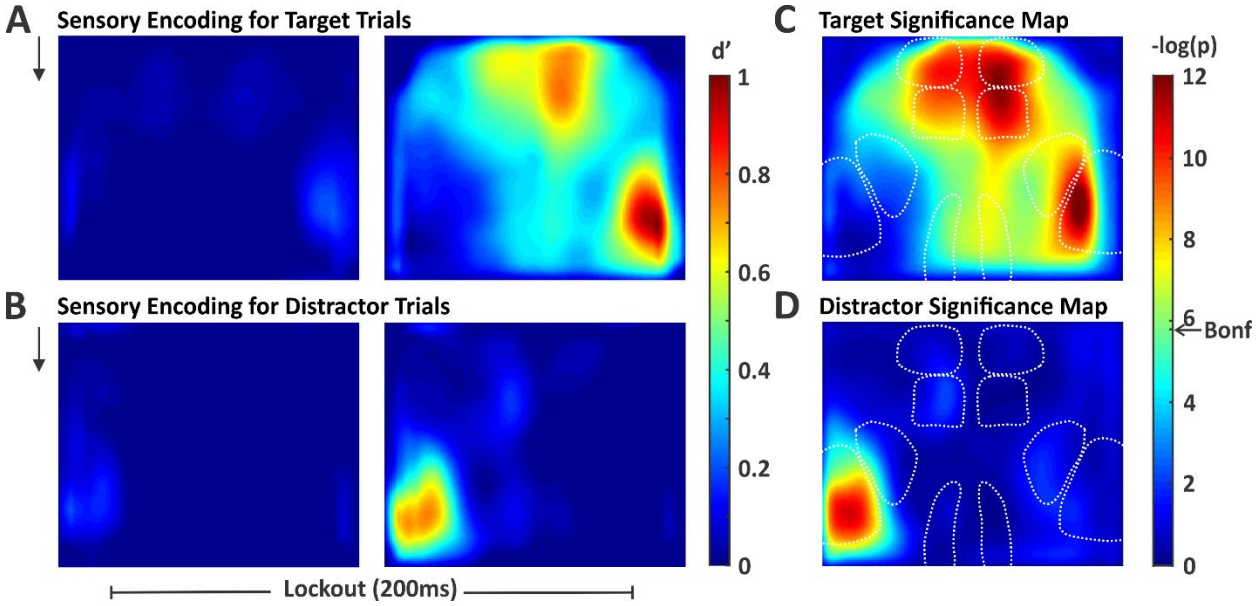

Figure 5: Spatial Maps of Stimulus Encoding
We quantified stimulus encoding as the separation between stimulus absent and stimulus present d', computed pixel-by-pixel. **(A)** Map of target stimulus encoding during the two sequential frames of the lockout period (black arrow represents stimulus onset). **(B)** Map of distractor stimulus encoding during the same time windows as in [A]. **(C)** and **(D)** Significance maps of the right panels of [A] and [B], respectively. Significance threshold determined by the Bonferroni correction for multiple comparisons is indicated by the arrow on the color bar (Bonf). Pixels with smaller p-values (warmer colors) have d' values significantly above 0. For target stimuli, we observed widespread stimulus encoding including in multiple frontal and parietal regions. For distractor stimuli, significant stimulus encoding is restricted to S1.

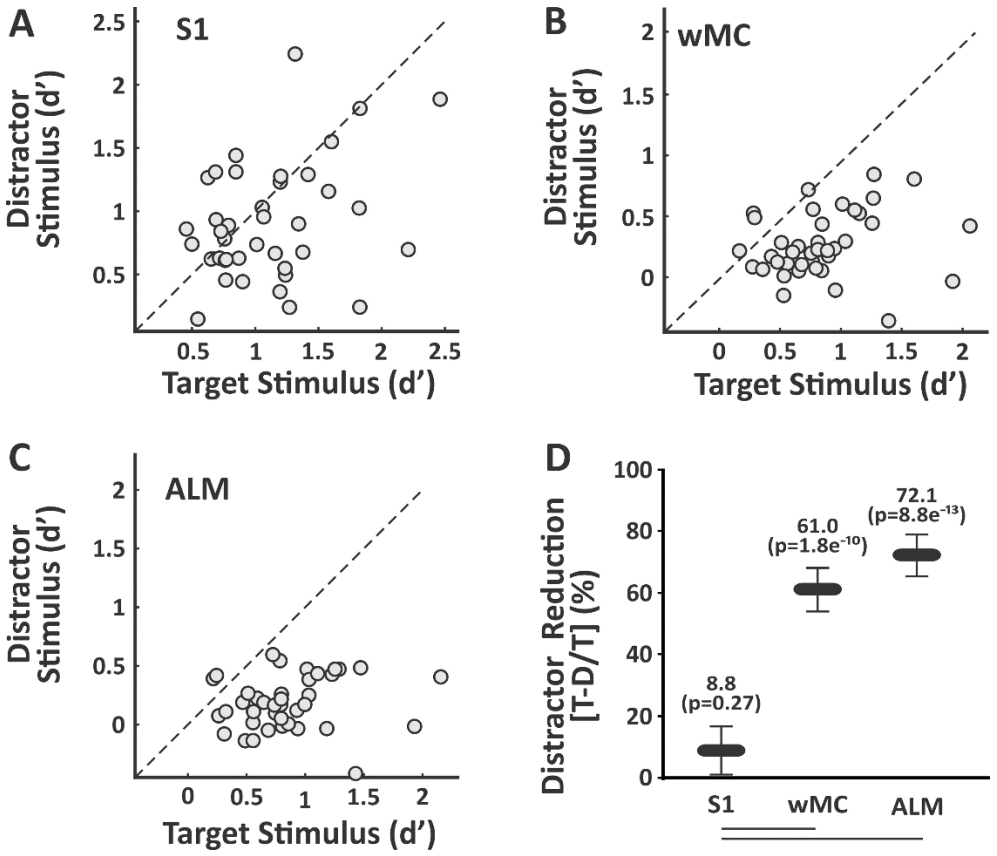

Figure 6: Quantification of Target vs Distractor Stimulus Propagation within Cortex

For each session, we compared target stimulus encoding in target-aligned cortices to distractor stimulus encoding in distractor-aligned cortex. **(A-C)** Scatter plots of target versus distractor encoding in S1 **(A)**, wMC **(B)** and ALM **(C)**. Each data point is one session (n=39 sessions). Note that the data are broadly distributed in S1, and highly biased towards stronger target encoding in wMC and ALM. **(D)** Summary data, comparing reductions in distractor encoding within each region (values above each data point) and between regions (lines below graph denote statistical significance). Reductions in distractor encoding are significantly larger in wMC and ALM compared to S1.

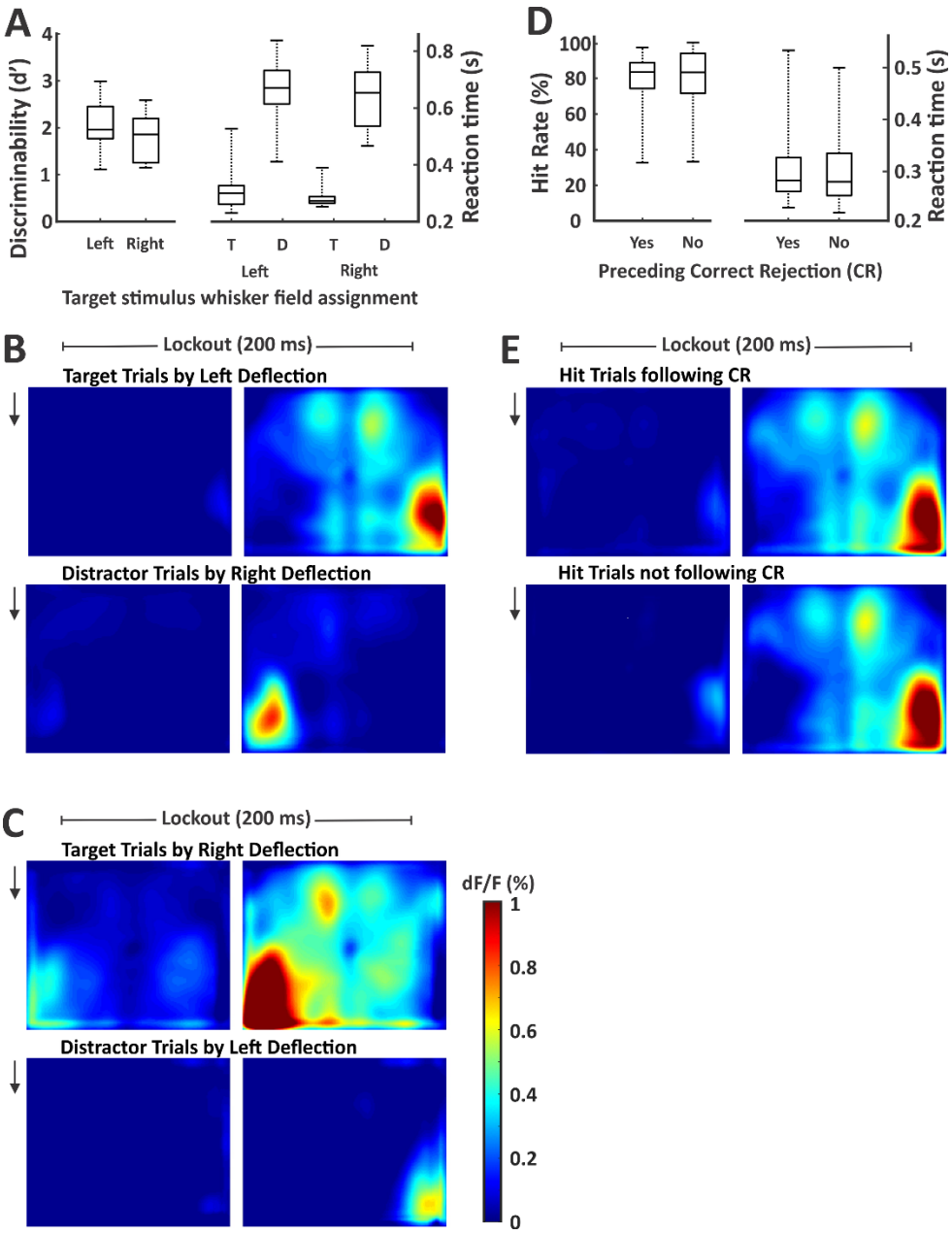
A
Discriminability (d')
Reaction time (s)
Left
Right
T
D
T
D
Left
Right
Target stimulus whisker field assignment
D
Hit Rate (%)
Reaction time (s)
Yes
No
Yes
No
Preceding Correct Rejection (CR)
B
Lockout (200 ms)
Target Trials by Left Deflection
Distractor Trials by Right Deflection
E
Lockout (200 ms)
Hit Trials following CR
Hit Trials not following CR
C
Lockout (200 ms)
Target Trials by Right Deflection
Distractor Trials by Left Deflection
dF/F (%)

Figure 7: Similar behavior and neural activity across target assignments and trial structures

(A) Discriminability d' and reaction times reported (box and whisker plots) separately for mice with left or right target whisker field assignment. None of the behavioral measures were significantly different between these two populations. **(B)** Cortical activity during the lockout period for target trials (top) and distractor trials (bottom) for sessions in which the target was assigned to the left whisker field (represented by the right cortical hemisphere) (n = 3 mice, n = 25 sessions). **(C)** Same as [B], but for sessions in which the target was assigned to the right whisker field (represented by the left cortical hemisphere) (n = 2 mice, n = 14 sessions). Signal propagation to frontal cortex correlated with target assignment. **(D)** Hit rates and reaction times reported (box and whisker plots) separately for target trials with and without a preceding correct rejection. None of the behavioral measures were significantly different between these two trial structures. **(E)** Cortical activity during the lockout period for hit trials following a correct rejection (top) and hit trials not following a correct rejection (bottom) (n=39 sessions for both).

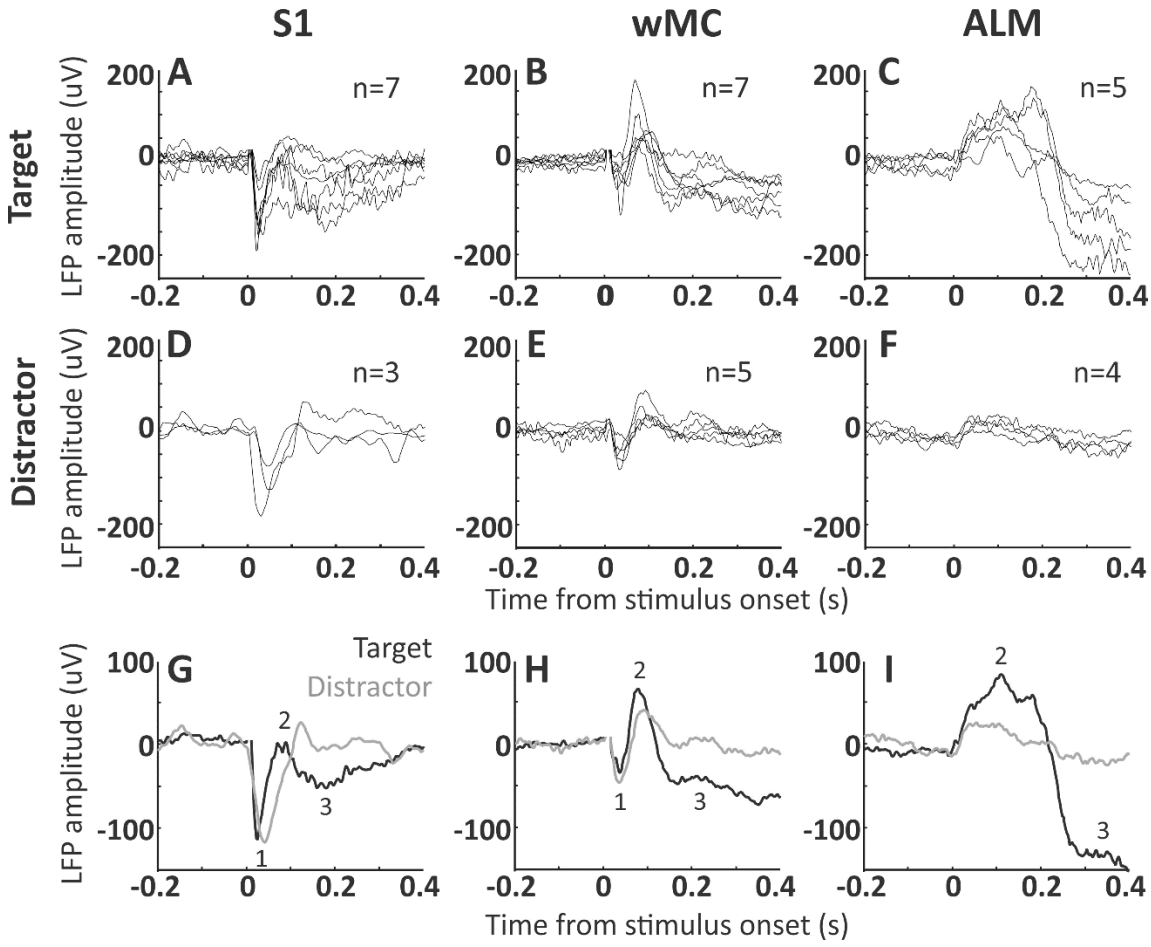

Figure 8: LFP signal transformation across S1, wMC and ALM

LFP signals were recorded from layer 5 of S1, wMC and ALM. (A-F) Each trace reflects average LFP signals from one session, across all target trials in target-aligned cortices (A-C) and across all distractor trials in distractor-aligned cortices (D-F). The count in each panel refers to the number of recorded sessions included. (G-I) Target-aligned (black) and distractor-aligned (grey) LFP signals, averaged across sessions. We observed three distinct event-related potentials, two negative-going (1 and 3) and one positive-going (2). Event 1, which is large in S1, small in wMC and absent in ALM, likely reflects the initial feedforward sensory sweep. This event is similar in target and distractor recordings. Event 3, which is large in ALM and moderate in wMC and S1, is highly dissimilar between target and distractor recordings.

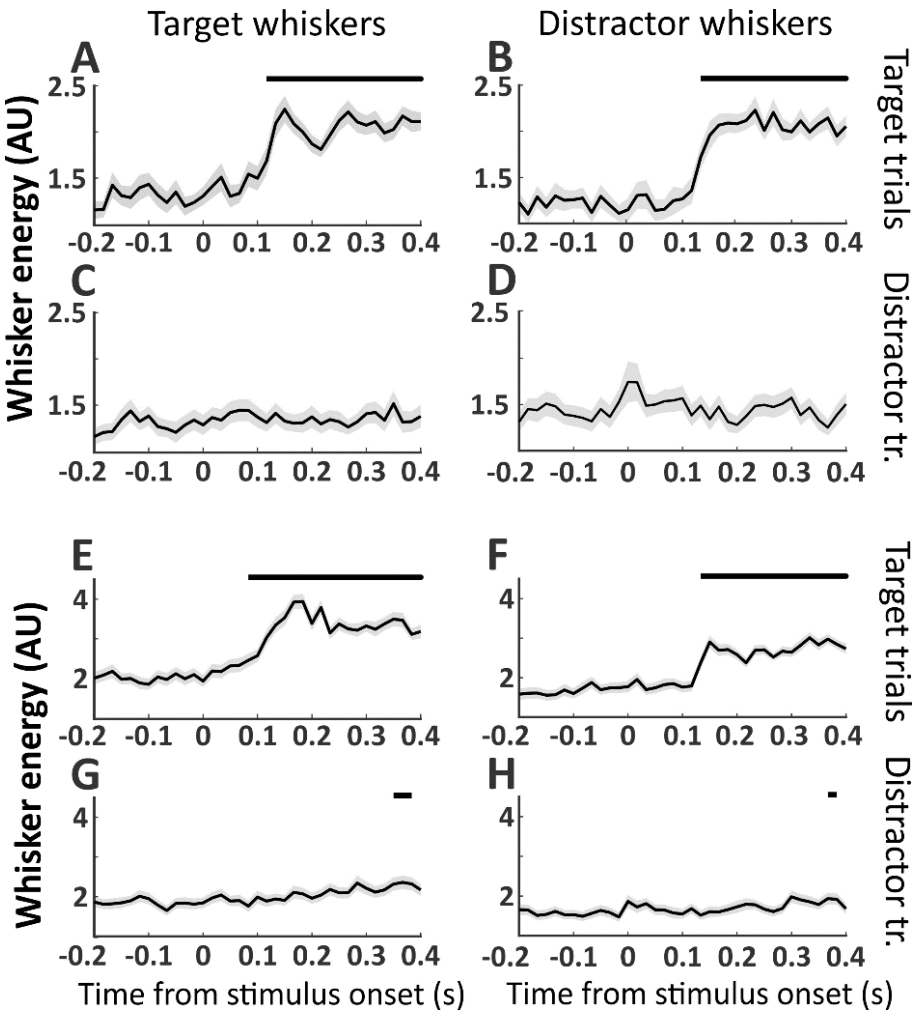

Figure 9: Bilateral whisker movements on target trials

Whisker movement energy was calculated from target or distractor whisker fields and plotted separately for target and distractor trials. Significant changes in post-stimulus compared to pre-stimulus whisker movements are indicated as black bars above each plot. Two example sessions are shown, session 1 (A-D) and session 2 (E-H). (A, E) Target whisker energy on target trials; (B, F) distractor whisker energy on target trials; (C, G) target whisker energy on distractor trials; (D, H) distractor whisker energy on distractor trials. Significant increases in whisker movements occurred for both target and distractor whiskers approximately 0.1 seconds after target stimulus onset (A, B, E, F). Target and distractor whisker movements to distractor stimuli were either non-significant throughout the trial (C, D) or delayed (G, H).

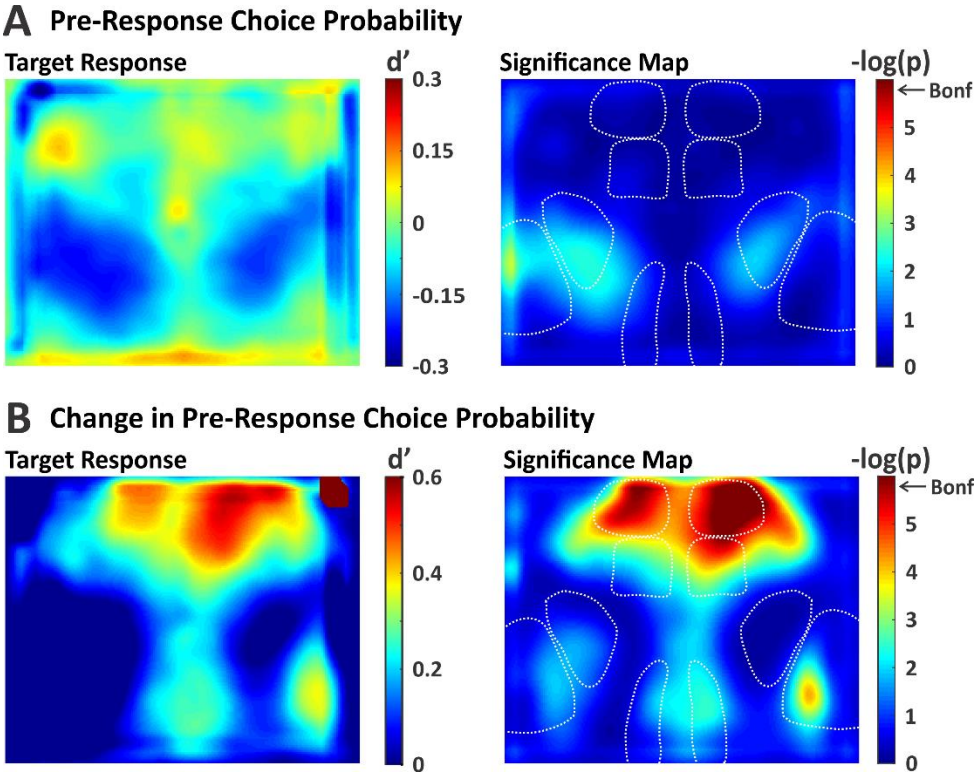

Figure 10: Spatial Maps of Choice Probability
We quantified choice probability as the separation between response absent and response present d', computed pixel-by-pixel. **(A)** Choice probability map (left) and significance map (right) during the last frame of the lockout period. None of the pixels reached significance after correcting for multiple comparisons (Bonferonni). **(B)** Same as in [A], except with choice probability computed on the difference in activity between the two lockout frames. With this approach, significant choice probability was observed in target-aligned wMC and bilateral ALM.

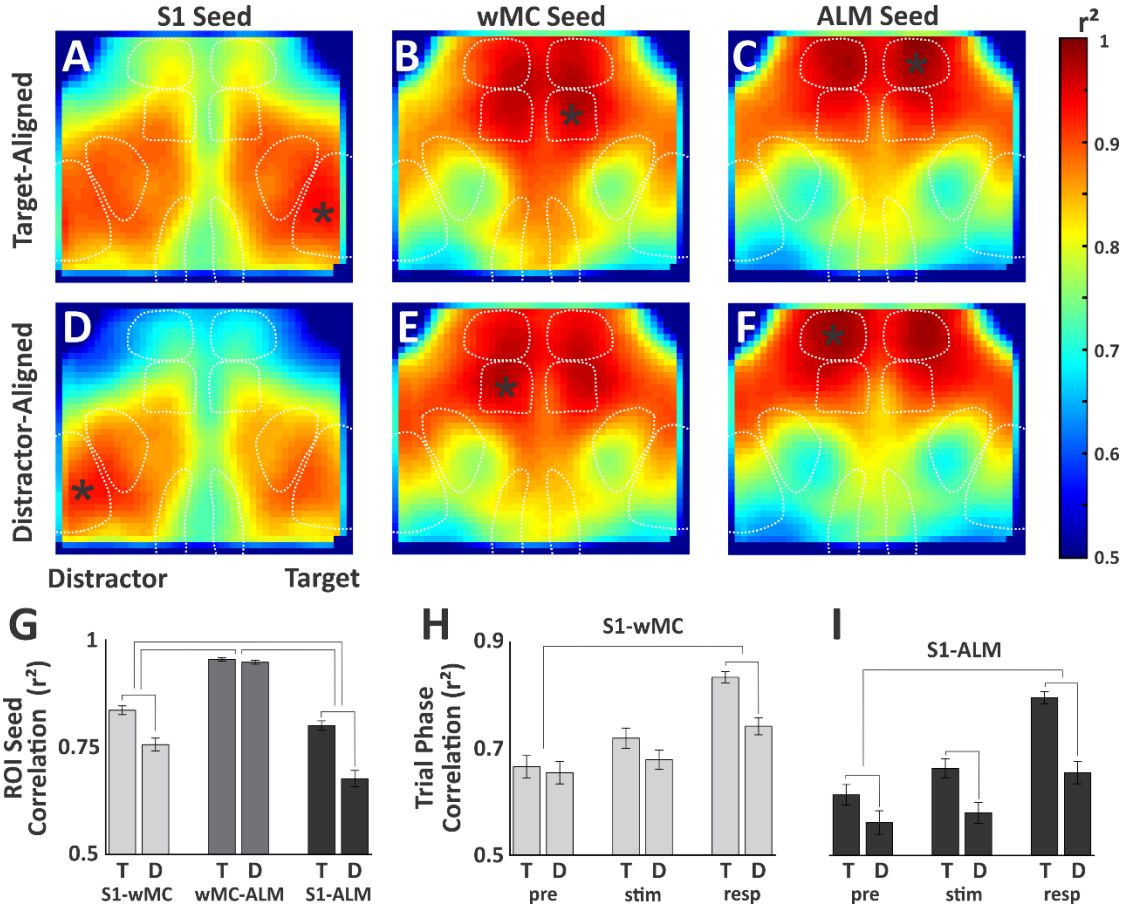

Figure 11: Spatial Correlation Analysis
(A-F) Correlation maps for full trial data. Seed regions of interest (marked by asterisk) included S1, wMC and ALM, in target-aligned **(A-C)** and distractor-aligned **(D-F)** cortices. **(G)** Summary data of average pairwise correlation values between S1-wMC, wMC-ALM and S1-ALM. Statistical comparisons were made between target-aligned (T) and distractor-aligned (D) correlations, with significance denoted by lines connecting adjacent columns. Statistical comparisons were also made based on the differences in target-aligned and distractor-aligned correlations between regions, with significance denoted by lines connecting pairs of columns. (H, I) Similar structure as in [G], except for comparisons of target-aligned and distractor-aligned correlations (H, S1-wMC; I, S1-ALM) for different trial phases (pre, pre-stimulus; stim, peri-stimulus; resp, response).

Chapter 3: Global, low amplitude prestimulus cortical state

Having identified an attenuating filter in the brain region situated between sensory and motor areas during distractor trials on the hemisphere aligned with the distractor, our subsequent focus aimed to investigate the impact of preparatory activity on learning and executing the selective detection task. We sought to reveal 1) whether the prestimulus activity impacts stimulus encoding and detection, and 2) whether such task-relevant prestimulus activity is focal and restricted to specific cortical regions or global and observed throughout neocortex. To achieve this, we isolated and averaged neural activity across the last 500ms preceding the stimulus onset. This approach allowed us to compare prestimulus and post-stimulus activity, enabling us to observe differences in both temporal and spatial aspects of the task.

Given that this work built upon the foundations laid in the previous manuscript (chapter 2) and utilized the same behavioral and neural dataset, my contributions overlap with those in the attenuation study (Aruljothi et al., 2020) , as well as conducting new analyses on both behavioral and neural data such as calculating the sliding window normalization to account for trial-by-trial variance and plotting the heat maps for the difference in prestimulus fluorescence (as shown in Figures 1-4).

Title: Global, Low Amplitude Cortical State Predicts Response Outcomes in a Selective Detection Task

Running title: Prestimulus Cortical State on Selective Detection

Authors: Krista Marrero[1*], Krithiga Aruljothi[2*], Chengchun Gao[3], Behzad Zareian[2], Zhaoran Zhang[1], Edward Zagha[1,2]

[1]Neuroscience Graduate Program, [2]Department of Psychology, [3]Department of Bioengineering, University of California Riverside, 900 University Avenue, Riverside CA 92521 USA

* equal contributors

Correspondence to: edward.zagha@ucr.edu

Abstract

Spontaneous neuronal activity strongly impacts stimulus encoding and behavioral responses. We sought to determine the effects of neocortical prestimulus activity on stimulus detection. We trained mice in a selective whisker detection task, in which they learned to respond (lick) to target stimuli in one whisker field and ignore distractor stimuli in the contralateral whisker field. During expert task performance, we used widefield Ca^{2+} imaging to assess prestimulus and post-stimulus neuronal activity broadly across frontal and parietal cortices. We found that lower prestimulus activity correlated with enhanced stimulus detection: lower prestimulus activity predicted response versus no response outcomes and faster reaction times. The activity predictive of trial outcome was distributed through dorsal neocortex, rather than being restricted to whisker or licking regions. Using principal component analysis, we demonstrate that response trials are associated with a distinct and less variable prestimulus neuronal subspace. For single units, prestimulus choice probability was weak yet distributed broadly, with lower than chance choice probability correlating with stronger sensory and motor encoding. These findings support a low amplitude, low variability, optimal prestimulus cortical state for stimulus detection that presents globally and predicts response outcomes for both target and distractor stimuli.

Keywords

Neocortex, widefield imaging, sensory detection, choice probability, prestimulus

Introduction

The brain is never silent. Throughout sleep and wakefulness, spontaneous neuronal activity reflects dynamic, self-organized states that affect the generation and propagation of neuronal signals (Arieli et al., 1995, 1996; Ferezou et al., 2007; McCormick et al., 2015; McGinley et al., 2015b; Niell & Stryker, 2010; Poulet et al., 2012; Zagha & McCormick, 2014). Changes in spontaneous activity impact the amplitude of neuronal sensory responses (Crochet & Petersen, 2006; Haider & McCormick, 2009; Poulet & Petersen, 2008; Sachdev et al., 2004; Shimaoka et al., 2018) and behavioral outcomes (Boly et al., 2007; Fiebelkorn & Kastner, 2021; Kim & Sejnowski, 2021; Mazaheri et al., 2011; McGinley et al., 2015b; van Kempen et al., 2021). In awake subjects, these changes correlate with changes in task engagement, movement, and internal (cognitive or egocentric) versus external (perceptive or allocentric) processing modes (Andreou & Borgwardt, 2020; Boly et al., 2007; de Lange et al., 2013; M. C. Murphy et al., 2018; Musall et al., 2019; Salkoff et al., 2020; Stringer et al., 2019). However, most studies of sensory processing and sensory detection normalize post-stimulus by prestimulus activity, thereby obscuring the impacts of spontaneous activity. And yet, understanding how spontaneous activity impacts neuronal signaling and task performance will reveal important principles of context-dependent sensory and motor processing.

This study focuses on prestimulus activity during a sensory detection task, for which many open questions remain. First, is the ability to detect a stimulus improved by high or low prestimulus activity (Figure 1A)? A common model of

decision-making is integration to bound, which proposes that a decision is made once neuronal activity reaches a specific threshold (Gold & Shadlen, 2007; Hanes & Schall, 1996; Roitman & Shadlen, 2002). Within this model, higher prestimulus activity may bring a network closer to decision threshold and/or increase the gain of a network and therefore promote stimulus detection (Haider & McCormick, 2009). Consistent with this framework, studies in primary visual cortex demonstrate that higher prestimulus activity leads to larger amplitude stimulus responses (Haider et al., 2007). However, higher prestimulus activity may reduce cortical stimulus responses (Hasenstaub et al., 2007), due to increased cortical inhibition and reduced intrinsic and synaptic excitability. Studies in the primary somatosensory and primary auditory cortices support this alternative noise suppression framework, demonstrating that lower prestimulus activity, or activity in a low-arousal synchronized state, leads to larger amplitude stimulus responses (McGinley et al., 2015; Petersen et al., 2003; Sachdev et al., 2004).

In somatosensory (whisker) detection tasks, impacts of prestimulus activity on stimulus encoding and detection have been studied at the level of membrane potential through whole cell patch clamp recordings. While prestimulus membrane potential activity of primary somatosensory cortical neurons did predict sensory response amplitudes (Sachidhanandam et al., 2013), it did not predict trial outcome (e.g., hit versus miss) (Sachidhanandam et al., 2013; H. Yang et al., 2016). However, these whole cell recording studies are limited by relatively small

samples sizes (10s of neurons) which may obscure the ability to resolve small yet widespread contributions of prestimulus activity to task performance.

A second open question is whether the prestimulus activity that impacts stimulus encoding and detection is focal and restricted to specific cortical regions or global and observed throughout neocortex (Figure 1B). Global activity may reflect changes in arousal and movement (Musall et al., 2019; Salkoff et al., 2020; Stringer et al., 2019) whereas focal changes may reflect shifts in, for example, attentional focus or response preparation (Fries et al., 2001; Ghose & Maunsell, 2002; Luck et al., 1997; Moore & Armstrong, 2003). It is currently unknown whether prestimulus activity in sensory compared to motor cortices have larger impacts on task performance, and whether the directionality of that impact is the same across neocortical regions (Shimaoka et al., 2018). In addition to considering different cortices individually, is there an 'optimal state' of prestimulus activity that includes the contributions of multiple cortices (Figure 1C)? A third open question is whether prestimulus activity has the same or different impacts on target (attended) versus distractor (unattended) stimulus encoding and detection (Figure 1A, C). For example, the same prestimulus activity may promote discrimination (response to targets, no response to distractors) or bias responses for detection (respond to or ignore all stimuli). Lastly, do the neurons that express task-relevant changes in prestimulus activity overlap with or are they distinct from the neuronal populations that express strong post-stimulus sensory and/or motor activity (Figure 1D)?

We address these questions in the context of a selective whisker detection task in mice. We trained mice to respond (lick) to deflections on one whisker field (target) and ignore deflections in the contralateral whisker field (distractor) (Aruljothi et al., 2020; Zareian et al., 2021). Using widefield Ca^{2+} imaging, we previously identified the cortical regions that are highly active post-stimulus and pre-response, and therefore may contribute to stimulus detection: the whisker region of primary somatosensory cortex (S1), the whisker region of primary motor cortex (wMC), and the pre-motor licking region anterior lateral motor cortex (ALM) (Aruljothi et al., 2020). We consider these cortical regions to be 'task-related' and all other cortical regions to be 'task-unrelated'. Here, we implement a sliding window normalization to preserve prestimulus fluctuations. We investigated the impacts of prestimulus activity levels on trial outcome, for both target and distractor stimuli. Additionally, we use dimensionality reduction of the imaging data to assess prestimulus variability across cortices. Lastly, we assess prestimulus choice probability of single units in task-related cortices to determine the distribution of these signals across the neuronal population.

Methods

The experimental datasets in this study were previously published, including the whisker monitoring, widefield GCaMP6 imaging (Aruljothi et al., 2020) and single unit recordings (Zareian et al., 2021). Below, we summarize these experimental methods and describe the new analyses used in this study.

Animal Subjects

Experiments were approved by the IACUC of University of California, Riverside. Both male and female adult mice were used, either wild type (C57BL/6J, BALB/cByJ) or transgenic (Snap25-2A-GCaMP6s-D, backcrossed to BALB/cByJ). GCaMP6s expressing transgenic mice were used for widefield Ca^{2+} imaging; wild type mice were used for whisker imaging and electrophysiology. Mice were housed in a 12-hour light/dark cycle; experiments were conducted during the light cycle.

Animal Surgery

For headpost implantation, mice were placed under isoflurane (1-2%), ketamine (100 mg/kg), and xylazine (10 mg/kg) anesthesia. The scalp was cut (10 mm x 10 mm) and resected to expose the skull. A lightweight metal headpost was fixed onto the skull using cyanoacrylate glue. An 8 mm × 8 mm headpost window exposed most of dorsal cortex. The skull was covered with a thin layer of cyanoacrylate gap-filling medium (Insta-Cure, Bob Smith Industries) to seal the exposed skull and enhance skull transparency; the window was sealed with a quick-dry silicone gel (Reynolds Advanced Materials). Mice were administered meloxicam (0.3 mg/kg)

and enrofloxacin (5 mg/kg) for three days post-op. Water restriction began after recovery from surgery (minimum of three days). Training on the behavior rig began after one day of water restriction. For electrophysiological recordings, craniotomies and durotomies (< 0.5 mm diameter) were performed under isoflurane anesthesia. Full recovery from anesthesia was allowed (up to 60 minutes) before placement on the behavioral rig.

Animal Behavior

Training stages, metrics of learning, and criterion for expert performance in the Go/NoGo selective whisker detection task were previously reported (Aruljothi et al., 2020). Briefly, head-fixed and water deprived mice were placed on a behavioral apparatus controlled by Arduino and custom MATLAB (MathWorks) scripts. Two paddles were placed in whisker fields on the opposite sides of the face, designated as target or distractor. Target and distractor designations were assigned at the beginning of training and remained constant. Following variable intertrial intervals, mice could receive a target trial (rapid deflection of the target paddle), distractor trial (rapid deflection of the distractor paddle) or catch trial (no whisker stimulus). Mice responded by licking at a central lick port. Hits (responses to target stimuli) were rewarded with ~5 μL of water, correction rejections (not responding to distractor stimuli) and correct withholdings (not responding during the catch trial) were rewarded with a shortened intertrial-interval (ITI) and a subsequent target trial. Licking during the ITI was punished by resetting the ITI, effectively a time-out.

Mice were considered expert once they achieved a discriminability *d'* > 1 (separation of hit and false alarm response rates) for three consecutive days:

$$discriminability\ d' = \phi^{-1}_{Hit\ rate} - \phi^{-1}_{False\ alarm\ rate}$$

All recordings were conducted in expert mice while performing the task.

Widefield Imaging

Widefield imaging during expert task performance was conducted as previously reported. The dataset consists of 38 behavioral/imaging sessions, recorded from 5 mice. The through-skull imaging window included bilateral dorsal parietal and frontal cortices. Illumination from a 470 nm LED source (Thorlabs) was band-pass filtered for excitation (Chroma ET480/40x) and directed onto the skull via a dichroic mirror (Chroma T510lpxrxt). Emitted fluorescence was band-pass filtered (Chroma ET535/50m) and collected using an RT sCMOS camera (Diagnostic Imaging, SPOT Imaging software). Images were acquired at 10 Hz with a final resolution of 142 x 170 pixels (41 μm per pixel). Image sequences were imported to MATLAB for subsequent analyses.

Electrophysiology

Single unit recordings during expert task performance were conducted as previously reported (Zareian et al., 2021). The dataset consists of 32 behavioral/recording sessions, recorded from 22 mice, yielding a total of 936 single units from three cortical regions (target-aligned whisker region of primary

somatosensory cortex [S1], whisker region of motor cortex [wMC], and anterior lateral motor cortex [ALM]). Coordinates (mm, from bregma): S1 3.2-3.7 lateral, 1-1.5 posterior; wMC 0.5-1.5 lateral, 1-2 anterior; ALM 1-2 lateral, 2-2.5 anterior. Recordings were targeted to layer 5 of S1, wMC, and ALM, approximately 500 to 1100 μm below the pial surface. Electrophysiological recordings were conducted using a silicon multielectrode probe (NeuroNexus A1x16-Poly2-5mm-50s-177), positioned using a Narishige micro-manipulator. Neuralynx amplifier (DL 4SX 32ch System) and software were used for data acquisition and spike sorting.

Whisker imaging

Whisker imaging during expert task performance was conducted as previously reported (Aruljothi et al., 2020). The dataset consists of 9 behavioral/recording sessions, recorded from 4 mice. Images were acquired with a CMOS Camera (Thorlabs DCC3240M camera with Edmund Optics lens 33-301) at either 20 or 60 Hz. No systematic difference between 20 and 60 Hz was observed (data not presented). The imaging field of view included both paddles and the mouse's head (including whiskers and snout).

Data Analysis

Data analyses were performed in MATLAB using custom scripts.

Engagement period

To ensure that analyses were conducted during task engagement, 'engaged periods' were defined as continuous behavioral performance of at least 10 minutes without 60 seconds of no responding. For sessions with more than one engaged period, the longest engaged period was used for further analyses. Furthermore, sessions were included in subsequent analyses only if performance was at expert level: discriminability d'>1. For sessions with multiple stimulus amplitudes, trials were combined for further analyses only when the differences in response rates were 15% or less.

Sliding Window Normalization and Trial-Based Neuronal Activity

The trial-based imaging time window consisted of the prestimulus epoch (1 s), the stimulus and lockout epoch (0.2 s), and the allowable response epoch (1 s), a total of 2.2 s. A raw movie F was created by concatenating fluorescence activity from consecutive trials, where $F_n(i,j,f)$ is the fluorescence of each pixel (row *i* and column *j*) in frame *f* for each trial *n*. To generate normalized fluorescence values, we first determined the sliding window local mean for each pixel, computed every 2 s using a +/- 200 s window size [$F_{SW}(i,j,n)$]. Then, we calculated the normalized fluorescence (Salkoff, 2020 #1244) (see also Supplemental Figure 1) for each pixel at each frame as:

$$dF_{SW}/F_{SW}(i,j,n) = [F_n(i,j,f) - F_{SW}(i,j,n)]/F_{SW}(i,j,n)$$

Trialwise average movies were then compiled by first indexing outcome type (*hit*, *miss*, *false alarm*, *correct rejection*) and then by averaging pixelwise activity across corresponding frames of corresponding trials. Frames were aligned to the stimulus onset frame (stimulus-aligned) where stimulus occurred or aligned to the first frame containing the response (response-aligned) where response occurred. Trials with responses during the lockout period were considered *premature* and excluded from the analysis. Trials with responses before the stimulus but within the prestimulus imaging period were considered *spontaneous*, dF/F reported but not further analyzed. Grand average movies were aligned to bregma, flipped at bregma according to target-distractor assignment, and then averaged across all sessions.

Difference in Prestimulus Fluorescence

Fluorescence differences for target and distractor assignment were calculated per trial type per session. Prestimulus frames 6 to 10 (capturing the last 500 ms of the prestimulus window, before stimulus onset) were trialwise and pixelwise averaged per session. Session data were excluded from this analysis if there were fewer than 5 incorrect trials in the session (excluding 9 sessions for target Miss, 6 sessions for distractor FA). For target fluorescence difference frames (n = 29 sessions), Hits fluorescence mean frame was subtracted from Miss fluorescence mean frame. For distractor fluorescence difference frames (n = 32 sessions), FA fluorescence mean frame was subtracted from CR fluorescence mean frame. Response prestimulus frames were subtracted from no response prestimulus

frames because no response fluorescence activity was generally higher than response fluorescence activity. Prestimulus difference frames were aligned, assigned, and averaged across all sessions (as above). To normalize for differences in changes in fluorescence across regions, we performed a z-score normalization of the dF/F values for each pixel as the pixelwise mean divided by the pixelwise standard deviation ($\mu_{i,j}/\sigma_{i,j}$). For quantification of target versus distractor prestimulus difference, normalized difference (index), and significance, frames were averaged across pixels for scalar values.

Regression analyses between Prestimulus Activity and Reaction Time for Response Trials:

The correlation between activity during prestimulus period (dF/F) and reaction times (RT) for response trials (Hits and FAs) were computed as a linear regression from which we obtained the slope of the linear fit with 95% confidence interval and coefficient of determination, R^2, as the goodness of fit (Zareian et al., 2021) (Curve Fitting Toolbox in Matlab). For this analysis, we assigned prestimulus dF/F as the independent variable and reaction time as the dependent variable.

Stimulus Encoding in Post-Stimulus Fluorescence

Stimulus encoding was quantified as the neurometric *d'* (Britten et al., 1992) of prestimulus fluorescence (stimulus absent) and post-stimulus fluorescence (stimulus present) during the lockout epoch, as previously applied to imaging data (Aruljothi et al., 2020). We excluded session data from this analysis if there were

fewer than 4 incorrect trials in the session (excluding 5 sessions for target Miss, 2 sessions for distractor FA). Neurometric *d'* was calculated separately according to target and distractor assignment and then according to trial type outcome. This resulted in 6 different datasets for stimulus encoding: all target, all distractor, hit trials, miss trials, false alarm trials, and correct rejection trials. Prestimulus and post-stimulus fluorescence histograms were plotted into receiver operating characteristic (ROC) curves and the area under the curve (AUC) was converted to *d'* as the neurometric:

$$fluorescence\ d'_{Stimulus} = \sqrt{2} * Z_{AUC}$$

Region specific pixel values were identified as the maximum value within the defined regions of interest (ROI), performed for target-aligned and distractor-aligned regions of S1, wMC, and ALM. The difference in stimulus encoding in S1 between the response and the no response trials for both target and distractor stimuli was calculated as the percentage:

$$\%_{difference} = \frac{response\ trial - no\ response\ trial}{(response\ trial + no\ response\ trial)/2} * 100$$

Whisker Motion Energy During Behavior

The imaging window was cropped by region of interest: target or distractor paddle stimulus or whisker fields. The function *vision.VideoFileReader* was used for optimal reading of video frames into MATLAB. Whisker movement per frame

(*Δframe*) was calculated as the pixelwise frame by frame mean gray value (*MGV*) difference (ΔMGV_{pixel}). Whisker motion energy (*WME*) was defined as the sum of the squares across pixels:

$$WME = (\Delta l)^2 = \sum_{pixels} \left(\frac{\Delta MGV_{pixel}}{\Delta frame}\right)^2$$

WME traces of the cropped videos of the paddles were used to detect stimulus events (target/distractor). This was performed by using a constant threshold and aligning detected events from the video to their temporally closest events recorded using Arduino. The traces from the cropped videos of whisker fields were transformed (z-scored) to have a mean of zero and standard deviation of 1 for the purpose of comparison across sessions. Subsequently, WME data were temporally aligned by trial type to stimulus onset (target/distractor) determined from the videos.

Principal Component Analysis of Fluorescence

Fluorescence was averaged across anatomic masks [target and distractor S1, wMC, ALM, and retrosplenial (RSP) cortex] per frame per trial per session. Mean regions were normalized and placed into a covariance matrix. The covariance matrix was decomposed into an eigenmatrix, eigenvectors were sorted by eigenvalue weight, and eigenvectors were projected into component space. All frames were separated by trial type, plotted in PC space, and differentiated by trial

epoch (prestimulus, post-stimulus and pre-response lockout, and allowable response window). Component data for prestimulus frames were further analyzed: confidence area ellipses of 1 standard deviation, σ, was defined by the ellipsoid distribution of prestimulus frames in PC space per session. Centroids were defined as the geometric mean of prestimulus frames in PC space per session.

Spike Sort and Cluster of Single Units

Using Neuronalynx recording system, signals were sampled at 32 kHz, band-pass filtered from 0.1Hz to 8000 Hz, and high-pass filtered at 600 Hz to 6000 Hz. Putative spikes crossed thresholds of 20 to 40 μV, isolated from baseline noise. KlustaKwik algorithm in SpikeSort3D software was used for spike sorting and clustering. Clusters were defined by waveform and cluster location in feature space (peaks and valleys); movement artifacts (atypical waveforms or those occurring across all channels) were removed, as previously reported (Zareian et al., 2021). Subsequent analyses were conducted using MATLAB software (MathWorks).

Sensory and Motor Encoding of Single Units

Sensory and motor encoding of single units was performed as previously reported (Zareian et al., 2021). Sensory encoding was quantified by the neurometric *d'* using stimulus absent spiking (300 ms prestimulus) and stimulus present spiking (100 ms post-stimulus). Motor encoding was quantified by the neurometric *d'* using response absent spiking (300 ms prestimulus) and response present spiking (100

ms pre-response). Distributions were plotted into ROC curves and the AUC was converted to *d'* as a neurometric:

$$spike\ d'_{sensory}\ or\ d'_{motor} = \sqrt{2} * Z_{AUC}$$

Choice Probability of Single Units

For choice probability analyses, we ensured that there was a minimum of 5 trials per trial type (minimum 5 Hits and 5 Miss). Choice probability (%) was quantified as the separation of prestimulus spiking in Hits versus Miss trials. ROC and AUC were calculated from the distributions of Hits and Miss across trials, 500 ms to 0 ms before stimulus onset, averaged over 50 ms nonoverlapping intervals, as previously reported (Zareian et al., 2021).

Statistical Analyses

For imaging statistics, threshold for statistical significance was corrected for multiple comparisons with a Bonferroni correction. Fluorescence difference (Miss – Hits, CR – FA), statistical analyses determined whether dF/F frames were significantly different than zero across sessions (one sample t-test). For whisker analyses statistics, since the number of samples in the whisking data were low, we used one-sample Kolmogorov-Smirnov test (*kstest* in MATLAB) to test for normality assumptions. Since the data mostly violated the normality assumption, Wilcoxon signed rank (*signrank* in MATLAB) and rank sum (*ranksum* in MATLAB) tests were used for comparisons between prestimulus and post-stimulus whisking

and between trial types (Hits vs. Miss, FA vs. CR), respectively. For stimulus encoding (neurometric d'), statistical analyses determined whether the trialwise (Hits, Miss, FA, CR) maximum pixel value in S1 was significantly different than zero across sessions (one sample t-test). For differences in stimulus encoding, statistical analyses determined whether the stimulus-aligned S1 maximum pixel value was significantly different between response (Hits, FA) and no response (Miss, CR) outcome types across sessions (two sample t-test). For PCA ellipsoid variance and centroid distribution, statistical analysis determined whether ellipsoid variance or centroid distribution was significantly different between response and no response prestimulus frames, evaluated per component. Box whisker plots show the distribution of prestimulus frames or ellipsoid centroids per trial type with outliers, evaluated per component. For choice probability of single units, statistical analysis determined whether distributions within regions were significantly different from chance (one-sample t-test, chance level 50%) and whether distributions between regions were significantly different from each other (ANOVA and post-hoc Tukey test). For the significance assessment of sensory and motor encoding of single units, one-sample t-test was used to compare d-prime distributions to zero. For the relationship between sensory and motor encoding and choice probability of single units, statistical analysis determined whether regression slopes were significantly different from zero (95% confidence bounds for slopes). Box whisker plots were used to show distributions of sensory encoding, motor encoding, and

choice probability of single units evaluated within regions. Average data are presented as mean +/- standard error of the mean, unless otherwise indicated.

Results

Global prestimulus activity predicts response outcomes

We considered how prestimulus activity may influence sensory detection (Figure 1A-D). High prestimulus activity may promote detection of target and distractor stimuli; alternatively, low prestimulus activity may promote detection of target and distractor stimuli or discrimination of target from distractor stimuli (Figure 1A). The prestimulus activity that influences behavioral outcomes may present focally in specific task-related regions or globally across neocortex (Figure 1B). A low variability, specific 'optimal state' configuration may promote stimulus detection or target/distractor discrimination (Figure 1C). At the level of single units, prestimulus contextual signals and post-stimulus sensory and motor signals may be carried by distinct neuronal ensembles (sparse coding) or overlapping neuronal ensembles (dense coding) (Figure 1D). We tested these possibilities in a selective whisker detection task, in which head-fixed mice learn to respond to rapid deflections in one whisker field (target) and ignore identical deflections in the opposite whisker field (distractor) (Figure 1E). In this task, the possible trial outcomes include hit (response to target), miss (no response to target), false alarm (FA, response to distractor), and correct rejection (CR, no response to distractor) (Figure 1F). Prior to each stimulus was a variable inter-trial interval (ITI), in which mice were required to withhold responding or else reset the ITI. The prestimulus epoch we used for analyses is the last 1 second of the ITI immediately prior to stimulus onset (Figure 1G).

We used widefield Ca^{2+} imaging to measure neuronal activity during expert task performance in frontal and parietal cortices, bilaterally (Figure 1F). Our imaging dataset consists of 38 imaging sessions from 5 mice, using a single task-engaged period per session (see Methods). Due to the highly lateralized cortical whisker representation, we could clearly define target-aligned and distractor-aligned cortical regions, contralateral to the side of the whisker stimulus. To preserve activity fluctuations prestimulus, we normalized raw fluorescence activity using a sliding window method (400 s sliding window, see Methods and Supplemental Figure 1).

In Figure 2 we present grand average fluorescence activity for each trial outcome, aligned to the onsets of both the stimulus and response. In the first column of Figure 2 we show the last prestimulus frame, which is representative of the full prestimulus epoch. We note stark differences in prestimulus activity for different trial outcomes, particularly when comparing hit (Figure 2A) and miss (Figure 2D) trials. We observed lower prestimulus activity for hit versus miss and for FA versus CR trials, indicating that lower prestimulus activity precedes 'response' compared to 'no response' outcomes. Interestingly, low prestimulus activity appears to be specifically related to stimulus detection rather than response preparation. This is evidenced by higher activity preceding spontaneous responses (Spont, a response during the ITI, Figure 2C) compared to stimulus-related responses (hits and FA, Figures 2A and 2B). The magnitude of the prestimulus differences is large, on the same scale as the post-stimulus activity.

Additionally, prestimulus activity suppression preceding response trials appears to be widely distributed throughout dorsal neocortex, rather than being focused on the task-related regions of S1, wMC and ALM.

We quantified the differences in prestimulus activity between response and no response trials for target and distractor stimuli (Figure 3A-F). Shown in this figure are data from the last 500 ms of the prestimulus (similar results were obtained using 100 ms or 1 s prestimulus epochs, data not shown). We subtracted the average prestimulus fluorescence activity of hit from miss trails (Figure 3A). The positive values indicate higher activity preceding miss compared to hit trials (n=29 sessions, averaged across the entire field of view: dF/F $\mu_{[Miss-Hits]}$=2.1%±0.3%; one-sample t-test, t(28)=8.1, p=7.9e-09). The largest differences were not in the task-related whisker or licking regions but appear to be focused on the limb regions of somatosensory cortex. While dF/F is already a normalized metric, we sought to further control for possible regional differences in imaging sensitivity. Therefore, we conducted the same subtraction analysis, but on dF/F values that were additionally normalized by z-score, using the mean and standard deviation of the entire session. With this analysis (Figure 3B), the activity differences are more uniformly distributed across frontal and parietal cortices, with an average miss-hit difference of 1.2 standard deviations.

To determine the spatial regions of significance, on each pixel we performed a paired, two-sample t-test on average prestimulus fluorescence activity in hit versus miss sessions (p-value of each pixel shown in Figure 3C). All neocortical

regions within our field of view demonstrated statistical significance, even with a Bonferroni corrected alpha level to control for multiple comparisons (28,960 pixels). Thus, lower prestimulus activity on upcoming target trials is predictive of hit versus miss outcomes. This is observed for all cortical regions within our field of view, including task-related and task-unrelated regions.

There were some notable similarities and differences for distractor trials (Figure 3D-F). Similar to target trials, higher activity was observed preceding no response (CR) versus response (FA) trials (n=32 sessions, averaged across the entire field of view: dF/F $\mu_{[CR-FA]}$= 0.36± 0.11% one-sample t-test, t(31)=3.38, p=0.002). However, the fluorescence differences were approximately 5-fold higher for target trials compared with distractor trials (dF/F $\mu_{[Miss-Hits]}$=2.1% versus $\mu_{[CR-FA])}$=0.36%). A second difference is that for distractor trials, the focus on the somatosensory limb regions was observed in dF/F, z-score, and p-value maps (Figure 3D-F, respectively). The regions with the lowest p-value were slightly above the Bonferroni corrected alpha level. Thus, while lower activity preceding distractor trials was also predictive of a response, the effect size was smaller and less widespread.

In addition to predicting response outcome, we also sought to determine whether prestimulus activity levels predict reaction time on response trials (Figure 3G-J). For these analyses, we determined the slope and coefficient of determination (R^2) of linear fits for prestimulus dF/F versus reaction time for Hit and FA trials (separately) for each session. As shown in the example session in

Figure 3G, a positive slope indicates a correlation between higher prestimulus activity and longer post-stimulus reaction times. Across all sessions, we found a significant positive correlation (positive slope) on Hit trials between prestimulus activity and reaction time (n=30 sessions, slope=0.64±0.23, one-sample t-test: t(29)=2.73, p= 0.011; R^2=0.074±0.023) (Figure 3H). Thus, for target stimuli, lower prestimulus activity predicts both Hit versus Miss outcomes and faster reaction times.

We performed the same correlation analyses for FA trials (Figure 3I,J). In contrast to Hit trials, FA trials across sessions did not show a consistent correlations between prestimulus activity and reaction time (n=32 sessions, slope=-0.45±1.48, one-sample t-test: t(31)=-0.3, p=0.76; R^2=0.12±0.021) (Figure 3J).

Contributions of stimulus encoding and movement on trial outcomes

Next, we assessed whether the differences in trial outcome were reflected in differences in stimulus responses in the neocortex. We quantified the stimulus encoding during the lockout period (200 ms post-stimulus and pre-response) for each trial type (Figure 4). For each pixel, we measured stimulus encoding as the neurometric sensitivity index d' (Figure 4A-F) and determined whether these values were significantly different from zero (Figure 4G-L). We observed significant stimulus encoding in the stimulus-aligned primary somatosensory cortex (S1) for each trial type (one-sample t-test, n= 38, hits: 38, miss: 33, FA: 36, CR: 38, hits: d'

μ_{S1}=0.98±0.06, t(37)=15.58, p=7.79e-18; miss: d' μ_{S1}=0.69±0.08, t(32)=9.08, p=2.26e-10; FA: d' μ_{S1}=1.05±0.09, t(35)=12.08, p=4.87e-14; CR: d' μ_{S1}=0.58±0.049, t(37)= 11.89, p=3.32e-14). Thus, significant stimulus responses occur in S1 for both response and no response trials. However, we did observe a 40-60% reduction in S1 stimulus encoding in no response compared to response trials for target and distractor stimuli (hits vs. miss: d' $\mu_{\%\ difference}$=39.84±7.44%, paired-sample t-test, t(32)= 4.51, p=8.26e-05; FA vs. CR: d' $\mu_{\%\ difference}$=61.62±7.26%, paired-sample t-test, t(35)= 6.72, p=8.75e-08, see Methods). In summary, response trials are associated with reduced prestimulus activity and enhanced post-stimulus sensory responses.

Recent studies have demonstrated widespread neuronal activity increases due to movement (Musall et al., 2019; Salkoff et al., 2020; Stringer et al., 2019). Therefore, in a separate set of recordings, we determined the magnitude of prestimulus and post-stimulus whisker movements on different trial outcomes. Whisker movement was quantified as whisker motion energy (WME, normalized by z-score, see Methods). In Figure 5A-C we present these analyses for one example session for target stimuli. On hit trials, WME increased dramatically post-stimulus (Figure 5A, purple trace). We interpret this as whisking being part of the 'uninstructed' behavioral response sequence (Musall et al., 2019). Importantly, we also observed differences in WME prestimulus, with higher WME on miss compared to hit trials (mean +/- STD WME μ_{Hits}=-0.45 ± 0.32, WME μ_{Miss}=0.19 ± 0.71, rank sum=1516, p=0.001, two-sided Wilcoxon rank sum test; Figure 5A and

5B). In Figure 5C, we show prestimulus WME for each target trial, with the color of the bar indicating trial outcome. High prestimulus WME was more likely to result in a miss trial, even though many miss trials were not preceded by high prestimulus WME. Similar results were observed across all sessions (n=9 session, Figure 5D, Wilcoxon sign rank test, mean +/- STD prestimulus WME μ_{Hits}=-0.12 ± 0.17 vs. prestimulus WME μ_{Miss}=0.12 ± 0.15, signed rank=1, p=0.008). Thus, high prestimulus movement was associated with some, but not all, of the miss trials.

Differences in prestimulus WME were not as pronounced on distractor trials (Figure 5E-H). We did notice a trend towards increased WME on CR trials. However, this effect was not statistically significant across sessions (n=9 session, Figure 5H, Wilcoxon sign rank test: prestimulus WME μ_{FA}=-0.14 ± 0.2 vs. prestimulus WME μ_{CR}=-0.04 ± 0.10, signed rank=8, p=0.098). Notably, the effects of prestimulus movement on target and distractor trial outcomes parallel the effects of prestimulus neuronal activity: low prestimulus neuronal activity and low prestimulus WME predict response outcomes, yet these effects are much more pronounced for target compared to distractor trials.

Analyses of prestimulus activity variance and subspace in reduced spatial dimensions

Next, we sought to characterize frame-by-frame variability in our imaging data. To accomplish this, we used principal component analysis (PCA) to reduce the spatial dimensionality (Figure 6). First, we extracted regional single-trial fluorescence

activity using anatomic masks from the dorsal neocortex centered on regions of interest: target/distractor S1, RSP, wMC, and ALM (Figure 6A). We concatenated data from all frames, trials, sessions, and mice and performed PCA on this combined matrix. This enabled us to convert all sessions into the same lower-dimensional axes. Most of the variability in our imaging data could be explained by the first component (~91%) and the first two components explained ~96% of the variance (Figure 6B-D). Therefore, further analyses focused on these first two spatial components.

We determined the distributions of prestimulus activity from single frames within this PCA space (Figure 7). In Figure 7A, we plot the data from two example sessions, in which each data point is a single prestimulus frame preceding a hit (purple) or miss (yellow) trials. We noticed that the data from hit trials were more tightly clustered than the data from miss trials. To quantify this observation, first we fit the data from each trial type with a covariance ellipse. The shaded ellipses in Figure 7A represent a confidence area of 1 standard deviation, σ, which we used as a measure of framewise variability. Figure 7B plots the confidence area for prestimulus activity on hit and miss trials for all sessions (n=29 sessions). The prestimulus activity variance is significantly lower for hit compared to miss trials (effect size, Cohen's d=1.92; paired t-test, t(28)= 9.43, p=1.74e-10).

We conducted the same analyses for distractor trials and obtained similar results. The two example sessions in Figure 7C show more tightly clustered prestimulus activity for response (FA) compared to no response (CR) trials. Across

all sessions (n=32), the confidence areas are significantly lower for FA compared to CR trials (effect size, Cohen's d=1.11; paired t-test, t(31)= 7.40, p=1.22e-8, Figure 7D). Thus, for both target and distractor trials, lower framewise prestimulus variability predicts response outcomes.

In addition to differences in variability, we also noticed that the prestimulus activity resides in different subspaces preceding response and no response trials. As evident in Figure 7A, *within* each session the centroids of the hit and miss confidence areas are offset, whereas *between* these two sessions the hit centroids occur at similar positions. In Figure 7E, we plot the centroid position for all sessions (n=29 sessions). Indeed, we find that across all sessions the centroid positions preceding hit trials are separated from the centroid positions preceding miss trials. This separation is significant, for both PC1 and PC2 axes (Figure 7F, PC1: d=2.19, paired t-test, t(28)=8.55, p=1.34e-9; PC2: d=1.24, t(28)=4.01, p=2.07e-4). In contrast, for distractor trials, the centroids of prestimulus activity show greater overlap for response (FA) and no response (CR) trials (Figure 7G). However, we do still find significantly different centroid positions on distractor trials along PC1 (Figure 7H, PC1: d=0.57, paired t-test, t(31)=2.99, p=0.0027; PC2: d=0.43, t(31)=1.30, p=0.10). These data indicate that the neuronal activity across dorsal neocortex preceding response trials is less variable than no response trials and occupies a separate subspace. Similar to prestimulus neural activity (Figure 3) and movement (Figure 5), the differences in variability and subspace position are larger

for target compared to distractor trials. Taken together, these data specify an optimal neuronal and behavioral state for stimulus detection.

Distribution of prestimulus choice probability among single units

The above analyses of widefield imaging data assessed population neuronal activity. In this final series of analyses, we sought to determine the distribution of task-relevant prestimulus activities among single units (Figure 8). During the same selective whisker detection task, we recorded 936 single units, from target-aligned S1 (377 units), target-aligned wMC (338 units) and target-aligned ALM (221 units). First, we quantified the prestimulus choice probability of all units on target trials. Choice probabilities (CP) of single units in each region were marginally below chance (Figure 8A, CP μ_{S1}=49.10 ± 0.16, one-sample t-test, t(376)=-5.72, p=2.21e-8, CP μ_{wMC}=49.44 ±0.2, one-sample t-test, t(337)=-2.82, p=0.005, CP μ_{ALM}=49.64 ±0.19, one-sample t-test, t(220)=-1.92, p=0.06). These distributions were not significantly different across the three regions (two-way ANOVA: F(2,933)= 2.18, p=0.11 and post hoc Tukey: S1 vs. wMC, p=0.33; wMC vs. ALM, p=0.76; S1 vs. ALM, p=0.12). Prestimulus choice probability below chance indicates that lower activity predicts hit compared to miss outcomes, and therefore is consistent with the widefield imaging data. However, the distributions of these data indicate that only a small portion of single units show strong prestimulus choice probability.

Given this variability of single units, we next asked whether the units with strong prestimulus choice probability overlap with the units with strong post-stimulus sensory and pre-response motor encoding. To test this, we plotted prestimulus choice probability against post-stimulus sensory (Figure 8A) and pre-response motor (Figure 8B) encoding. The negative regression slopes show correlations between choice probability and sensory encoding for S1, and between choice probability and motor encoding for S1, wMC, and ALM (Figure 8C and 8D, one-sample t-test, sensory encoding slope: m_{S1}=-1.96 ± 0.31, t(375)=-6.34, p=6.56e-10; one-sample t-test, motor encoding slope: m_{S1}=-2.05 ± 0.28, t(375)=-7.35, p=1.23e-12 , m_{wMC}=-0.64 ± 0.26, t(336)=-2.49, p=0.013, m_{ALM}=-0.96 ± 0.28, t(219)=-3.46, p=6.41e-4). Thus, units in these regions have combined neuronal representations such that those representing prestimulus behavior context overlap with those with post-stimulus (sensory) and pre-response (motor) task-relevant encoding. This overlap may be influenced by a common factor such as firing rate (Supplemental Figure 2). Nevertheless, these analyses demonstrate that the subset of neurons that show the largest prestimulus suppression on hit trials are the same neurons that strongly encode task features.

Discussion

The primary focus of this study is to determine whether and how neuronal activity before stimulus onset predicts trial outcomes during goal-directed behavior. We assessed this for both target and distractor stimulus detection. We find that lower prestimulus activity predicts detection of both target and distractor stimuli (Figures 2 and 3) and faster reaction times on Hit trials (Figure 3). This low activity state is distributed globally throughout dorsal cortex (Figure 3), maps onto a distinct, less variable subspace than activity preceding no response trials (Figure 7) and is represented most robustly in the subset of neurons also encoding post-stimulus sensory and pre-response motor task features (Figure 8).

The impacts of spontaneous activity on stimulus responses have been explored extensively in both physiological and computational studies. Increased spontaneous activity has been proposed to increase response gain by two primary mechanisms: depolarization to reduce membrane potential distance to spike threshold and increased variance to amplify the impacts of weak inputs (Cardin et al., 2008; Haider et al., 2007; Haider & McCormick, 2009; Hô & Destexhe, 2000; Rudolph & Destexhe, 2003; Shu et al., 2003). Therefore, we were surprised to find that reduced prestimulus activity correlated with both enhanced stimulus detection (Figures 2 and 3) and increased sensory responses (Figure 4). And yet, our data are consistent with studies in primary somatosensory and auditory cortices, demonstrating increased sensory responses with reduced prestimulus activity (Cardin et al., 2008; Hasenstaub et al., 2007; McGinley et al., 2015; Sachdev et

al., 2004). Future studies are required to determine the cellular and network mechanisms underlying increased responsiveness with low activity, with possibilities including reduced membrane conductance (Chance et al., 2002), reduced inhibition, and reduced synaptic depression.

Our study was conducted in the context of a somatosensory (whisker) detection task. It is not currently known, however, whether these findings will generalize to other sensory modalities and other types of tasks. Reduced network activity and reduced synaptic variance have been shown to predict a network with a discrete, all-or-none input-output function (Hô & Destexhe, 2000). This configuration may improve distinguishing the presence versus absence of a stimulus as needed for stimulus detection. Such a network state, though, would be predicted to poorly encode the precise features of a stimulus. Therefore, we speculate that tasks requiring discrimination of fine stimulus details may be optimal in a high activity network state with a continuous input-output function. However, this remains to be tested.

Most studies of the impacts of spontaneous activity on sensory responses focus on primary sensory areas. However, stimulus detection tasks require the contributions of multiple cortices (De Lafuente & Romo, 2006). Indeed, we have recently shown that the task in this study activates multiple sensory and motor cortices, including S1, wMC, and ALM (Aruljothi et al., 2020; Zareian et al., 2021). In this study we demonstrate that the prestimulus activity predictive of trial outcome is global, involving all regions of dorsal neocortex. This global cortical state may

reflect the coordination amongst multiple cortices, to improve not just stimulus encoding in primary sensory cortex, but the propagation of task-relevant signals throughout neocortex. Interestingly, we found prestimulus activity suppression to be largest in the same neurons that also strongly encode post-stimulus sensory and pre-response motor features, in S1, wMC, and ALM. This organization may ensure coordination not just between cortical regions, but among the specific neuronal ensembles involved in this stimulus detection task. Low activity in these specific neuronal ensembles may increase excitability and transmission by increasing membrane resistance and reducing synaptic depression.

Global changes in cortical state, as observed here, are traditionally associated with changes in arousal, driven by widespread ascending neuromodulatory systems (Zagha & McCormick, 2014). More recently, studies have shown that movement is associated with global increases in neocortical activity (Musall et al., 2019; Salkoff et al., 2020; Stringer et al., 2019). As with low activity preceding response trials, we also find that whisker movements are reduced preceding hit trials (Figure 5), consistent with previous reports (Kyriakatos et al., 2017; Ollerenshaw et al., 2012). We suspect that whisker movements impair detection for multiple reasons: 1) reafference signals from self-generated movements (Fee et al., 1997) may obscure stimulus-evoked afferent signals, 2) self-generated movements may evoke top-down sensory gating and thereby suppress stimulus evoked signals (Chakrabarti & Schwarz, 2018), and 3) centrally-mediated cortical activation associated with whisker movements (Poulet et al.,

2012) may reduce network excitability. And yet, our findings support a view of cortical state as higher dimensional than stationary versus moving (McGinley et al., 2015; Zagha & McCormick, 2014). Among Hit trials, we find a positive correlation between prestimulus activity and reaction time (Figure 3). This suggests that even within overt changes in arousal, the precise levels of cortical activity impact performance in our task, with the lowest prestimulus activity correlating with optimal performance. Dissecting the physiological mechanisms underlying the low amplitude cortical state permissive for whisker stimulus detection is a focus of ongoing investigations.

Acknowledgements

This work was supported by the Whitehall Foundation (Research Grant 2017-05-71 to E.Z.) and the National Institutes of Health (R01NS107599 to E.Z.). We thank Drs. Hongdian Yang and David Salkoff for many helpful discussions throughout the project. The authors declare no competing financial interests.

References

Andreou, C., & Borgwardt, S. (2020). Structural and functional imaging markers for susceptibility to psychosis. *Molecular Psychiatry*, *25*(11), 2773–2785. https://doi.org/10.1038/s41380-020-0679-7

Arieli, A., Shoham, D., Hildesheim, R., & Grinvald, A. (1995). Coherent spatiotemporal patterns of ongoing activity revealed by real-time optical imaging coupled with single-unit recording in the cat visual cortex. *Journal of Neurophysiology*, *73*(5), 2072–2093. https://doi.org/10.1152/jn.1995.73.5.2072

Arieli, A., Sterkin, A., Grinvald, A., & Aertsen, A. (1996). Dynamics of Ongoing Activity: Explanation of the Large Variability in Evoked Cortical Responses. *Science*, *273*(5283), 1868 LP – 1871. https://doi.org/10.1126/science.273.5283.1868

Aruljothi, K., Marrero, K., Zhang, Z., Zareian, B., & Zagha, E. (2020). Functional Localization of an Attenuating Filter within Cortex for a Selective Detection Task in Mice. *Journal of Neuroscience*, *40*(28), 5443–5454. https://doi.org/10.1523/JNEUROSCI.2993-19.2020

Boly, M., Balteau, E., Schnakers, C., Degueldre, C., Moonen, G., Luxen, A., Phillips, C., Peigneux, P., Maquet, P., & Laureys, S. (2007). Baseline brain activity fluctuations predict somatosensory perception in humans. *Proceedings of the National Academy of Sciences*, *104*(29), 12187 LP – 12192. https://doi.org/10.1073/pnas.0611404104

Britten, K. H., Shadlen, M. N., Newsome, W. T., & Movshon, J. A. (1992). The analysis of visual motion: a comparison of neuronal and psychophysical performance. *The Journal of Neuroscience*, *12*(12), 4745 LP – 4765. https://doi.org/10.1523/JNEUROSCI.12-12-04745.1992

Cardin, J. A., Palmer, L. A., & Contreras, D. (2008). Cellular Mechanisms Underlying Stimulus-Dependent Gain Modulation in Primary Visual Cortex Neurons In Vivo. *Neuron*, *59*(1), 150–160. https://doi.org/10.1016/j.neuron.2008.05.002

Chakrabarti, S., & Schwarz, C. (2018). Cortical modulation of sensory flow during active touch in the rat whisker system. *Nature Communications*, *9*(1), 3907. https://doi.org/10.1038/s41467-018-06200-6

Chance, F. S., Abbott, L. F., & Reyes, A. D. (2002). Gain modulation from background synaptic input. *Neuron*, *35*(4), 773–782. https://doi.org/10.1016/s0896-6273(02)00820-6

Crochet, S., & Petersen, C. C. H. (2006). Correlating whisker behavior with membrane potential in barrel cortex of awake mice. *Nature Neuroscience*, *9*(5), 608–610. https://doi.org/10.1038/nn1690

De Lafuente, V., & Romo, R. (2006). Neural correlate of subjective sensory experience gradually builds up across cortical areas. *Proceedings of the National Academy of Sciences of the United States of America*, *103*(39), 14266–14271. https://doi.org/10.1073/pnas.0605826103

de Lange, F. P., Rahnev, D. A., Donner, T. H., & Lau, H. (2013). Prestimulus Oscillatory Activity over Motor Cortex Reflects Perceptual Expectations. *The Journal of Neuroscience*, *33*(4), 1400 LP – 1410. https://doi.org/10.1523/JNEUROSCI.1094-12.2013

Fee, M. S., Mitra, P. P., & Kleinfeld, D. (1997). Central Versus Peripheral Determinants of Patterned Spike Activity in Rat Vibrissa Cortex During Whisking. *Journal of Neurophysiology*, *78*(2), 1144–1149. https://doi.org/10.1152/jn.1997.78.2.1144

Ferezou, I., Haiss, F., Gentet, L. J., Aronoff, R., Weber, B., & Petersen, C. C. H. (2007). Spatiotemporal Dynamics of Cortical Sensorimotor Integration in Behaving Mice. *Neuron*, *56*(5), 907–923. https://doi.org/10.1016/j.neuron.2007.10.007

Fiebelkorn, I. C., & Kastner, S. (2021). Spike Timing in the Attention Network Predicts Behavioral Outcome Prior to Target Selection. *Neuron*, *109*(1), 177-188.e4. https://doi.org/10.1016/j.neuron.2020.09.039

Fries, P., Reynolds, J. H., Rorie, A. E., & Desimone, R. (2001). Modulation of Oscillatory Neuronal Synchronization by Selective Visual Attention. *Science*, *291*(5508), 1560 LP – 1563. https://doi.org/10.1126/science.1055465

Ghose, G. M., & Maunsell, J. H. R. (2002). Attentional modulation in visual cortex depends on task timing. *Nature*, *419*(6907), 616–620. https://doi.org/10.1038/nature01057

Gold, J. I., & Shadlen, M. N. (2007). The Neural Basis of Decision Making. *Annual Review of Neuroscience*, *30*(1), 535–574. https://doi.org/10.1146/annurev.neuro.29.051605.113038

Haider, B., Duque, A., Hasenstaub, A. R., Yu, Y., & McCormick, D. A. (2007). Enhancement of Visual Responsiveness by Spontaneous Local Network Activity In Vivo. *Journal of Neurophysiology*, *97*(6), 4186–4202. https://doi.org/10.1152/jn.01114.2006

Haider, B., & McCormick, D. A. (2009). Rapid Neocortical Dynamics: Cellular and Network Mechanisms. *Neuron*, *62*(2), 171–189. https://doi.org/10.1016/j.neuron.2009.04.008

Hanes, D. P., & Schall, J. D. (1996). Neural Control of Voluntary Movement Initiation. *Science*, *274*(5286), 427 LP – 430. https://doi.org/10.1126/science.274.5286.427

Hasenstaub, A., Sachdev, R. N. S., & McCormick, D. A. (2007). State Changes Rapidly Modulate Cortical Neuronal Responsiveness. *The Journal of Neuroscience*, *27*(36), 9607 LP – 9622. https://doi.org/10.1523/JNEUROSCI.2184-07.2007

Hô, N., & Destexhe, A. (2000). Synaptic Background Activity Enhances the Responsiveness of Neocortical Pyramidal Neurons. *Journal of Neurophysiology*, *84*(3), 1488–1496. https://doi.org/10.1152/jn.2000.84.3.1488

Kim, R., & Sejnowski, T. J. (2021). Strong inhibitory signaling underlies stable temporal dynamics and working memory in spiking neural networks. *Nature Neuroscience*, *24*(1), 129–139. https://doi.org/10.1038/s41593-020-00753-w

Kyriakatos, A., Sadashivaiah, V., Zhang, Y., Motta, A., Auffret, M., & Petersen, C. C. H. (2017). Voltage-sensitive dye imaging of mouse neocortex during a whisker detection task. *Neurophotonics*, *4*(3), 031204. https://doi.org/10.1117/1.NPh.4.3.031204

Luck, S. J., Chelazzi, L., Hillyard, S. A., & Desimone, R. (1997). Neural Mechanisms of Spatial Selective Attention in Areas V1, V2, and V4 of Macaque Visual Cortex. *Journal of Neurophysiology*, *77*(1), 24–42. https://doi.org/10.1152/jn.1997.77.1.24

Mazaheri, A., DiQuattro, N. E., Bengson, J., & Geng, J. J. (2011). Pre-Stimulus Activity Predicts the Winner of Top-Down vs. Bottom-Up Attentional Selection. *PLOS ONE*, *6*(2), e16243. https://doi.org/10.1371/journal.pone.0016243

McCormick, D. A., McGinley, M. J., & Salkoff, D. B. (2015). Brain state dependent activity in the cortex and thalamus. *Current Opinion in Neurobiology*, *31*, 133–140. https://doi.org/https://doi.org/10.1016/j.conb.2014.10.003

McGinley, M. J., David, S. V., & McCormick, D. A. (2015). Cortical Membrane Potential Signature of Optimal States for Sensory Signal Detection. *Neuron*, *87*(1), 179–192. https://doi.org/10.1016/j.neuron.2015.05.038

Moore, T., & Armstrong, K. M. (2003). Selective gating of visual signals by microstimulation of frontal cortex. *Nature*, *421*(6921), 370–373. https://doi.org/10.1038/nature01341

Murphy, M. C., Chan, K. C., Kim, S.-G., & Vazquez, A. L. (2018). Macroscale variation in resting-state neuronal activity and connectivity assessed by simultaneous calcium imaging, hemodynamic imaging and electrophysiology. *NeuroImage*, *169*, 352–362. https://doi.org/https://doi.org/10.1016/j.neuroimage.2017.12.070

Musall, S., Kaufman, M. T., Juavinett, A. L., Gluf, S., & Churchland, A. K. (2019). Single-trial neural dynamics are dominated by richly varied movements. *Nature Neuroscience*, *22*(10), 1677–1686. https://doi.org/10.1038/s41593-019-0502-4

Niell, C. M., & Stryker, M. P. (2010). Modulation of Visual Responses by Behavioral State in Mouse Visual Cortex. *Neuron*, *65*(4), 472–479. https://doi.org/10.1016/j.neuron.2010.01.033

Ollerenshaw, D. R., Bari, B. A., Millard, D. C., Orr, L. E., Wang, Q., & Stanley, G. B. (2012). Detection of tactile inputs in the rat vibrissa pathway. *Journal of Neurophysiology*, *108*(2), 479–490. https://doi.org/10.1152/jn.00004.2012

Petersen, C. C. H., Grinvald, A., & Sakmann, B. (2003). Spatiotemporal Dynamics of Sensory Responses in Layer 2/3 of Rat Barrel Cortex Measured In Vivo by Voltage-Sensitive Dye Imaging Combined with Whole-Cell Voltage Recordings and Neuron Reconstructions. *The Journal of Neuroscience*, *23*(4), 1298 LP – 1309. https://doi.org/10.1523/JNEUROSCI.23-04-01298.2003

Poulet, J. F. A., Fernandez, L. M. J., Crochet, S., & Petersen, C. C. H. (2012). Thalamic control of cortical states. *Nature Neuroscience*, *15*(3), 370–372. https://doi.org/10.1038/nn.3035

Poulet, J. F. A., & Petersen, C. C. H. (2008). Internal brain state regulates membrane potential synchrony in barrel cortex of behaving mice. *Nature*, *454*(7206), 881–885. https://doi.org/10.1038/nature07150

Roitman, J. D., & Shadlen, M. N. (2002). Response of Neurons in the Lateral Intraparietal Area during a Combined Visual Discrimination Reaction Time Task. *The Journal of Neuroscience*, *22*(21), 9475 LP – 9489. https://doi.org/10.1523/JNEUROSCI.22-21-09475.2002

Rudolph, M., & Destexhe, A. (2003). A Fast-Conducting, Stochastic Integrative Mode for Neocortical Neurons InVivo

The Journal of Neuroscience, *23*(6), 2466 LP – 2476. https://doi.org/10.1523/JNEUROSCI.23-06-02466.2003

Sachdev, R. N. S., Ebner, F. F., & Wilson, C. J. (2004). Effect of Subthreshold Up and Down States on the Whisker-Evoked Response in Somatosensory Cortex. *Journal of Neurophysiology*, *92*(6), 3511–3521. https://doi.org/10.1152/jn.00347.2004

Sachidhanandam, S., Sreenivasan, V., Kyriakatos, A., Kremer, Y., & Petersen, C. C. H. (2013). Membrane potential correlates of sensory perception in mouse barrel cortex. *Nature Neuroscience*, *16*(11), 1671–1677. https://doi.org/10.1038/nn.3532

Salkoff, D. B., Zagha, E., McCarthy, E., & McCormick, D. A. (2020). Movement and Performance Explain Widespread Cortical Activity in a Visual Detection Task. *Cerebral Cortex*, *30*(1), 421–437. https://doi.org/10.1093/cercor/bhz206

Shimaoka, D., Harris, K. D., & Carandini, M. (2018). Effects of Arousal on Mouse Sensory Cortex Depend on Modality. *Cell Reports*, *22*(12), 3160–3167. https://doi.org/10.1016/j.celrep.2018.02.092

Shu, Y., Hasenstaub, A., Badoual, M., Bal, T., & McCormick, D. A. (2003). Barrages of Synaptic Activity Control the Gain and Sensitivity of Cortical Neurons. *The Journal of Neuroscience*, *23*(32), 10388 LP – 10401. https://doi.org/10.1523/JNEUROSCI.23-32-10388.2003

Stringer, C., Pachitariu, M., Steinmetz, N., Reddy, C. B., Carandini, M., & Harris, K. D. (2019). Spontaneous behaviors drive multidimensional, brainwide activity. *Science*, *364*(6437), eaav7893. https://doi.org/10.1126/science.aav7893

van Kempen, J., Gieselmann, M. A., Boyd, M., Steinmetz, N. A., Moore, T., Engel, T. A., & Thiele, A. (2021). Top-down coordination of local cortical state during selective attention. *Neuron*, *109*(5), 894-904.e8. https://doi.org/10.1016/j.neuron.2020.12.013

Yang, H., Kwon, S. E., Severson, K. S., & O'Connor, D. H. (2016). Origins of choice-related activity in mouse somatosensory cortex. *Nature Neuroscience*, *19*(1), 127–134. https://doi.org/10.1038/nn.4183

Zagha, E., & McCormick, D. A. (2014). Neural control of brain state. *Current Opinion in Neurobiology*, *29*, 178–186. https://doi.org/https://doi.org/10.1016/j.conb.2014.09.010

Zareian, B., Zhang, Z., & Zagha, E. (2021). Cortical localization of the sensory-motor transformation in a whisker detection task in mice. *eNeuro*, *8*(1), 1–14. https://doi.org/10.1523/ENEURO.0004-21.2021

Figures and Legends

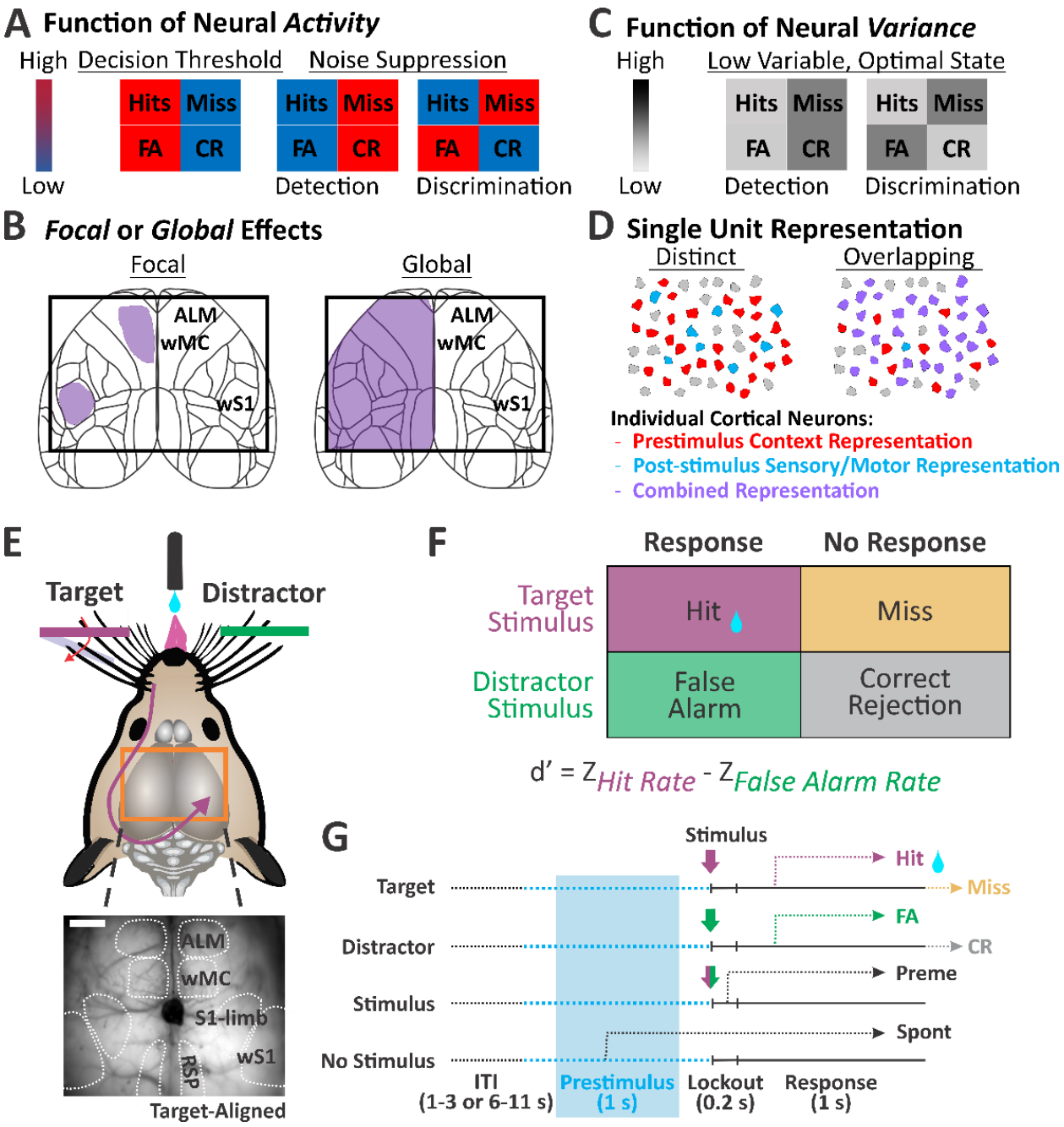

Figure 1: Predictions and experimental design for testing impacts of prestimulus activity on sensory detection and discrimination. (A-D) Potential mechanisms of task-relevant prestimulus activity. (E-G) Experimental design. (E). Head-fixed mice are trained to discriminate between target whisker deflections (purple) and distractor whisker deflections (green), within opposite whisker fields. Mice report detection by licking a central lickport. The orange rectangle reflects the widefield Ca^{2+} imaging window. The inset below is a sample imaging frame, demarcating neocortical regions of interest in bilateral frontal and parietal cortices. (F) Classification of trial types and outcomes. Task performance is quantified by discrimination d' as the separation between hit and false alarm rates. z, inverse cumulative function of the normal distribution. G. Trial structure, including a variable inter-trial interval, 1 s prestimulus window, 0.2 s stimulus and lockout (delay) window, and 1 s response window. The prestimulus window of interest in this study is the last 1 s of the inter-trial interval (blue shade), immediately before stimulus onset. Spont, spontaneous responses during the prestimulus window; Preme, premature responses during the lockout window. Scale bar in (E) is 1 mm.

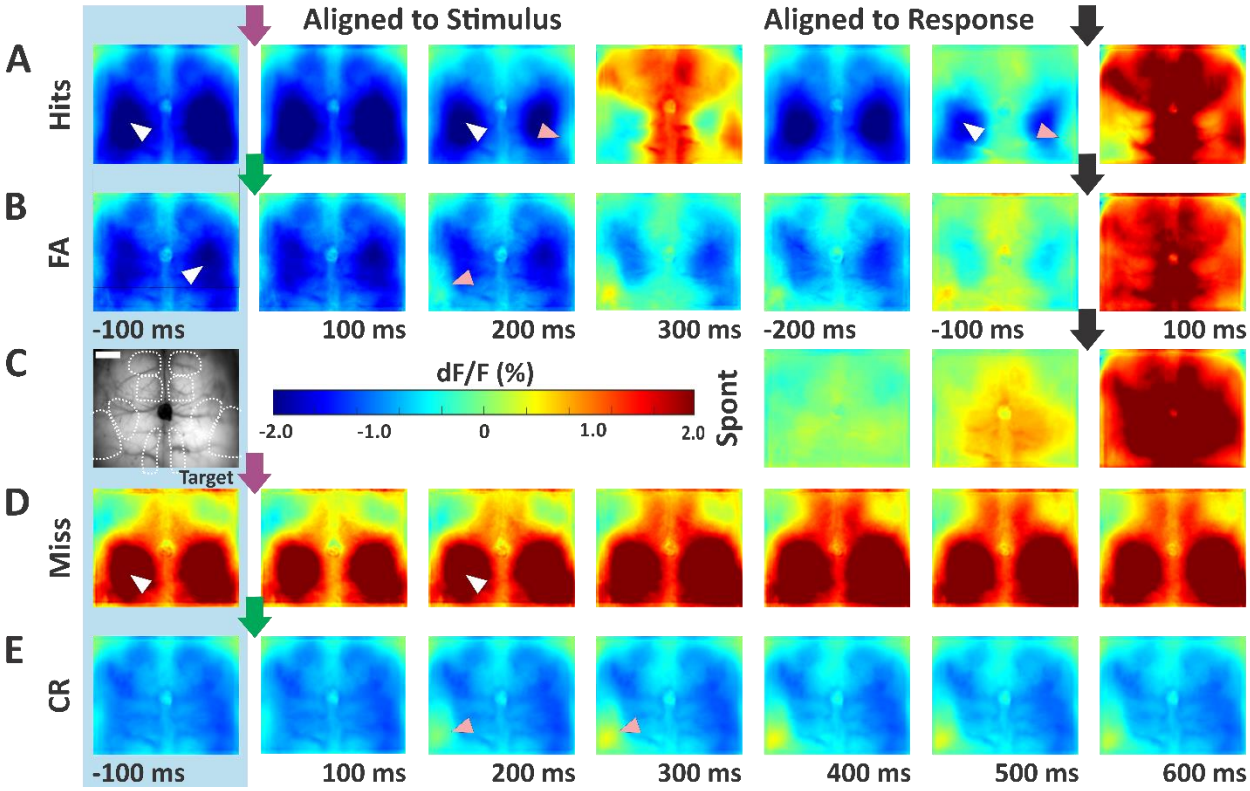

Figure 2: Sliding window normalized grand average fluorescence activity (dF/F). Data are averages across all mice and all sessions (n=38 sessions). Activity in specific imaging frames is aligned to the stimulus onset (left, purple and green arrows for target and distractor stimuli, respectively) or response onset (right, black arrows, in rows A, B, and C). Warmer colors indicate higher activity. The pink arrowheads specify stimulus-aligned whisker regions of S1, whereas the white arrowheads specify limb regions of S1 (see atlas in leftmost panel in row C). The last prestimulus frame is shown in the first column (blue shade). Shown are hit trials (A), false alarm trials (B), spontaneous trials (C), miss trials (D), and correct rejection trials (E). Note the low (negative due to normalization) dF/F prestimulus activity in response trials (hit and false alarm), compared to the high dF/F prestimulus activity in miss trials. Scale bar in (C) is 1 mm.

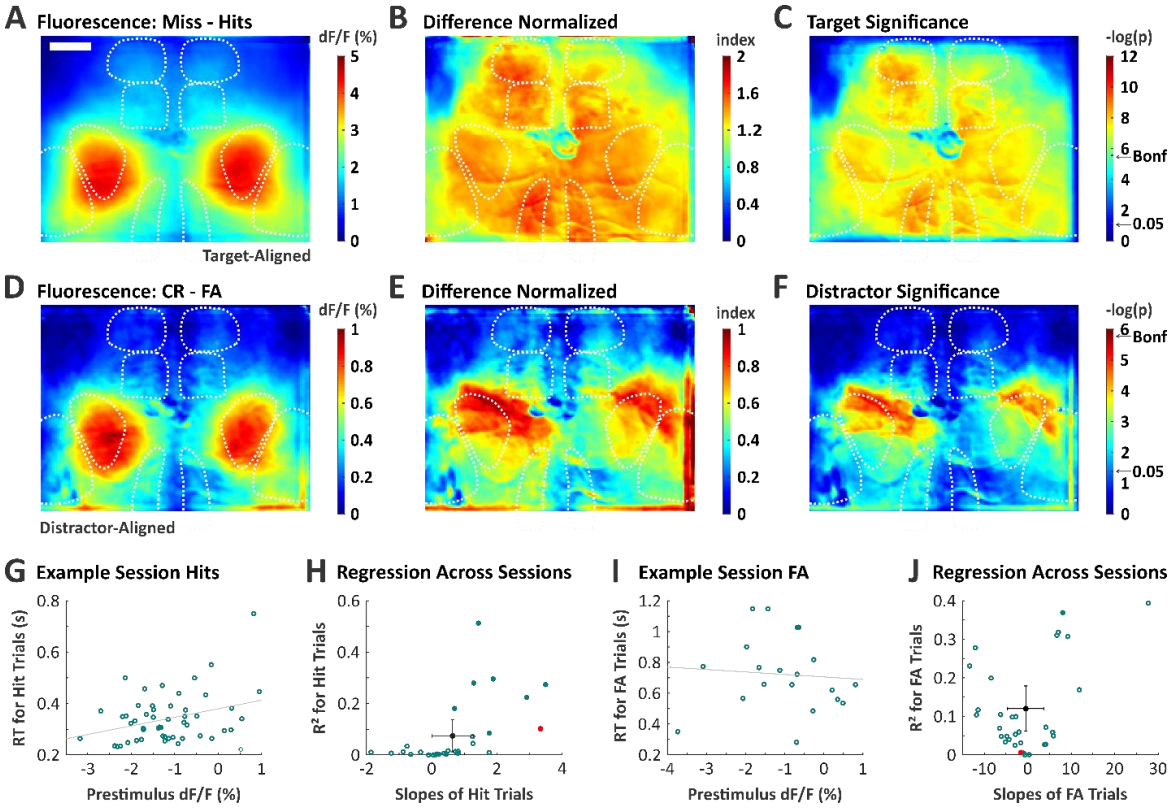

Figure 3: Prestimulus neuronal activity differences between response and no response trials and correlations with reaction time. (A) Grand average of prestimulus dF/F for miss minus hit trials. All pixel values within neocortex are greater than 0, indicating higher global activity preceding miss trials. (B) Similar to [A], except that the individual session dF/F signals were further normalized by z-score to control for differences in fluorescence fluctuations. (C) Significance map for the data in [A]. Significance threshold with Bonferroni correction for multiple comparisons is indicated by the arrow (Bonf). For target trials, higher activity preceding no response trials is statistically significant throughout dorsal cortex. (D-F) Same structure as [A-C], except for CR minus FA trials. Note the more restricted range of scale bars in each panel, compared to target data. For distractor trials, higher activity preceding no response trials is marginally significant, most prominent in the S1 limb regions. Scale bar in (A) is 1 mm. (G) An example session showing a positive correlation between prestimulus activity (dF/F) and reaction time for individual Hit trials (slope=3.34, R^2=0.10, dotted line is the linear regression). (H) Regression analyses across all sessions for Hit trials. The red data point is the example session in [G], the black data reflect the mean ± standard deviation across sessions (n=30 sessions). (I) FA trials in an example session, with a non-significant negative correlation between prestimulus activity and reaction time (slope=-1.6, R^2=0.006). (J) Same as H but for FA trials (n=32 sessions).

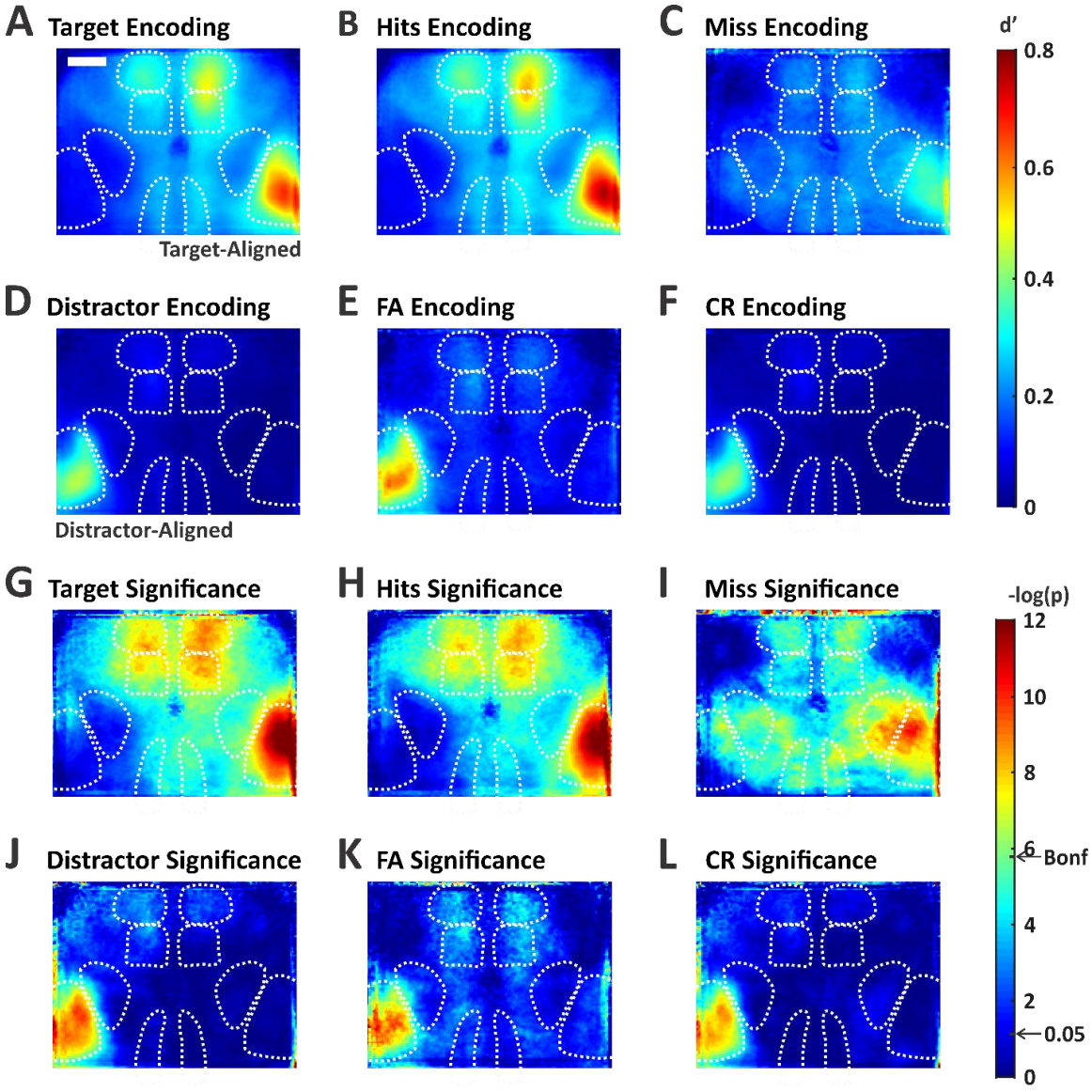

Figure 4: Quantification of stimulus encoding for each trial type. (A-F) Neurometric d' values were calculated for each pixel during the last frame of the lockout: after stimulus presentation and before the allowed response window. Data are grand average d' maps from all sessions, showing all target trials (A), hit trials (B), miss trials (C), all distractor trials (D), FA trials (E), and CR trials (F). Note the larger stimulus encoding in response trials (B and E compared to C and F). Significance maps of the data in [A-F], respectively. Significance threshold with Bonferroni correction for multiple comparisons is indicated by the arrow (Bonf). For all trial types there is significant stimulus encoding in the stimulus-aligned S1 whisker region. Scale bar in (A) is 1 mm.

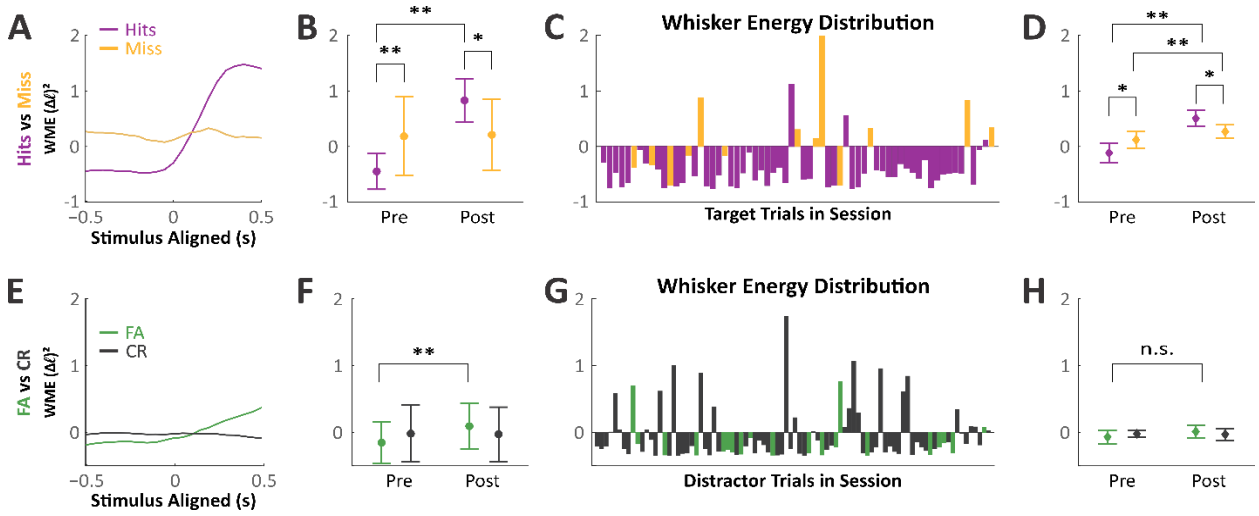

Figure 5: Prestimulus and post-stimulus whisker movements in each trial type. (A) Peristimulus whisker motion energy (WME) on target trials in an example session, hits (purple) and misses (orange). On hits trials there was a dramatic increase in WME post-stimulus and during the response window. Prestimulus, however, WME on hits trials was reduced compared to miss trials. (B) Quantification of data in [A], comparing prestimulus (pre) and post-stimulus WME for hit and miss trials. (C) Prestimulus WME values for each trial in the example session. (D) Summary data for all sessions (n=9). Note the reduced WME preceding hit compared to miss trials. (E-H) Same as above, but for distractor trials. While this example session shows moderately reduced WME preceding false alarm trials (E-G), this trend was not statistically significant across the full dataset (H). Data are presented as mean +/- STD, *p<0.05, **p<0.005.

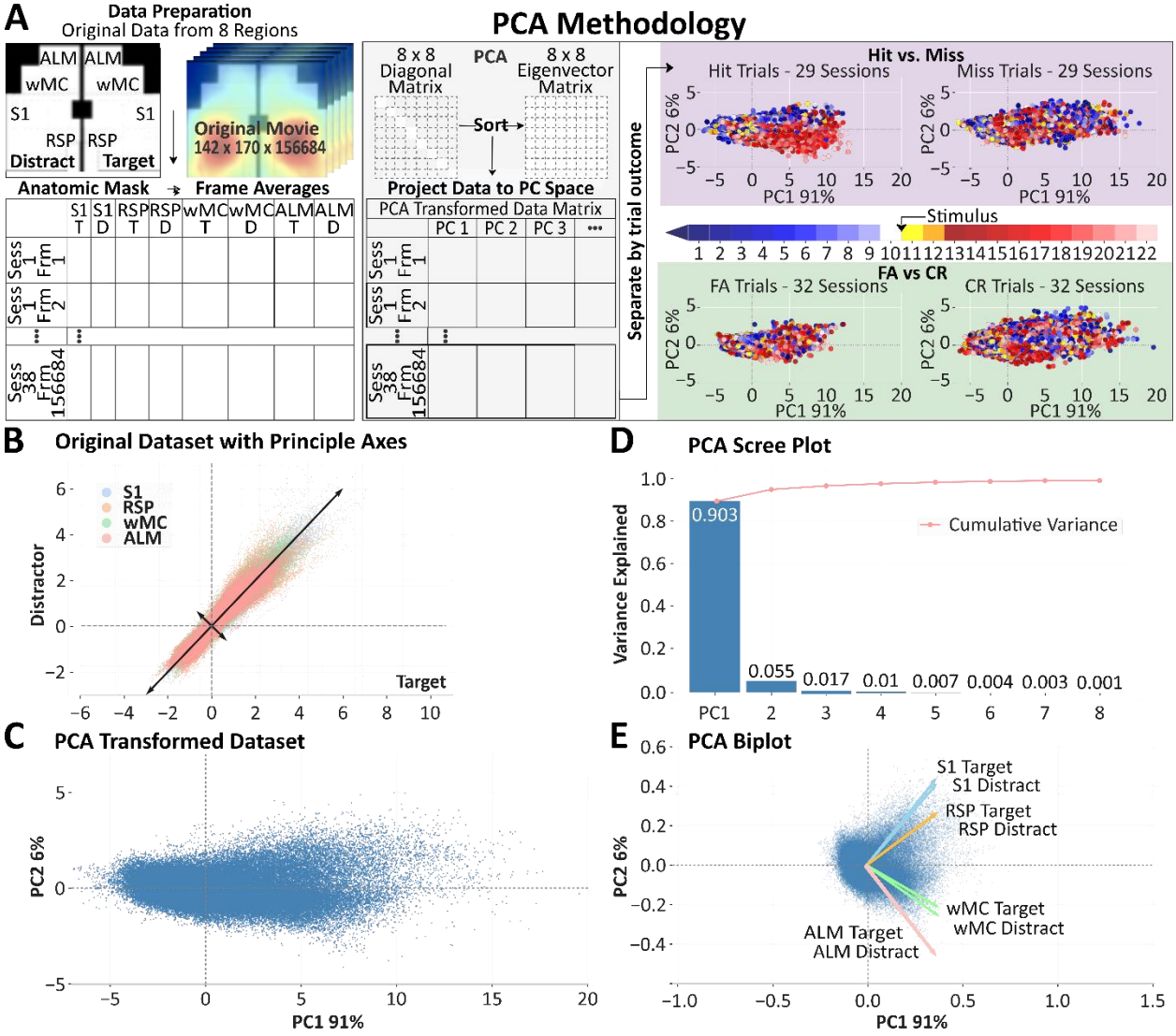
A
Data Preparation
Original Data from 8 Regions
PCA Methodology
ALM
wMC
S1
RSP
Distract
Target
Original Movie
142 x 170 x 156684
Anatomic Mask
Frame Averages
8 x 8 Diagonal Matrix
PCA
8 x 8 Eigenvector Matrix
Sort
Project Data to PC Space
PCA Transformed Data Matrix
PC 1
PC 2
PC 3
Separate by trial outcome
Hit vs. Miss
Hit Trials - 29 Sessions
Miss Trials - 29 Sessions
PC2 6%
PC1 91%
Stimulus
FA vs CR
FA Trials - 32 Sessions
CR Trials - 32 Sessions
B
Original Dataset with Principle Axes
S1
RSP
wMC
ALM
Distractor
Target
C
PCA Transformed Dataset
PC2 6%
PC1 91%
D
PCA Scree Plot
Variance Explained
Cumulative Variance
0.903
0.055
0.017
0.01
0.007
0.004
0.003
0.001
PC1
E
PCA Biplot
S1 Target
S1 Distract
RSP Target
RSP Distract
wMC Target
wMC Distract
ALM Target
ALM Distract
PC2 6%
PC1 91%

Figure 6: Spatial dimensionality reduction for single trial analyses. (A) Methodology for using principal component analysis (PCA) to reduce spatial dimensionality. Left, full images were parsed into 8 regional masks. Average dF/F within each mask for all trials and all sessions were appended into a single matrix, upon which PCA was performed. Right, frames with different trial outcomes were back-projected to the first principal component (PC1) and plotted against their projection onto the second principal component (PC2). Transformed samples are colored based on their frame index: prestimulus (blue to white), post-stimulus and pre-response (yellow and orange), response (red to pink). (B) Original dataset, each data point represents a sample frame ROI-specific average, plotted against its change in fluorescence (dF/F) between target (x-axis) and distractor (y-axis) hemispheres. Black arrows represent the first two principal vectors. (C) Transformed dataset, each data point represents a sample frame plotted against its projection onto PC1 and PC2. (D) PCA scree plot. PCs are plotted according to their rank in variance, with accumulated variance plotted in red. The first two PCs were chosen for further analysis as they explain >95% variance of the untransformed dataset (PC1, 91%, PC2, 6%). (E) PCA biplot. Samples plotted against their normalized projection onto PC1 and PC2, with vectors representing individual ROIs according to their loadings.

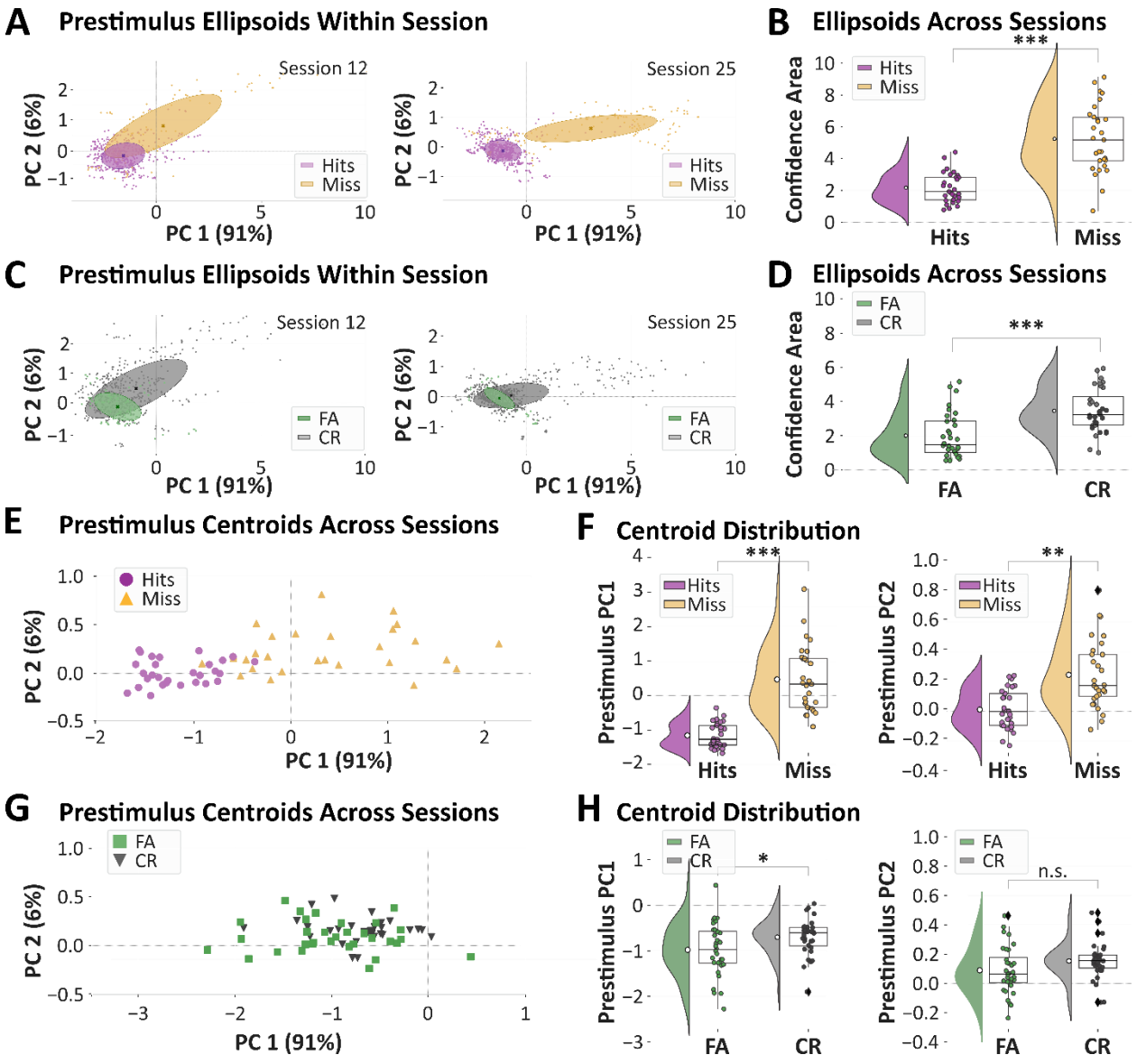
A
Prestimulus Ellipsoids Within Session
Session 12
Session 25
PC 2 (6%)
PC 1 (91%)
Hits
Miss
B
Ellipsoids Across Sessions
Confidence Area
***
C
Prestimulus Ellipsoids Within Session
FA
CR
D
Ellipsoids Across Sessions
E
Prestimulus Centroids Across Sessions
F
Centroid Distribution
Prestimulus PC1
Prestimulus PC2
**
G
Prestimulus Centroids Across Sessions
H
Centroid Distribution
*
n.s.

Figure 7: Single trial analyses of prestimulus subspace variance and position according to trial outcomes. All data presented are from the last 500 ms of the prestimulus window (frames 6 to 10 of Figure 6A). (A) Prestimulus activity in PC space for hit (purple) and miss (yellow) trials of two example sessions. Each data point represents a single prestimulus frame. Overlaid are covariance ellipses for both trial outcome types (major radius, 1σ along PC1; minor radius, 1σ along PC2). Note the reduced area and distinct position of the covariance ellipses for hit compared to miss trials. (B) Comparison of the ellipse area, as a measure of variability, across all sessions. (C and D) Same as [A] and [B], except for FA (green) and CR (gray) trials. Response trials (hit and FA) are preceded by less variable prestimulus activity compared to no response trials (miss and CR). (E) Centroid positions of the covariance ellipses in PC space for all sessions, for hit and miss trials (same color designation as above). Each data point represents the hit or miss centroid from one session. (F) Quantification of centroid positions on axes PC1 (left) and PC2 (right). (G and H) Same as [E] and [F], except for FA and CR trials. Prestimulus activity occupies distinct subspaces for response and no response trials, along both PC1 and PC2 for target trials and along PC 1 for distractor trials. *p<0. 01; **p<0.001; ***p<0.0001; n.s., non-significant.

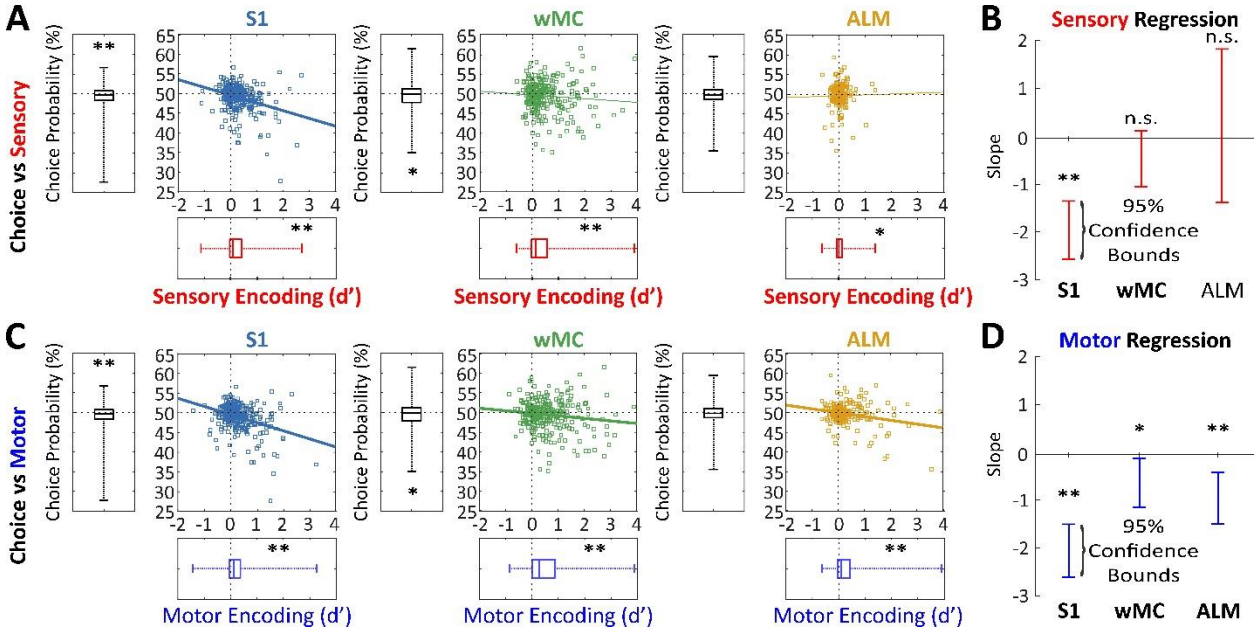

Figure 8: Distribution of prestimulus choice probability, post-stimulus sensory, and pre-response motor encoding across single units in S1, wMC and ALM. (A) Plots of sensory encoding (d') versus choice probability (%) for single units in target-aligned S1 (left), wMC (center), and ALM (right). Asterisks above box plots reflect comparisons of individual measures to chance (d'=0 and choice probability=50%). Scatter plots include linear fits of the single unit data. Single units in each of these three cortical regions show below chance prestimulus choice probability (tending yet not significant for ALM (p=0.06), significant for S1 and wMC) and positive post-stimulus sensory encoding. (B) 95% confidence bounds of the linear regression slope values. (C and D) Same as [A] and [B], but for pre-response motor encoding. The significant negative slope values indicate an overlap between the single units with lower than chance prestimulus choice probability and positive post-stimulus sensory encoding (for S1) and pre-response motor encoding (for S1, wMC, and ALM). *p<0.05; **p<0.005; n.s., non-significant.

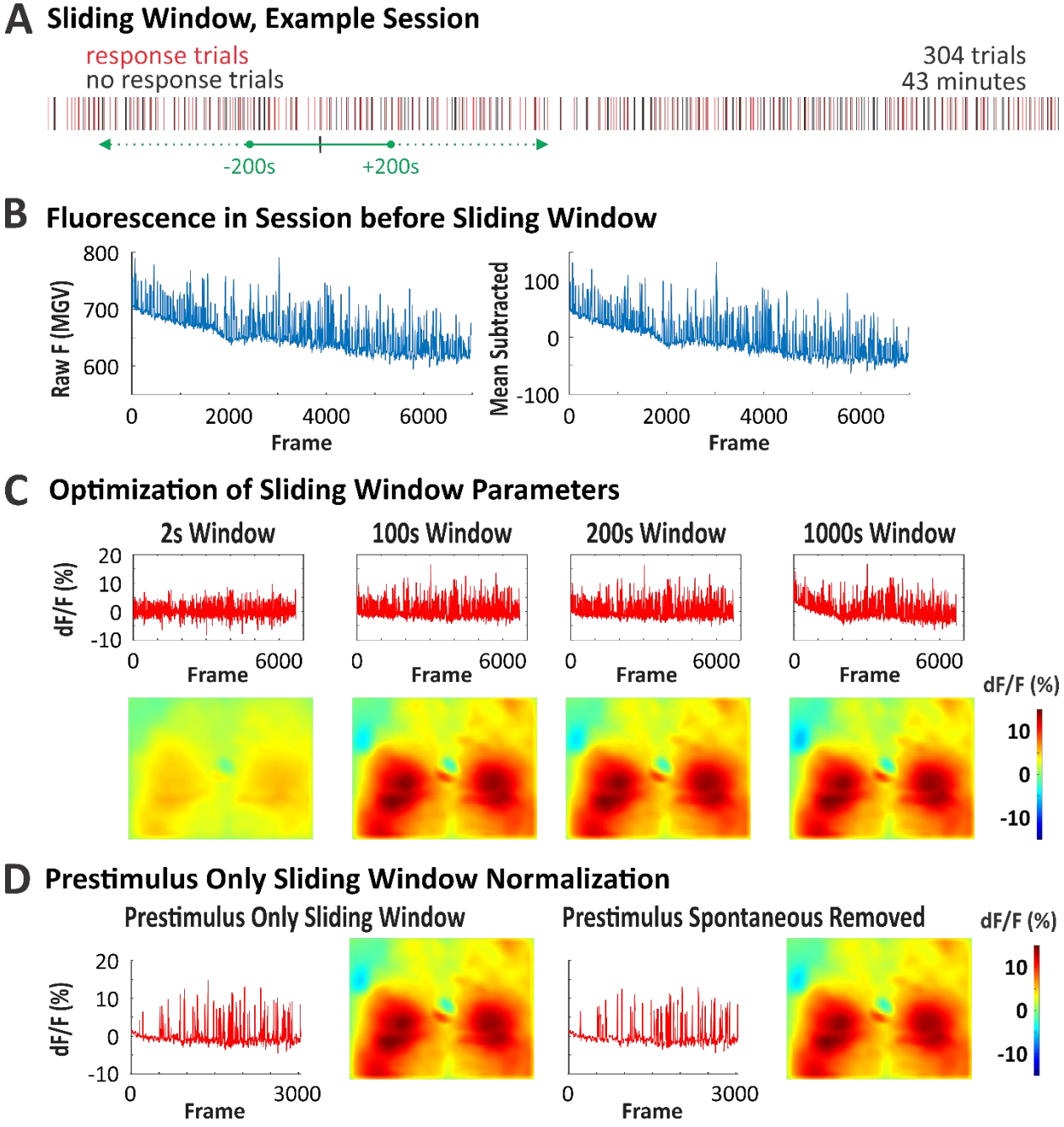
A Sliding Window, Example Session
response trials
no response trials
304 trials
43 minutes
-200s
+200s
B Fluorescence in Session before Sliding Window
Raw F (MGV)
800
700
600
0
2000
4000
6000
Frame
Mean Subtracted
100
0
-100
0
2000
4000
6000
Frame
C Optimization of Sliding Window Parameters
2s Window
100s Window
200s Window
1000s Window
dF/F (%)
20
10
0
-10
0
Frame
6000
dF/F (%)
10
0
-10
D Prestimulus Only Sliding Window Normalization
Prestimulus Only Sliding Window
Prestimulus Spontaneous Removed
dF/F (%)
20
10
0
-10
0
Frame
3000
dF/F (%)
10
0
-10

Supplemental Figure 1, Related to Methods, Figures 1-3: Sliding window normalization method and robustness of window size. (A) Depiction of response trials (red), no response trials (black) and sliding window (green) used for an example session. This session consisted of 304 trials over 43.4 minutes. Each sliding window segment included an average of 46 trials. (B) Rundown in raw fluorescence per frame and mean subtracted raw fluorescence per frame acquired across example session. (C) Different sliding windows considered for optimization of method used in this study. Top row: dF/F using a sliding window every 2s; 2s half-width (far left), 100s half-width (center left), 200s half-width (center right), 1000s half-width (far right). Bottom row: Mean to Hits difference using sliding window indicated in top row. This normalization method is robust to a range of sliding window sizes, between 50s to 200s. If the window is too small (left) single trial differences are normalized out. If the window is too large (right) fluorescence rundown is not corrected. (D) Sliding window method (200s) applied to prestimulus frames only and applied to prestimulus frames with spontaneous trials removed. Left to right: dF/F per frame across prestimulus frames in example session (far left), Miss to Hits difference using only prestimulus frames (left center), dF/F per frame across prestimulus frames, spontaneous trials removed, in example session (right center), Miss to Hits difference using prestimulus frames, spontaneous trials removed (far right). Excluding post-stimulus frames and spontaneous trials does not impact our sliding window prestimulus analyses.

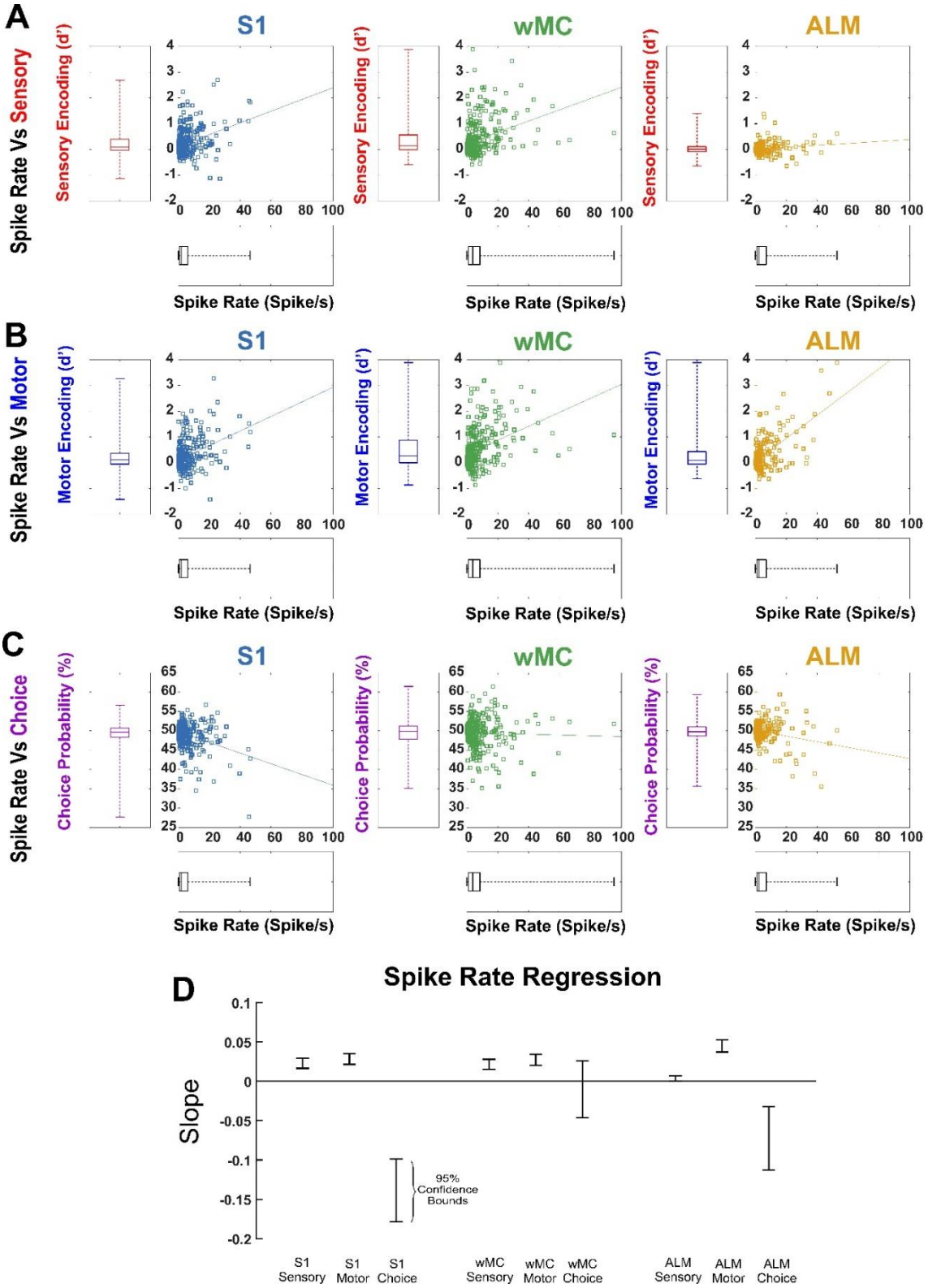
A
Spike Rate Vs Sensory
S1
wMC
ALM
Sensory Encoding (d')
Spike Rate (Spike/s)
B
Spike Rate Vs Motor
Motor Encoding (d')
C
Spike Rate Vs Choice
Choice Probability (%)
D
Spike Rate Regression
Slope
95% Confidence Bounds
S1 Sensory
S1 Motor
S1 Choice
wMC Sensory
wMC Motor
wMC Choice
ALM Sensory
ALM Motor
ALM Choice

Supplemental Figure 2, Related to Figure 8: Relationship between spike rate and prestimulus choice probability and post-stimulus sensory and pre-response motor encoding across single units in S1, wMC and ALM. (A) Plots of sensory encoding (d') versus spike rate (Hz) for single units in target-aligned S1 (left), wMC (center), and ALM (right). Scatter plots include linear fits of the single unit data. Single units in each of these three cortical regions show positive relationship between spike rate and post-stimulus sensory encoding. (B and C) Same as [A], but for pre-response motor encoding (B) and prestimulus choice probability (C). (D) 95% confidence bounds of the linear regression slope values for all scatter plots. These data identify spike rate as a common factor that correlates with both post-stimulus sensory and motor encoding (positive correlation) and prestimulus choice probability (negative correlation).

Chapter 4

Correlation of behavioral measures and neural modulations in dorsal cortex across learning of a selective whisker detection task in mice

Introduction

The optimal performance of a motor task hinges on the ability to learn and accurately respond to certain stimuli while disregarding others, as exemplified in a simple go/no-go task. In the context of mice mastering the whisker selective detection task, we anticipate cortical activation to undergo changes in tandem with behavioral modifications related to both sensory and motor events. While previous research on rodents has predominantly implicated changes in the motor cortex to underlie motor skill learning and execution (Kawai et al., 2015; Komiyama et al., 2010; Laubach et al., 2000; Peters et al., 2017) and changes in sensory cortex to underlie sensory detection (Huber et al., 2012b) and sensory discrimination (Pai et al., 2011; Rudebeck & Murray, 2008), extensive research has demonstrated the challenges of categorizing brain regions strictly into sensory and motor systems. Traditionally considered motor areas have been found to exhibit sensory receptive fields (di Pellegrino et al., 1992; J. T. Murphy et al., 1978) and neural activity associated with sensory decision-making (Romo et al., 2002, 2004). Motor experience can induce selective expansions in sensory regions of the brain (Xerri et al., 1996). Moreover, alterations in motor function have been shown to impact the processing of visual (Brown et al., 2007), acoustic (Shiller et al., 2009), and

proprioceptive stimuli (Cressman & Henriques, 2010), highlighting the intricate interaction between motor and sensory systems within the brain.

Consequently, we set out to test two hypotheses: 1) learning in a selective detection task involves cortex-wide alterations in sensory and motor regions, and 2) changes in the learning of specific behavioral measures can be attributed to distinct cortical modulations. This exploration was anticipated to yield multiple hypotheses regarding the neural mechanisms underpinning the acquisition of diverse behavioral processes within a singular task.

We conducted widefield calcium imaging throughout the learning phase of the selective detection behavioral paradigm. Pixel-wise correlation maps of neural activation were generated to identify patterns that correlated with changes in behavioral measures. Our findings revealed that the learning process encompasses extensive neocortical changes as mice progress to expert-level performance in the task.

Materials and Methods

Animals and Surgery

All experiments conducted in this study received approval from the Institutional Animal Care and Use Committee (IACUC) of the University of California, Riverside. Mice utilized in the study were procured from Jackson Laboratories (JAX). Neural imaging data related to the task were derived from mice expressing GCaMP6s under the Snap25-2A-GCaMP6s-D promoter (JAX #025111). The SNAP25-2A-

GCaMP6s mouse line expresses GCaMP6s pan-neuronally, encompassing both excitatory and inhibitory neurons throughout the brain (Madisen et al., 2015). Transgenic mice were backcrossed into the BALB/cByJ background (JAX 000651). Both male and female mice participated in the experiments.

Mice were housed in a controlled environment with a 12-hour light/12-hour dark cycle. All training and recordings were conducted with mice securely head-fixed in the behavioral apparatus. Headpost implantation was performed on mice aged between 2 to 5 months under anesthesia induced by a combination of isoflurane (1-2%), ketamine (100 mg/kg), and xylazine (10 mg/kg). A 10 mm x 10 mm section of the scalp was removed to expose the skull. The exposed skull was cleared of connective tissue, and a custom-built headpost (made of lightweight titanium or stainless steel, measuring 3 cm in length and weighing 1.5 grams) was affixed to the skull with cyanoacrylate glue. The headpost featured a 5 mm x 7 mm central window for imaging and recording.

For in vivo widefield Ca2+ imaging, a thin layer of cyanoacrylate gap-filling medium (Insta-Cure, Bob Smith Industries) was applied to the window to seal the exposed skull and enhance skull transparency. Silicone elastomer (Reynolds Advanced Materials) was additionally applied above the imaging window. Post-surgery, mice were placed on a heating pad for recovery and administered meloxicam (0.3 mg/kg) and enrofloxacin (5 mg/kg) for three days. Mice were given a minimum of three days to recover from surgery before undergoing water restriction and

behavioral training. Recordings under anesthesia were conducted immediately after headpost implantation.

Animal Behavior

The training stages, learning metrics, and criteria for expert performance in the Go/NoGo selective whisker detection task were previously detailed in our previous works (Aruljothi et al., 2020; Marrero et al., 2022; Zareian et al., 2021b, 2023; Zhang & Zagha, 2023). In summary, mice, fixed in a head restraint and subjected to water deprivation, were positioned on a behavioral apparatus governed by Arduino and custom MATLAB scripts. Two paddles were strategically located in whisker fields on opposite sides of the face, designated as either target or distractor. These designations were established at the onset of training and remained fixed.

After variable intertrial intervals, mice encountered target trials (involving a rapid deflection of the target paddle), distractor trials (involving a rapid deflection of the distractor paddle) or catch trials (involving no whisker stimulus). Mice expressed their responses through licking at a central port. Hits (responses to target stimuli) resulted in a reward of approximately 5 μL of water. Correct rejections (non-responses to distractor stimuli) and correct withholdings (non-responses during catch trials) were rewarded with a shortened intertrial interval (ITI) and a subsequent target trial.

Licking during the ITI incurred a penalty, resetting the ITI and acting as a time-out. Mice achieved expert status upon maintaining a discriminability (d') greater than 1 (indicating a distinction between hit and false alarm response rates) for three consecutive days:

$$discriminability\ d' = \phi^{-1}_{Hit\ rate} - \phi^{-1}_{False\ alarm\ rate}$$

Widefield Calcium Imaging

Widefield imaging in head-fixed mice performing the selective detection task was conducted through-skull. The imaging setup utilized a Macroscope IIa (RedShirtImaging) with the beam diverter removed, a 75 mm inverted lens featuring 0.7x magnification and a 16 mm working distance. The lens (NA 0.4) was directly positioned over the cranial window, providing a field of view measuring 7 mm x 5 mm, encompassing most of the dorsal parietal and frontal cortex on both sides.

Illumination was achieved using a mounted 470 nm LED (Thorlabs M470L3), dispersed through a collimating lens (Thorlabs ACL2520-A), band-pass filtered (Chroma ET480/40x), and directed through the macroscope using a dichroic mirror (Chroma T510lpxrxt). Fluorescent light returning from the brain underwent band-pass filtering (Chroma ET535/50m) before reaching an RT sCMOS camera (SPOT Imaging). Employing on-camera 2x2 binning and post-processing image size reduction, the final resolution was 142 x 170 pixels at 41 μm per pixel with a 12-bit

depth. Image acquisition occurred at a temporal resolution of 10 Hz, synchronized with the trial structure. TIF image sequences were imported into MATLAB for preprocessing and subsequent analysis.

Data Analysis

Data analyses were performed in MATLAB using custom scripts.

Behavioral learning analyses

Behavioral analyses were performed and reported in our latest publication (Marrero et al., 2023). Scatter plots were generated, where each point represented individual mouse sessions across mice (n=52 mice). The means were depicted as mouse sessions, resampled to 20 sessions per mouse, and then averaged across all mice (n=52 mice). Transitions are considered 'increasing' if the slopes across mice were significantly positive and as 'decreasing' if the slopes were significantly negative. These measures were considered to have a monotonic transition across learning. If slopes of the behavioral measures first showed an increase and then a decrease across learning, then these measures were considered to have a biphasic transition across learning. In this chapter, we focused on five out of the 11 measures, selecting them based on their dependence on trial types. Specifically, for target trials, we opted for hit rate and target reaction times as behavioral measures reflecting pure target responses. For distract trials, we selected false alarm rate as a behavioral measure representing pure distractor responses. Additionally, as measures encompassing both target and distractor trials, we

included discrimination d' and wait AUC, which gauges the mice's ability to withhold licking during the inter-trial interval (ITI) period.

Sliding Window Normalization and Trial-Based Neuronal Activity

The imaging time window for each trial comprised the prestimulus epoch (1 s), the stimulus and lockout epoch (0.2 s), and the allowable response epoch (1 s), totaling 2.2 s. A raw movie F was constructed by concatenating fluorescence activity from consecutive trials, where Fn(i,j,f) represents the fluorescence of each pixel (row i and column j) in frame f for each trial n. To obtain normalized fluorescence values, we initially determined the sliding window local mean for each pixel, calculated every 2 s using a +/- 200 s window size [FSW(i,j,n)]. Subsequently, we computed the normalized fluorescence (following the method of Salkoff et al., 2020) for each pixel at each frame as follows:

$$dF_{SW}/F_{SW}(i,j,n) = [F_n(i,j,f) - F_{SW}(i,j,n)]/F_{SW}(i,j,n)$$

Average movies were created by initially categorizing stimulus type (target and distractor trials), followed by averaging pixel-wise activity across corresponding frames of the respective trials. The resulting averages were then aligned to bregma.

Difference in Prestimulus Fluorescence

Fluorescence variations for target and distractor categorization were computed for each trial type in every session. The prestimulus frames 6 to 10, encompassing

the final 500 ms of the prestimulus window before stimulus onset, were averaged on a per-trial and per-pixel basis for each session. Sessions with fewer than 5 incorrect trials were excluded from this analysis. For target fluorescence difference frames, the mean frame of Hits fluorescence was subtracted from the mean frame of Miss fluorescence.

Defining Cortical Regions of Interest

For both task-relevant and task-irrelevant cortical regions, we established a center pixel based on the pixel resolution (41 μm) and alignment with bregma, calculated as center pixel value = [coordinates from bregma (in mm)]/0.041 mm. This allowed the conversion of bregma-based coordinates (mm) [wS1 ±3.4 lateral, 1.4 posterior; wM1 ±1 lateral, 1 anterior; ALM ±1.5 lateral, 2.5 anterior; RSP ±0.4 lateral, 2.4 posterior; limb S1 ±2.0 lateral, 0.6 posterior] to coordinates from bregma in pixels. The coordinates and wires were adapted from the Allen Brain Institute's common coordinates framework (CCF) (Wang et al., 2020).

Stimulus Encoding in Post-Stimulus Fluorescence

The quantification of stimulus encoding involved calculating the neurometric d' (Britten et al., 1992) for prestimulus fluorescence (stimulus absent) and post-stimulus fluorescence (stimulus present) for one frame after the lockout epoch (200- 300ms from stimulus onset), adapted from the methodology previously applied to imaging data (Aruljothi et al., 2020c; Marrero et al., 2022). Neurometric d' was computed separately based on target and distractor assignment and further

categorized according to trial type outcome. Prestimulus and post-stimulus fluorescence histograms were translated into receiver operating characteristic (ROC) curves, and the area under the curve (AUC) was transformed into d' as the neurometric measure.

$$fluorescence\ d'_{Stimulus} = \sqrt{2} * Z_{AUC}$$

The neurometric d' was computed separately for naïve and expert days, considering the average of the last three days, for all six mice trained in the task. The stimulus encoding average for naïve days was subsequently subtracted from that of the expert days, with alignment to the bregma.

Statistical Analyses

For imaging statistics, threshold for statistical significance was set at a confidence interval of 99% (α = 0.01). For all dF/F, dF/F differences (Miss–Hits) and d', statistical analyses determined whether each pixel of the frames were significantly different than zero across sessions (one sample t-test).

Results

Sensory-motor attenuation of distractor trials in distractor-aligned hemisphere occurs out of S1:

To address whether the attenuation of distractor-aligned sensory-motor propagation is a result of target selection or distractor inhibition, we conducted neural encoding analyses following the methodologies outlined in chapters 2 and 3. One potential scenario is that, in naïve mice, both target and distractor sensory cortical signals propagate to the frontal cortices, and attenuation emerges through the process of distractor inhibition as mice learn to achieve expert performance. Specifically, the propagation from distractor VPM to sensory cortex and sensory cortex to motor cortex signals are inhibited, while target signal propagation remains unaffected. Alternatively, the hypothesis posits that, in naïve mice, neither target nor distractor sensory cortical signals propagate to frontal cortices. Instead, the emergence of attenuation occurs through a process of target selection during learning, where, in expert mice, target VPM and sensory cortical signals propagate to the frontal cortex while distractor signals do not.

For this analysis, we averaged the data from the first frame following the lockout period, excluding trials with reaction times less than 300 ms. This selection is made because this specific frame exhibits a robust sensory and sensory-motor propagation signal compared to the last frame of the lockout period. The average of this frame across mice reveals that, in naïve mice, both target and distractor

trials exhibit clear sensory cortex to motor cortex propagation (Figure 1A *left* and Figure 1B *left*). With learning, the sensory cortex to motor cortex propagation remains unchanged in target trials, while in distractor trials, sensory cortex to motor cortex propagation undergoes significant reduction (Figure 1A *right* and Figure 1B *right*). Based on this observation, the hypothesis that attenuation arises through the process of distractor inhibition during learning is supported. Consequently, our observations lead us to conclude that there is a consistent reduction in S1 and wM1 activation with learning in the distractor hemisphere for distractor trials. This observation is further validated through the subtraction of the average naive neural d' from the average expert neural d' across all six mice (n=6) [Figure 1C]. The heat maps for both target and distractor trials were generated across each pixel using a one-sample t-test with $\alpha = 0.01$ ($-\log10(p)=1$ on significance maps). The heat map for target trials indicates a noteworthy trend toward activation in the preferred tjMC, bilateral ALM, the cortical areas associated with licking. Conversely, for distractor trials, the heat map demonstrates a pronounced suppression in the preferred wS1, wM1, and bilateral ALM and limb S1, indicating attenuation in the sensory cortex to motor cortex propagation and to other projection areas. (figure 1D). While the target trials show a process of sensory selection (enhancement) downstream of cortical whisker regions, distractor trials show the suppression of sensory-motor propagation (attenuation) within cortical whisker regions.

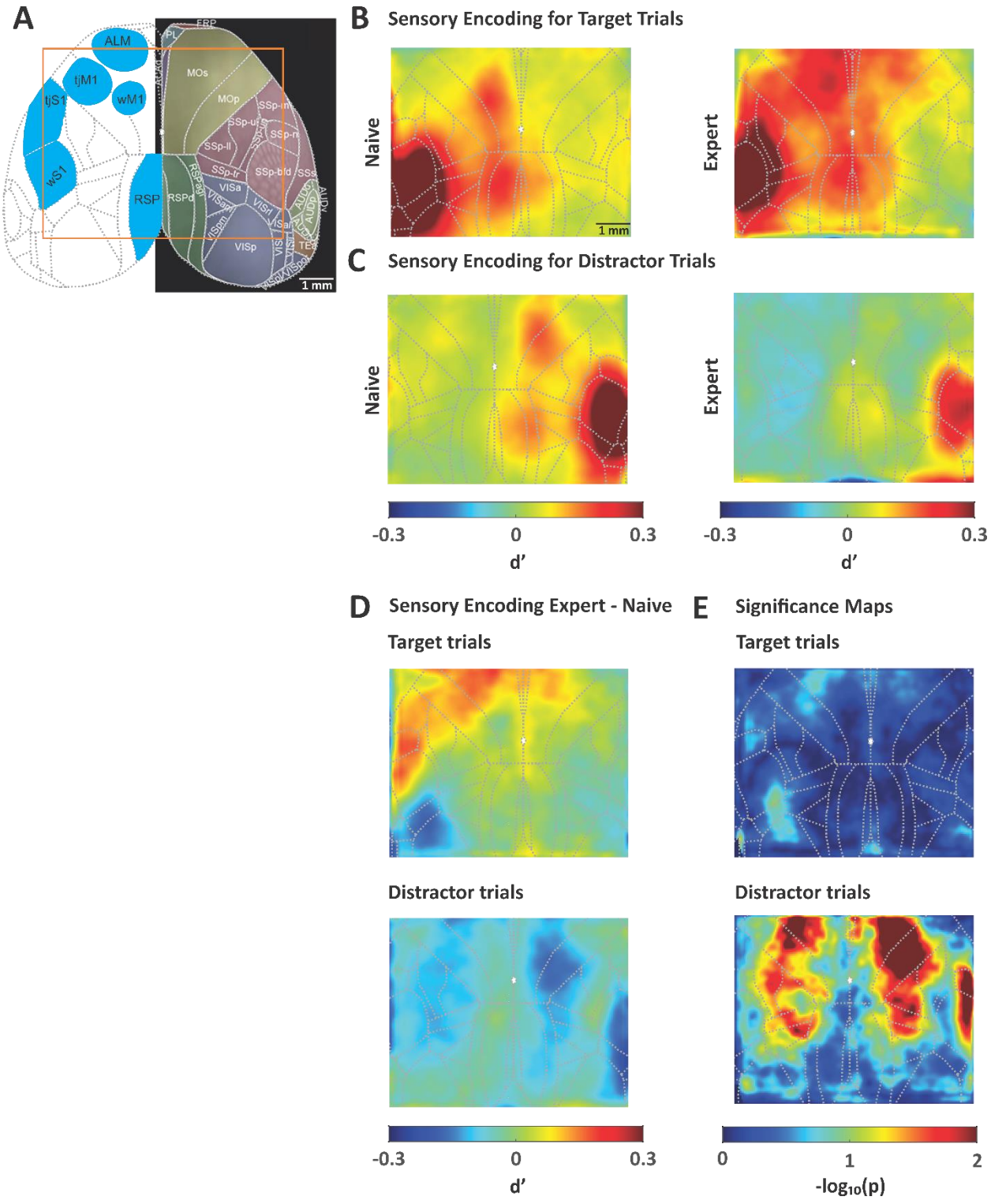
A
ALM
tjM1
wM1
tjS1
wS1
RSP
MOs
MOp
SSp-m
SSp-ul
SSp-n
SSp-ll
SSp-tr
SSp-bfd
SSs
VISa
RSPd
VISp
TEa
FRP
PL
1 mm
B
Sensory Encoding for Target Trials
Naive
Expert
1 mm
C
Sensory Encoding for Distractor Trials
Naive
Expert
-0.3
0
0.3
d'
D
Sensory Encoding Expert - Naive
Target trials
Distractor trials
-0.3
0
0.3
d'
E
Significance Maps
Target trials
Distractor trials
0
1
2
-log10(p)

Figure 1: Sensory-motor attenuation of distractor trials in distractor-aligned hemisphere occurs within S1 and wM1. (*A*) Reference brain and areas of interest in the dorsal cortex with the imaging window highlighted in orange ***(B)*** Sensory encoding for target trials. *Left,* Sensory encoding in naïve mice (average across n=6 mice) showing clear stimulus representation in target-aligned sensory cortex, sensory cortex to motor cortex propagation and propagation to retrosplenial cortex (RSP). *Right,* Sensory encoding in expert mice (average across n=6 mice) showing similar stimulus encoding in target-aligned whisker sensory cortex (wS1), and robust propagation to the licking-associated cortical areas (ALM and tjMC). ***(C)*** Sensory encoding for distractor trials. *Left,* Sensory encoding in naïve mice (average across n=6 mice) showing similar encoding patterns as the naïve mice for target trials. *Right,* Sensory encoding in expert mice (average across n=6 mice) showing clear but diminished stimulus representation in distractor-aligned wS1 and strong attenuation of sensory-motor propagation. ***(D)*** Difference between sensory encoding in expert and naïve sessions for target and distractor trials. *Top,* Difference in target trials (expert – naïve), showing enhancement in stimulus encoding in target-aligned tjMC and bilateral ALM in expert sessions. *Bottom,* Difference in distractor trials (expert – naïve), showing reductions in the S1 and wM1 in the distractor-aligned hemisphere and other parietal and frontal regions bilaterally. ***(E)*** Significance maps for the top and bottom panels of C respectively. The color bar indicates the range of p-value. For target trials, we observed only a trend towards significance. For distractor trials, we observed suppression in the distractor-aligned wS1, wM1, and bilateral ALM and limb S1.

Correlation between activation of brain regions for stimulus encoding with behavioral measures:

Subsequently, we focused on determining the neuronal activation patterns that correlate with changes in various behavioral measures throughout learning. To address this, we selected behavioral measures based on their reliance on trial types: Hit rate and target reaction time (RT) for target trials, False Alarm rate for distractor trials, and the discrimination d’ and wait AUC for target trials vs distractor trials. Figure 2 illustrates the phasic learning transitions of 11 behavioral measures across a total of 52 mice. The 5 measures highlighted in this chapter exhibit distinct learning trajectories among mice. Specifically, the hit rate, a measure of target response, demonstrates a monotonically increasing transition. In contrast, target reaction times exhibit a monotonically decreasing transition. The false alarm rate, representing distractor responses, displays a biphasic transition, indicating an initial increase followed by a decrease as mice progress to expert levels in the task. The two measures shared between target and distractor trials—discrimination d' and wait AUC— both exhibit an increasing transition throughout the learning process.

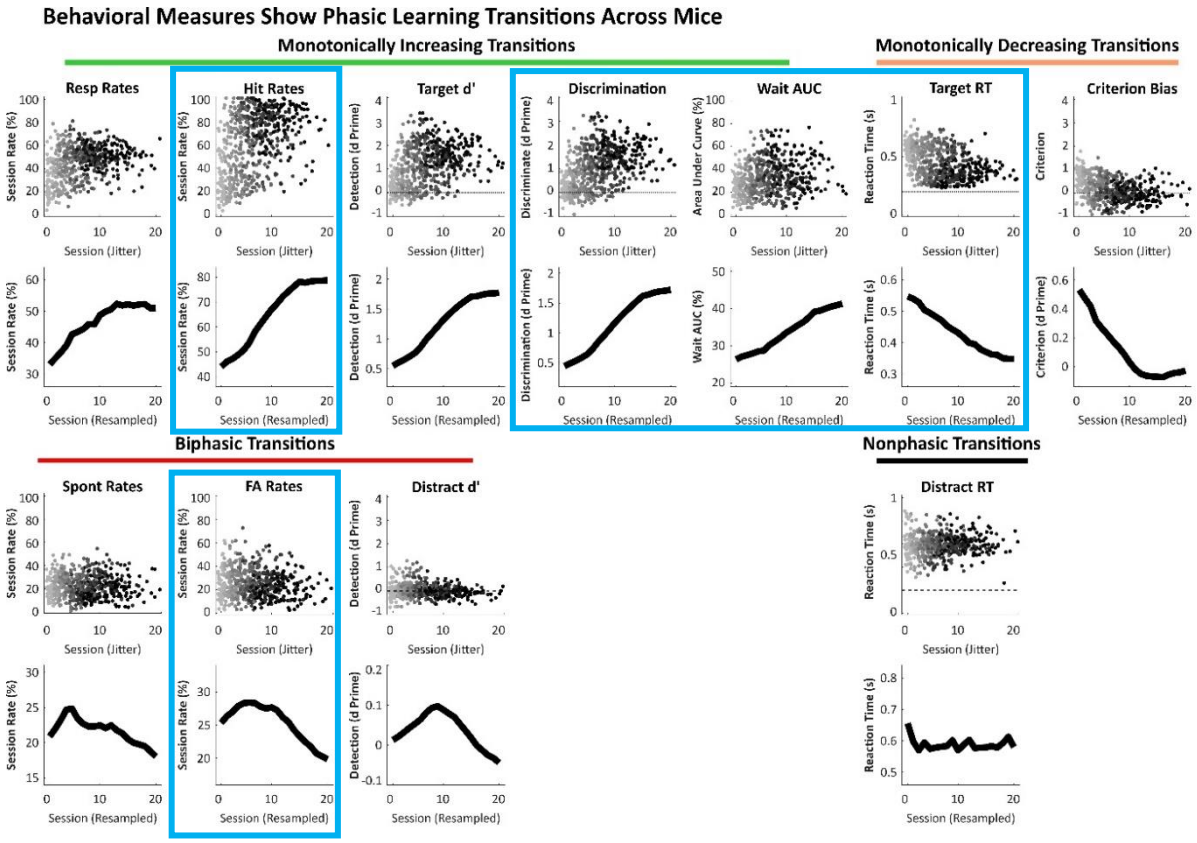

Figure 2: Behavioral measures show phasic learning transitions across mice. *Top row,* Scatterplots with each point representing individual mouse sessions across mice (n=52 mice). *Bottom row*, Means resampled to 20 sessions per mouse and averaged across all mice (n=52 mice). Behavioral measures of interest are highlighted in blue.

We then generated pixel-by-pixel correlation maps for the neural d' of the target and distractor trials in relation to each behavioral measure to discern correlation patterns. For these analyses, we used all training days, from naïve through expert performance, and correlated neuronal and behavioral measures across days.

Figure 3A illustrates that, for target trials, the activation of licking areas (target-aligned tjMC and bilateral ALM) exhibits a significantly positive correlation with hit rate across the learning period. Intriguingly, the activation of these same areas demonstrates a significantly negative correlation with target reaction time (Figure 3B), suggesting that these two behavioral measures are influenced by common neural mechanisms. In the case of distractor trials, Figure 3C reveals that the activation of distractor-aligned ALM and bilateral tjMC significantly positively correlates with False Alarm rate (FAR), mirroring the effects observed in the target trials vs hit rate correlation map. These observations might indicate that the response to either stimulus (HR and FAR) and target reaction times are all driven by similar neural mechanisms – that is, the ability for stimuli to activate licking-associated regions. Notably, these behavioral measures are not correlated with activation of whisker-associated sensory or motor cortices (for target or distractor-related measures). Together, these findings indicate that the stimulus evoked responses in the cortex are predictive of the upcoming motor response (licking) and not indicative of the sensory response and that common neural correlates are associated with the behavioral measures. So far, these data are consistent with the low dimensional learning theory.

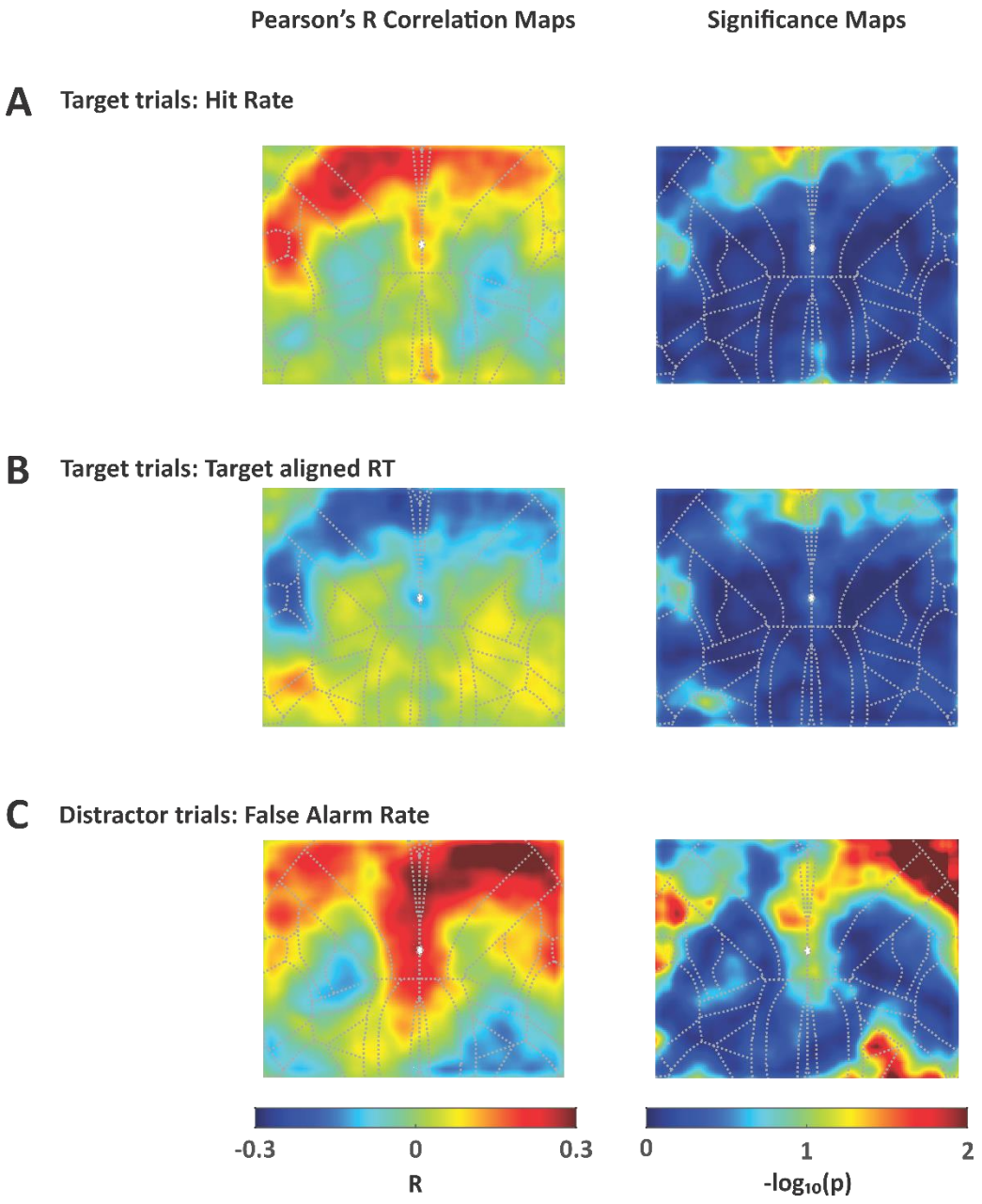

Figure 3: Correlation between activation of brain regions for stimulus encoding with behavioral measures. ***(A)*** *left,* Correlation map between stimulus encoding for target trials and hit rate. Activation of licking areas, particularly in the target-aligned hemisphere, are positively correlated with hit rate. *Right,* Color map as generated in Figure 2. ***(B)*** *left,* Correlation map between stimulus encoding for target trials and target reaction times. *Right,* Significance map as in A. ***(C)*** *left,* Correlation map between stimulus encoding for distractor trials and false alarm rate. *Right,* Significance map as in A and B.

Next, we analyzed the correlation of behavioral measure discrimination d’ vs target trials and distractor trials individually. Figure 4A indicates that, for target trials, the activation of licking areas (preferred tjMC and ALM) exhibits a positive correlation with discrimination d’, closely resembling the effects observed in Figure 3A, though the significance map only shows a trend towards the observed effects. In Figure 4B, for distractor trials, the global suppression of the dorsal cortex is positively correlated with discrimination d’, strongly supported by the significance map. The observed effect diverges significantly from the patterns identified in the correlation maps of response rates (hit rate and false alarm rate), target reaction times, and discrimination d' for target trials. This discrepancy suggests the presence of an entirely distinct mechanism influencing the correlation map for distractor neural d' and behavioral discrimination d'. Such findings hint at the possibility that learning processes may not be adequately described by a low-dimensional model.

Figures 4C and 4D portray the correlation between wait AUC and the neural d’ for target trials and distractor trials, respectively. The activation of the target-aligned parietal cortex displays a positive correlation with waiting AUC for target trials (Figure 4C), while the significant suppression of bilateral retrosplenial cortex (RSP) and distractor-aligned tjMC and ALM are negatively correlated with waiting AUC for distractor trials (Figure 4D). While the wait AUC was correlated to the sensory area for target trials (target-aligned parietal cortex), it was correlated more to the response aligned areas (distractor-aligned tjMC, ALM and bilateral RSP) for

distractor trials, indicating that they are influenced by distinct neural mechanisms. Considering the various effects evident in Figures 3 and 4, we hypothesize that multiple mechanisms contribute to establishing the correlation between neural and behavioral measures throughout the learning process. This speculation supports the notion that learning is likely characterized by high dimensionality.

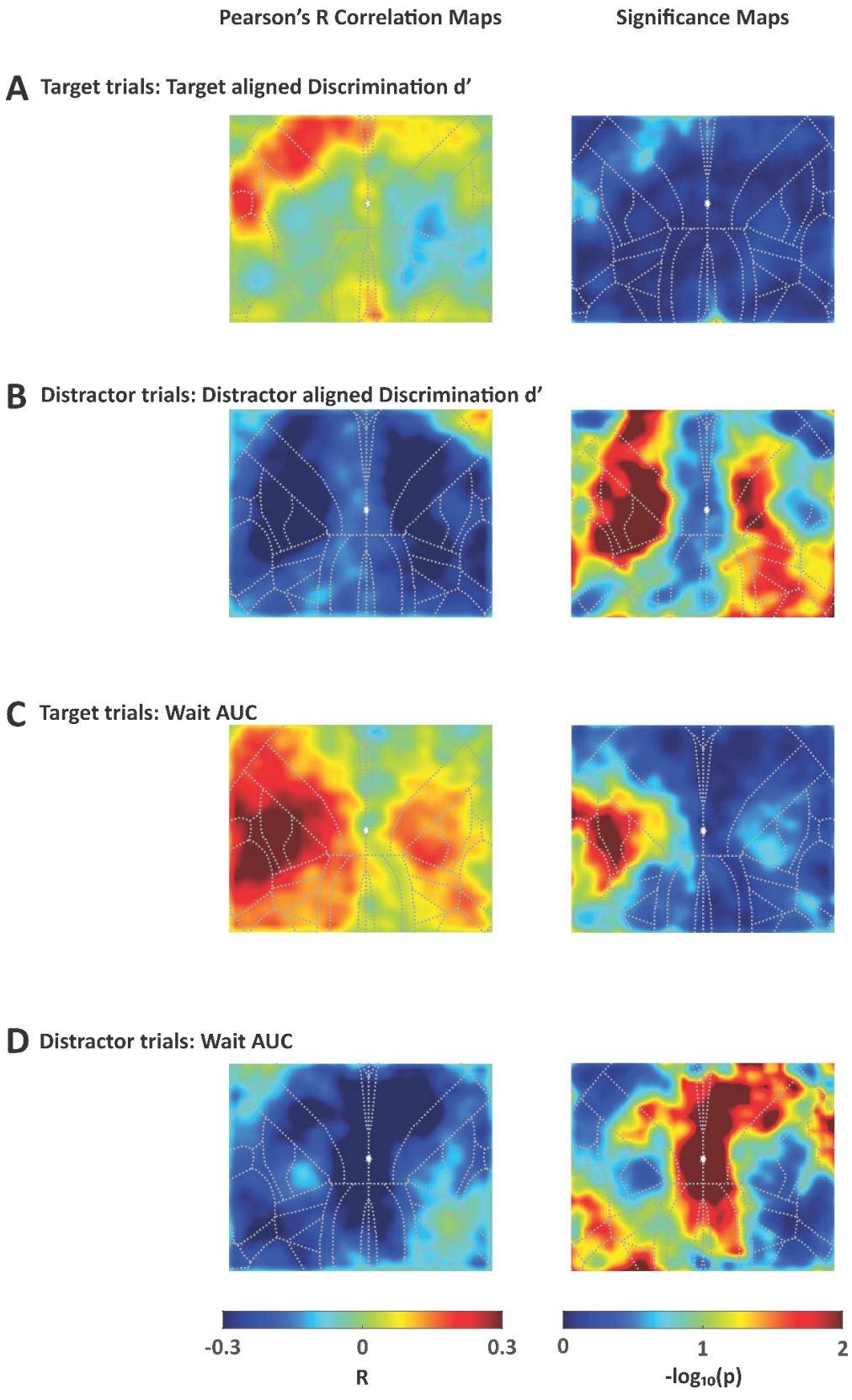
Pearson's R Correlation Maps
Significance Maps
A Target trials: Target aligned Discrimination d'
B Distractor trials: Distractor aligned Discrimination d'
C Target trials: Wait AUC
D Distractor trials: Wait AUC
-0.3
0
0.3
R
0
1
2
-log10(p)

Figure 4: Correlation between activation of brain regions for stimulus encoding with behavioral measures. ***(A)*** *left,* Correlation map between stimulus encoding for target trials and discrimination d'. Activation of licking areas are positively correlated similar to hit rate in Figure 3A. *Right,* Significance map as generated in Figures 2 and 3. ***(B)*** *left,* Correlation map between stimulus encoding for distractor trials and discrimination d'. Global suppression of the dorsal cortex is positively correlated with discrimination d'. *Right,* Significance map. ***(C)*** *left,* Correlation map between stimulus encoding for target trials and Wait AUC. Activation of the target-aligned parietal cortex displays a positive correlation with waiting AUC. *Right,* Significance map. ***(D)*** *left,* Correlation map between stimulus encoding for distractor trials and Wait AUC. Suppression of bilateral retrosplenial cortex (RSP) and distractor-aligned tjMC and ALM are negatively correlated with waiting AUC for distractor trials. *Right,* Significance map.

Correlation between activation of brain regions for prestimulus misses-hits rate of change of fluorescence for target trials with behavioral measures:

In Ch 3 we found that global cortical suppression predicted response outcomes and reaction times. Across training, what is the relationship between cortical suppression and task learning for specific behavioral measures? We identified the correlation between specific behavioral measures and prestimulus cortical suppression for each pixel. We chose hit rate, target reaction time, and discrimination d' as our behavioral measures, comparing them against the prestimulus fluorescence change (miss-hit, dF/F) as discussed in Chapter 3. Separation in prestimulus fluorescence change between hits and misses was positively correlated with hit rate as supported by the significant map in Figure 5A. This indicates that as the mice learn to respond more to the target stimulus, stronger the separation between prestimulus hits and misses dF/F. The same is true for discrimination d' as observed in Figure 5C. However, the miss-hits prestimulus dF/F is negatively correlated with the target reaction times, indicating that as the mice respond faster to the target stimulus, the separation between prestimulus hits and misses dF/F increases (Figure 5B).

The correlation profiles of the three behavioral measures- hit rate, target reaction times and discrimination d'- with the neural measures are similar between the pre- and post-stimulus epochs but the regions of correlation in the dorsal neocortex are distinctly different between the two epochs. The activation of paw regions in the

prestimulus epoch as opposed to the activation of distinct regions in the post stimulus epoch might be indicative of a preparatory state before the stimulus onset.

In summary, with this study, we were able to determine that the emergence of attenuation of distractor signal across learning of our selective detection task is due to the selective enhancement in the licking areas for target trials and the suppression of sensory encoding and sensory motor propagation for distractor trials (Figure 2). We also were able to establish the correlation between select behavioral measures and neural measures both pre- and post-stimulus presentation and speculate on the cellular mechanisms involved in those processes (figures 3-5).

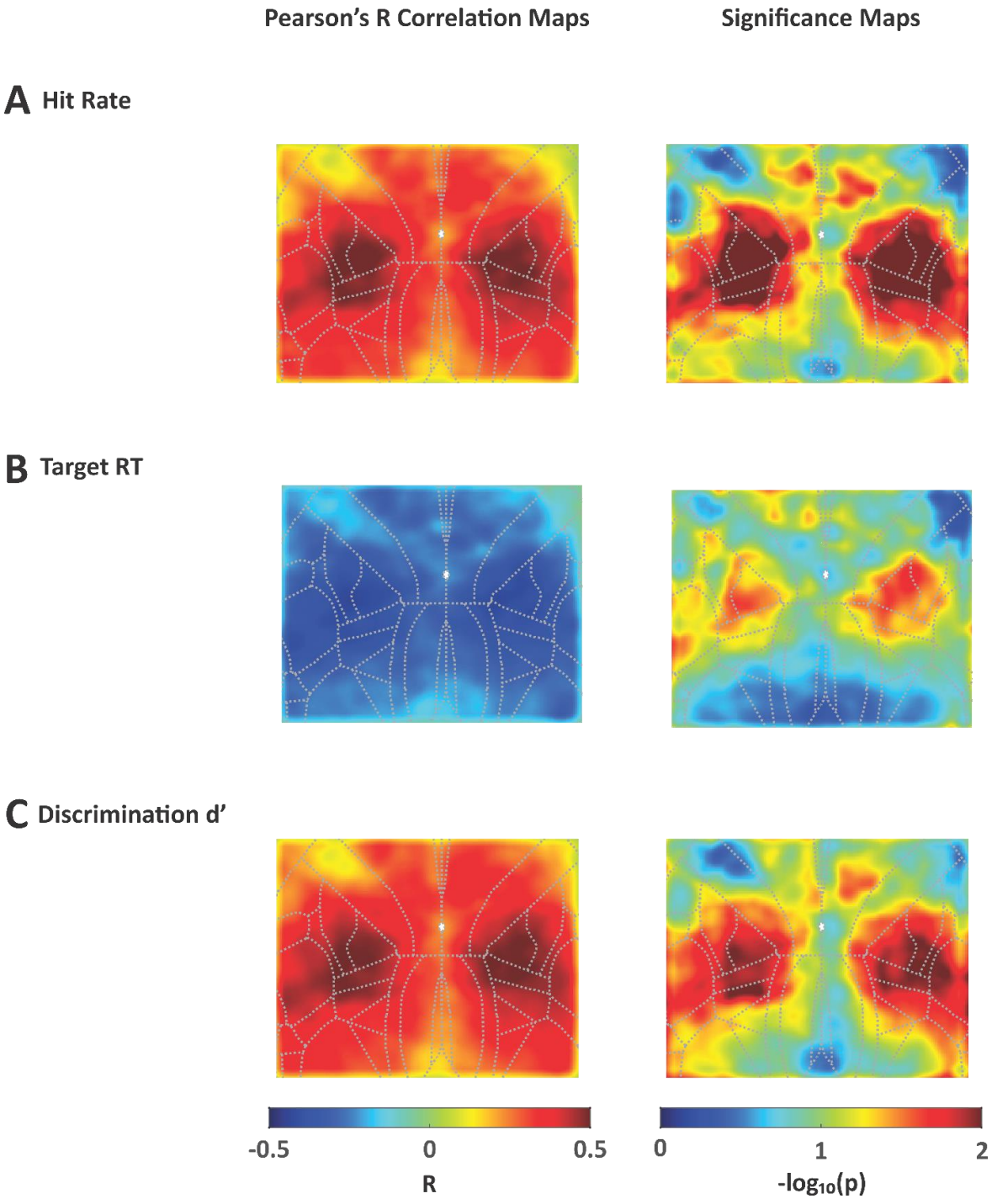
Pearson's R Correlation Maps
Significance Maps
A Hit Rate
B Target RT
C Discrimination d'
-0.5
0
0.5
R
0
1
2
-log10(p)

Figure 5: Correlation between activation of brain regions for prestimulus rate of change of fluorescence for target trials with behavioral measures. ***(A)*** *left,* Correlation map between prestimulus miss-hit dF/F and hit rate. Separation in prestimulus fluorescence change between hits and misses was positively correlated with hit rate globally across the dorsal neocortex. *Right,* Significance map as generated in previous figures. ***(B)*** *left,* Correlation map between prestimulus miss-hit dF/F and target reaction times. Separation in prestimulus fluorescence change between hits and misses was negatively correlated with target reaction times globally across the dorsal neocortex. *Right,* Significance map. ***(C)*** *left,* Correlation map between prestimulus miss-hit dF/F and discrimination d'. Separation in prestimulus fluorescence change between hits and misses was positively correlated with discrimination d' globally across the dorsal neocortex, as observed in *(A)*. *Right,* Significance map.

Discussion

Our aim was to observe the longitudinal evolution of behavioral performance and its corresponding neural activity in mice engaging in a go/no-go selective detection task. The central inquiry guiding our investigation was the emergence of the attenuation filter in the distractor hemisphere during distractor trials and its temporal evolution through learning. As depicted in Figure 1, our findings indicate that selective enhancement occurs in the licking related areas of tjMC and ALM for target trials and the attenuation occurs in the whisker related areas for distractor trials. This observation implies the involvement of multiple cortical regions in the attenuation process, rather than the isolated influence of a singular brain region. This suggests the involvement of a cognitive process known as associative learning in the brain, where the animal forms a connection between the stimulus (whisker deflection) and the desired response (licking for a reward). In our prior investigations (chapters 2 and 3), we noted an improvement in sensory-motor propagation (from whisker somatosensory cortex, wS1, to motor cortex, wM1) in expert mice following the stimulus. Initially, we assumed this enhancement was solely triggered by the stimulus. However, upon examining the neural activity during task learning, we realized that the increased activation in the licking areas indicated the "response" aspect of associative learning was initiating the effect. Conversely, for distractor trials, the attenuation remained evident in the whisker-related areas, suggesting that attenuation is primarily a stimulus-triggered process.

Building on this, our focus shifted to unraveling the relationship between established behavioral measures, as outlined in our parallel behavioral study (Marrero et al., 2023), and the neural correlates as potential drivers of those behavioral measures. Figure 2 shows the phasic learning transition of 11 behavioral measures across 52 mice. The 5 measures of interest all show different transition profiles throughout learning. The target response measures hit rate and reaction tikes show a monotonically increasing and decreasing transition profiles respectively. The distractor response measure false alarm rate shows a biphasic transition profile whereas, the two measures common for target and distractor trials- discrimination d' and wait AUC- both show a monotonic increase of the transition profile (Figure 2, *bottom row*). Figures 3 and 4 demonstrate that analogous neural mechanisms correlate with key behavioral measures positively such as hit rate (HR), target reaction times (target RT), and discrimination d' for target trials, and with false alarm rates (FAR) for distractor trials. The distinctive correlation patterns between discrimination d' and waiting AUC for target trials versus distractor trials, as depicted in Figure 3, suggest the involvement of multiple processes in preparatory activity preceding responses to target versus distractor stimuli. Figure 3 shows how the 'go' or 'response' measures are triggered in the licking areas of the brain (tjMC and ALM) while figure 4 shows how the other two measures are triggered distinctively in the brain. The process of decision-making developing across learning calls for some speculations in terms of the mechanisms involved. As discussed in the results section for each observation and to

summarize, the behavioral response measures and discrimination d' aligned with targets exhibit a positive correlation with the activation of the brain areas related to licking. In contrast, distractor-aligned discrimination d' displays a global negative correlation with neural d'. Interestingly, the wait AUC for target and distractor trials reveals distinct patterns of correlated brain areas, suggesting the involvement of multiple mechanisms in these learning-related changes. This observation supports the idea that learning is a high-dimensional process.

Subsequently, we explored the activation of specific brain regions influencing the delineation between hits and misses during the prestimulus period. Figure 4 illustrates a positive correlation between hit rate, target reaction time, discrimination d', and the separation in prestimulus fluorescence changes between hits and misses. This implies that these three behavioral measures are governed by common neural mechanisms during both pre- and post-stimulus phases of the task.

However, this method has its limitations. While it informs us about the correlation of neuronal modulations with individual behavioral measures, it doesn't compare neuronal modulations across various behavioral processes. To address this, we propose using multiple linear regression analyses, a statistical method employing independent variables to predict the outcome of a dependent variable. Ridge regression can be applied, utilizing the five behavioral learning trajectories as regressors for each mouse's neuronal modulation trajectory (dependent variable). This analysis aims to ascertain the extent to which each behavioral learning

measure independently co-varies with neuronal modulations. The explained variance signifies the ratio of variance in the response variable that can be clarified by the predictor variable(s) within the regression model, providing insight into the individual contributions of each predictor variable to the observed changes in the model.

Although this study successfully identifies the brain regions associated with driving behavioral measures, the correlation maps alone cannot elucidate the extent to which each behavioral learning measure co-varies with individual neuronal modulations. To understand whether the behavior measures drive the neuronal changes we observed or vice versa, we need to establish causality through manipulations. This could be achieved by silencing the brain areas that get activated or suppressed for the behavioral measures they are correlated with. For instance, since the stimulus evoked response rates (HR and FAR) and discrimination d' show positive correlations with the stimulus-aligned licking areas (tjMC and ALM), silencing one of the two areas could potentially affect the response rates and discrimination d' accordingly.

References

Aruljothi, K., Marrero, K., Zhang, Z., Zareian, B., & Zagha, E. (2020). Functional Localization of an Attenuating Filter within Cortex for a Selective Detection Task in Mice. *The Journal of Neuroscience*, *40*(28), 5443 LP – 5454. https://doi.org/10.1523/JNEUROSCI.2993-19.2020

Brown, L. E., Wilson, E. T., Goodale, M. A., & Gribble, P. L. (2007). Motor force field learning influences visual processing of target motion. *The Journal of Neuroscience : The Official Journal of the Society for Neuroscience*, *27*(37), 9975–9983. https://doi.org/10.1523/JNEUROSCI.1245-07.2007

Cressman, E. K., & Henriques, D. Y. P. (2010). Reach adaptation and proprioceptive recalibration following exposure to misaligned sensory input. *Journal of Neurophysiology*, *103*(4), 1888–1895. https://doi.org/10.1152/jn.01002.2009

di Pellegrino, G., Fadiga, L., Fogassi, L., Gallese, V., & Rizzolatti, G. (1992). Understanding motor events: a neurophysiological study. *Experimental Brain Research*, *91*(1), 176–180. https://doi.org/10.1007/BF00230027

Huber, D., Gutnisky, D. A., Peron, S., O'Connor, D. H., Wiegert, J. S., Tian, L., Oertner, T. G., Looger, L. L., & Svoboda, K. (2012). Multiple dynamic representations in the motor cortex during sensorimotor learning. *Nature*, *484*(7395), 473–478. https://doi.org/10.1038/nature11039

Kawai, R., Markman, T., Poddar, R., Ko, R., Fantana, A. L., Dhawale, A. K., Kampff, A. R., & Ölveczky, B. P. (2015). Motor Cortex Is Required for Learning but Not for Executing a Motor Skill. *Neuron*, *86*(3), 800–812. https://doi.org/10.1016/j.neuron.2015.03.024

Komiyama, T., Sato, T. R., O'Connor, D. H., Zhang, Y.-X., Huber, D., Hooks, B. M., Gabitto, M., & Svoboda, K. (2010). Learning-related fine-scale specificity imaged in motor cortex circuits of behaving mice. *Nature*, *464*(7292), 1182–1186. https://doi.org/10.1038/nature08897

Laubach, M., Wessberg, J., & Nicolelis, M. A. L. (2000). Cortical ensemble activity increasingly predicts behaviour outcomes during learning of a motor task. *Nature*, *405*(6786), 567–571. https://doi.org/10.1038/35014604

Madisen, L., Garner, A. R., Shimaoka, D., Chuong, A. S., Klapoetke, N. C., Li, L., van der Bourg, A., Niino, Y., Egolf, L., Monetti, C., Gu, H., Mills, M., Cheng, A., Tasic, B., Nguyen, T. N., Sunkin, S. M., Benucci, A., Nagy, A., Miyawaki, A., … Zeng, H. (2015). Transgenic mice for intersectional targeting of neural sensors

and effectors with high specificity and performance. *Neuron*, *85*(5), 942–958. https://doi.org/10.1016/j.neuron.2015.02.022

Marrero, K., Aruljothi, K., Zareian, B., Gao, C., Zhang, Z., & Zagha, E. (2022). Global, Low-Amplitude Cortical State Predicts Response Outcomes in a Selective Detection Task in Mice. *Cerebral Cortex*, *32*(9), 2037–2053. https://doi.org/10.1093/cercor/bhab339

Marrero, K., Aruljothi, K., Zareian, B., Zhang, Z., & Zagha, E. (2023). Multiple Temporal and Object-Based Strategies Across Learning for a Selective Detection Task in Mice. *BioRxiv*. https://doi.org/10.1101/2023.02.13.528412

Murphy, J. T., Kwan, H. C., MacKay, W. A., & Wong, Y. C. (1978). Spatial organization of precentral cortex in awake primates. III. Input-output coupling. *Journal of Neurophysiology*, *41*(5), 1132–1139. https://doi.org/10.1152/jn.1978.41.5.1132

Pai, S., Erlich, J., Kopec, C., & Brody, C. (2011). Minimal Impairment in a Rat Model of Duration Discrimination Following Excitotoxic Lesions of Primary Auditory and Prefrontal Cortices. *Frontiers in Systems Neuroscience*, *5*. https://doi.org/10.3389/fnsys.2011.00074

Peters, A. J., Liu, H., & Komiyama, T. (2017). Learning in the Rodent Motor Cortex. *Annual Review of Neuroscience*, *40*, 77–97. https://doi.org/10.1146/annurev-neuro-072116-031407

Romo, R., Hernández, A., & Zainos, A. (2004). Neuronal correlates of a perceptual decision in ventral premotor cortex. *Neuron*, *41*(1), 165–173. https://doi.org/10.1016/s0896-6273(03)00817-1

Romo, R., Hernández, A., Zainos, A., Lemus, L., & Brody, C. D. (2002). Neuronal correlates of decision-making in secondary somatosensory cortex. *Nature Neuroscience*, *5*(11), 1217–1225. https://doi.org/10.1038/nn950

Rudebeck, P. H., & Murray, E. A. (2008). Amygdala and Orbitofrontal Cortex Lesions Differentially Influence Choices during Object Reversal Learning. *The Journal of Neuroscience*, *28*(33), 8338. https://doi.org/10.1523/JNEUROSCI.2272-08.2008

Shiller, D. M., Sato, M., Gracco, V. L., & Baum, S. R. (2009). Perceptual recalibration of speech sounds following speech motor learning. *The Journal of the Acoustical Society of America*, *125*(2), 1103–1113. https://doi.org/10.1121/1.3058638

Wang, Q., Ding, S.-L., Li, Y., Royall, J., Feng, D., Lesnar, P., Graddis, N., Naeemi, M., Facer, B., Ho, A., Dolbeare, T., Blanchard, B., Dee, N., Wakeman, W., Hirokawa, K. E., Szafer, A., Sunkin, S. M., Oh, S. W., Bernard, A., … Ng, L. (2020). The Allen Mouse Brain Common Coordinate Framework: A 3D Reference Atlas. *Cell*, *181*(4), 936-953.e20. https://doi.org/https://doi.org/10.1016/j.cell.2020.04.007

Xerri, C., Coq, J. O., Merzenich, M. M., & Jenkins, W. M. (1996). Experience-induced plasticity of cutaneous maps in the primary somatosensory cortex of adult monkeys and rats. *Journal of Physiology, Paris*, *90*(3–4), 277–287. https://doi.org/10.1016/s0928-4257(97)81438-6

Zareian, B., Lam, A., & Zagha, E. (2023). Dorsolateral Striatum is a Bottleneck for Responding to Task-Relevant Stimuli in a Learned Whisker Detection Task in Mice. *The Journal of Neuroscience*, *43*(12), 2126–2139. https://doi.org/10.1523/JNEUROSCI.1506-22.2023

Zareian, B., Zhang, Z., & Zagha, E. (2021). Cortical Localization of the Sensory-Motor Transformation in a Whisker Detection Task in Mice. *Eneuro*, *8*(1), ENEURO.0004-21.2021. https://doi.org/10.1523/ENEURO.0004-21.2021

Zhang, Z., & Zagha, E. (2023). Motor cortex gates distractor stimulus encoding in sensory cortex. *Nature Communications*, *14*(1), 2097. https://doi.org/10.1038/s41467-023-37848-4

Chapter 5: Discussion and Conclusion

Our investigations have delved into the neuronal correlates of goal-directed behavior, examining the neural underpinnings of task performance across the cortex, tracking learning behavior over time, and establishing connections between neural correlates and behavioral measures throughout the learning process. These discoveries have merely opened the door to further scrutiny, prompting additional potential avenues of research, raising new questions, and heightening awareness of the multifaceted aspects of our task.

Behavior Paradigm

We have deepened our understanding of the decision-making process associated with selectively responding to and ignoring similar stimuli. We trained mice to perform a whisker-based go/no-go selective detection task where they learn to respond to a target stimulus while withholding responses to a distractor stimulus. We used widefield calcium imaging in expert mice to analyze neural responses throughout dorsal cortex. In the first study, detailed in chapter 2, we observed robust sensory cortex to motor cortex propagation in the target-related hemisphere for target trials but attenuation of sensory-to-motor propagation for distractor trials. In chapter 3, we determined whether and how neuronal activity before stimulus onset predicts trial outcomes during goal-directed behavior. We found that lower prestimulus activity correlated with enhanced stimulus detection. The activity predictive of trial outcome was distributed through dorsal neocortex, rather than

being restricted to task-relevant sensory or motor regions. In chapter 4, we tracked the behavioral measures and their neural correlates across learning of the task and observed distinct correlations between the two measures.

One limitation of my thesis work is that this exploration has been limited to a behavioral paradigm where the opposing stimuli are well separated across hemifields and hence perceptually quite easy to discriminate. To investigate a more refined discrimination, our lab has chosen to introduce a conceptually minor yet significant modification to our existing task paradigm. This decision is based on the advantage of using the same established behavioral and neuronal outcome measures, eliminating the need to validate entirely new measures. The current task involves a directional (rostral-caudal) discrimination task within the same whisker field, requiring the differential filtering of stimuli within overlapping cortical populations. Another interesting direction to take would be to implement a switching task to observe behavioral flexibility. This task includes within-session changes in target and distractor assignment in block design, which requires dynamic changes in stimulus filtering across blocks (McBurney-Lin et al., 2022). For both the tasks, we suspect that there might be distractor filtering within wS1 and wM1 as observed in our original task.

Generalization across sensory modalities

Stimuli previously associated with rewards tend to capture attention, even when they lack robust physical salience, are currently irrelevant to the task, and no longer predict rewards (Anderson et al., 2011; Anderson & Halpern, 2017; Watson et al., 2019). This value-based attentional bias can extend to objects perceptually related to the rewarded stimuli (Mine & Saiki, 2018). However, investigations into the generalization of stimulus-reward associations have predominantly centered on perceptual cues within a single sensory modality. Semantic and cross-modal generalization of such associations have been largely understudied despite real-world learning applications (Dunsmoor & Murphy, 2015). Extending value-based attentional priority across sensory modalities in a semantic context would challenge existing assumptions about the neural mechanisms underlying reward history effects. This could offer new perspectives on maladaptive behaviors like addiction, given that attentional biases for drug cues significantly influence drug-seeking behavior and contribute to relapse (Anderson, 2016).

Mouse Models

Animal models are necessary for understanding the pathophysiology of neuropsychiatric disorders such as ADHD, Autism, Schizophrenia, etc. These disease models could show faster reaction times to ‘go’ signal and slower reaction times to the ‘stop’ signal or increase in overall impulsivity. The transgenic GCaMP mice used in our study had faster reaction times and generally higher spontaneous

licking. These may indicate deficits regarding attention and/or hyperactivity. Classical transgenic rodent models contribute to understanding loss of function for specific genes in psychiatric disorders using conventional KO mice. In addition, the advent of tissue-specific Cre-loxP system enables to investigate more regional and temporal deletion or overexpression of a gene (Baker et al., 2020). For example, the Fmr1 KO mouse exhibits symptoms akin to those seen in the human condition, such as hyperactivity, repetitive behaviors, and seizures (Larson et al., 2008). Furthermore, this model presents abnormalities in the density of dendritic spines, making it a promising candidate for our research. These mice would make great candidates to be trained in our behavior paradigm to observe whether the attenuating filter exists if the mice fail to learn to ignore the distractor stimulus.

The dysbindin-1 gene (DTNBP1: dystrobrevin binding protein 1) emerges as a notable susceptibility gene for schizophrenia. It predominantly localizes to neurons in the brain, contributing to the regulation of neurotransmitter release, expression of membrane-surface receptors, and synaptic plasticity. The Sandy mice, characterized by spontaneous Dtnbp1 deletion, exhibit behavioral abnormalities relevant to schizophrenia symptoms. These mice exhibit a range of behavioral abnormalities associated with schizophrenia symptoms, encompassing hypoactivity, heightened anxiety-like responses, diminished social interaction (Hattori et al., 2008), deficits in both long-term (FENG et al., 2008) and working memory (Takao et al., 2008), and challenges in contextual fear conditioning (Glen et al., 2014). The potential mechanisms underlying these behavioral abnormalities

in Sandy mice include diminished dopamine transmission in the forebrain (Hattori et al., 2008) and destabilization of snapin, a protein binding to SNAP25 that regulates calcium-dependent exocytosis (FENG et al., 2008). These mice also exhibit increased impulsive and compulsive behaviors relevant to psychiatric disorders. When trained on a reward-based operant task, the Dys KO mice produced more premature and timeout responses at the beginning of learning and significantly decreased these behaviors with learning (Carr et al., 2013).

Widefield calcium imaging

Exploring widefield calcium imaging posed an initial challenge in this research endeavor, given the relatively novel nature of the imaging technique. Once we had defined the behavior paradigm and identified the tool for assessing neural attributes to address our inquiries, the subsequent challenge arose in interpreting the results obtained through widefield imaging. Various methods were employed to process the raw fluorescence data, including mean grey value, baseline normalization, and sliding window normalization. In terms of quantitative analysis, decoding the fluorescence data provided valuable insights into our understanding of sensory encoding (distinguishing between stimulus present and stimulus absent), choice encoding (discerning response presence versus response absence), and so forth.

Using the widefield calcium imaging method, we successfully captured neural activity from the majority of the dorsal cortex, encompassing our regions of interest.

However, it's important to note that this method comes with limitations, resulting in the inability to image certain areas such as the medial prefrontal cortex (mPFC) (Allen et al., 2017; Harris et al., 2019; Makino et al., 2017) and secondary somatosensory cortex (S2) (Condylis et al., 2020; Rossi-Pool et al., 2021). These regions may play crucial roles in sensory selection, utilizing memory from past experiences to inform present decisions, and tactile object recognition—all of which are integral aspects of our study.

There are limitations in achieving cellular resolution with widefield imaging. For instance, if directional discrimination involves two spatially overlapping ensembles, widefield imaging may not be adequate to distinguish these populations. Additionally, the specific activities of distinct excitatory projection neurons or inhibitory neurons are not discernible. A promising avenue for future research would involve conducting widefield imaging exclusively from genetically or projection-defined neurons throughout the cortex. For instance, this could include imaging only PV neurons expressing GCaMP throughout the cortex or exclusively focusing on striatal-projecting neurons. This would also help with achieving pathway specificity of projection sites.

Behavioral vs Neural correlates

In exploring the impact of neural correlates on behavioral measures, we employed a simple yet effective method of analysis: examining the relationship through linear correlation, specifically reported as Pearson’s correlation (R). This analysis

provides insights into the degree of correlation between the measures. A positive R value indicates a linear correlation between the neural measure and the behavioral measure, occurring in phase with each other. Conversely, a negative R value signifies an inverse correlation between the neural measure and the behavioral measure.

One limitation of this approach is that while it informs us about whether and how neuronal modulations correlate with individual behavioral measures, it doesn't compare neuronal modulations across behavioral processes. Multiple linear regression analyses, a statistical method utilizing one or more independent variables to predict the outcome of a dependent variable, offer a solution. For each mouse's neuronal modulation trajectory (dependent variable), ridge regression can be applied using the four behavioral learning trajectories as regressors. These analyses aim to answer a crucial question: to what extent does each behavioral learning measure co-vary with each neuronal modulation?

Conducting a two-way ANOVA of the β-weights, followed by post-hoc pairwise comparisons, will enable the comparison of the main effects of neuronal modulation and behavioral measures. Additionally, for each behavioral measure, ranking the neuronal modulations with the highest β-weights provides insights into potential neuronal mechanisms that underlie the learning of specific behavioral processes.

This approach faces a few potential challenges. Firstly, there is the risk of collinearity among the regressors, which can complicate the assignment of model weights. To mitigate the impact of potential multicollinearity, ridge regression may be employed instead of the standard linear regression model, with the penalty term determined through cross-validation. It is worth noting that, in the behavioral-neuronal comparison, behavioral measures serve as predictors for each neuronal measure. Previous validation work, encompassing a substantial sample size (n=52 mice across learning, 6), has indicated low correlation among these behavioral measures, minimizing concerns about collinearity.

The second limitation is that our behavioral-neuronal comparisons are inherently correlational. Consequently, it is not possible to assert that neuronal modulations directly cause behavioral learning. However, we anticipate that future studies will generate numerous mechanistic hypotheses that can be rigorously tested in subsequent causal investigations by performing chronic lesions of specific brain legions or by utilizing transient optogenetic manipulations. Based on our findings in chapter 4, for example, as the response rates (HR and FAR) and discrimination d' exhibit positive correlations with the preferred licking areas (tjMC and ALM), silencing either of these areas by either chronic lesioning or optogenetic suppression might have a detrimental impact on response rates and discrimination d'.

Another consideration is that this method does not sample from vital non-surface cortices, such as the medial prefrontal cortex and orbitofrontal cortex. Sampling

these and sub-cortical structures will necessitate alternative approaches, such as silicon probe or Neuropixels recordings.

Cellular mechanisms of reward association and uncertainty

As our cortical research utilized a transgenic SNAP25 pan-neuronal promoter for calcium-related activity, the distinction between excitatory and inhibitory calcium-related activity remains undetermined. Consequently, the observed dynamic fluorescence can only suggest potential regions of interest for future investigations into task-related function and circuitry. Exploring excitatory versus inhibitory transgenic lines has been proposed as a means to address this differentiation. Additionally, we anticipate that the overall low activity in the prestimulus state and the dynamic propagation of signals post-stimulus would be contingent on a specific (potentially learned) neuromodulatory tone. One particularly important neuromodulator to investigate in our learning studies is dopamine (see below).

In the 1940s and 1950s, Hebb was among the pioneers proposing that alterations in synaptic strength, based on local patterns of activation, could elucidate the biophysical mechanisms behind conditioned reflexes. Bliss and Lomo (Bliss & Lomo, 1973) later established a connection between Hebb's theoretical proposal and the biophysical manifestation by demonstrating long-term potentiation (LTP) in the rabbit hippocampus. Subsequent biophysical studies have revealed several mechanisms for altering synaptic strength, closely tied to Hebb's theory and Bliss and Lomo's findings. (Wickens & Kötter, 1995)introduced a crucial concept known

as the three-factor rule, suggesting that synapses strengthen when presynaptic and postsynaptic activities coincide with dopamine release, and weaken in the absence of dopamine.

Temporal-difference (TD) learning is an extension of the Rescorla-Wagner model that also takes into account the timing of different events. In the context of reinforcement learning, when an animal encounters a significant positive reward prediction error, signaling an unexpected reward, the TD model indicates a need to increment the value assigned to the associated actions or sensations. Dopamine neurons release dopamine uniformly throughout frontocortical–basal ganglia loops under such circumstances (Barto, 1995; Houk et al., 1995; Joel et al., 2002). According to the three-factor rule, any dopamine receptor-equipped neuron active during a movement, for instance, will have its synapses strengthened when dopamine is present. This implies that when a positive prediction error occurs, the entire active segment of the frontocortical–basal ganglia loop has its synapses strengthened.

To understand the behavioral implications, consider neurons in the dorsal striatum forming maps of possible movements in extrapersonal space. Each time a movement occurs, the associated neurons are briefly active, and if followed by a positive prediction error, dopamine bathes the entire topographic map. This results in a permanent increase in synaptic strength among neurons associated with recent movements, encoding the expected value of those movements through repeated exposure to dopamine (Lau & Glimcher, 2007, 2008).

Crucially, all elements in this narrative align with preexisting observations of nervous system properties. Neurons in the striatum exhibit activity after movements, as posited by TD models. In prior research, it is observed that reward exerts an influence on both the primary motor (M1) and somatosensory (S1) cortices during both action and action observation (Marsh et al., 2015; D. McNiel et al., 2016; D. B. McNiel et al., 2016). Additionally, individual M1 neurons were revealed to multiplex information related to kinematics and reward (Marsh et al., 2015). Subsequent support for this work came from Ramakrishnan et al. 2017 (Ramakrishnan et al., 2017), where they similarly observed responses to reward prediction errors in both M1 and S1, highlighting the modulatory effect of reward on sensorimotor directional tuning curves. Dopamine releases a global prediction error signal throughout frontocortical–basal ganglia loops, and it induces LTP-like phenomena when correlated with underlying activity. After conditioning, synaptically driven action potentials in these areas encode the subjective values of actions, establishing the groundwork for implementing TD-class models of learning (Lau & Glimcher, 2007, 2008; Samejima et al., 2005). We could potentially express GCaMP in dopamine neurons and image their axons in dorsal cortex during learning. With that we can generate spatio-temporal maps of their activity during learning of the selective detection task.

The formation of the prediction error signal coded by dopamine neurons can also be envisioned. Neurons in the striatum encode learned action values in their firing rates, sending outputs to dopaminergic nuclei as a reward prediction. Additionally,

dopaminergic neurons receive direct inputs from sensory areas detecting and encoding reward magnitudes. Constructing a prediction error signal at dopamine neurons simply requires excitatory and inhibitory synapses to compute the difference between predicted and experienced rewards in the voltage of the dopamine neurons or their immediate predecessors (Glimcher, 2011).

We understand that dopamine stimulation plays a role in generating learning and behavior. Additionally, encountering rewards better than predicted stimulates dopamine neurons, suggesting that the dopamine response to natural rewards can directly influence behavioral learning and actions. Each instance of encountering a reward leads to dopamine neuron responses influencing subsequent behavior. An intriguing aspect is the dopamine response to positive prediction errors, where activation occurs when the received reward exceeds predictions. However, the challenge arises as each reward updates the prediction, making the previously larger-than-predicted reward the new norm, diminishing the dopamine prediction error response. Sustaining the same prediction error and dopamine stimulation would then necessitate consistently obtaining larger rewards (Schultz, 2016). Our lab is venturing into developing experiments to study predictive coding in the mice visual and whisker system, where the mice have to learn to respond to a sequence of stimuli and a mismatch in the sequence would lead to prediction errors. The anticipatory signals leading up to the motor response (licking) can be tracked with either electrophysiology or other calcium imaging techniques such as 2 photon

calcium imaging to observe the role of dopamine in behavioral learning and actions.

Final Remarks

In conclusion, we determined the neuronal changes in the cortex while mice learned to become experts in a selective detection task. However, the observations described here are limited by using specific tools and the task employed. Whether the neuronal and behavioral changes observed through learning are generated in the neocortex, or rather involve more complex signaling mechanisms involving sub-cortical structures are exciting topic of future explorations.

References

Allen, W. E., Kauvar, I. V, Chen, M. Z., Richman, E. B., Yang, S. J., Chan, K., Gradinaru, V., Deverman, B. E., Luo, L., & Deisseroth, K. (2017). Global Representations of Goal-Directed Behavior in Distinct Cell Types of Mouse Neocortex. *Neuron*, *94*(4), 891-907.e6. https://doi.org/10.1016/j.neuron.2017.04.017

Anderson, B. A. (2016). What is abnormal about addiction-related attentional biases? *Drug and Alcohol Dependence*, *167*, 8–14. https://doi.org/10.1016/j.drugalcdep.2016.08.002

Anderson, B. A., & Halpern, M. (2017). On the value-dependence of value-driven attentional capture. *Attention, Perception & Psychophysics*, *79*(4), 1001–1011. https://doi.org/10.3758/s13414-017-1289-6

Anderson, B. A., Laurent, P. A., & Yantis, S. (2011). Value-driven attentional capture. *Proceedings of the National Academy of Sciences of the United States of America*, *108*(25), 10367–10371. https://doi.org/10.1073/pnas.1104047108

Baker, M., Hong, S.-I., Kang, S., & Choi, D.-S. (2020). Rodent models for psychiatric disorders: problems and promises. *Laboratory Animal Research*, *36*(1), 9. https://doi.org/10.1186/s42826-020-00039-z

Barto, A. G. (1995). Adaptive critics and the basal ganglia. In *Models of information processing in the basal ganglia.* (pp. 215–232). The MIT Press.

Bliss, T. V, & Lomo, T. (1973). Long-lasting potentiation of synaptic transmission in the dentate area of the anaesthetized rabbit following stimulation of the perforant path. *The Journal of Physiology*, *232*(2), 331–356. https://doi.org/10.1113/jphysiol.1973.sp010273

Carr, G. V., Jenkins, K. A., Weinberger, D. R., & Papaleo, F. (2013). Loss of dysbindin-1 in mice impairs reward-based operant learning by increasing impulsive and compulsive behavior. *Behavioural Brain Research*, *241*, 173–184. https://doi.org/10.1016/j.bbr.2012.12.021

Condylis, C., Lowet, E., Ni, J., Bistrong, K., Ouellette, T., Josephs, N., & Chen, J. L. (2020). Context-Dependent Sensory Processing across Primary and Secondary Somatosensory Cortex. *Neuron*, *106*(3), 515-525.e5. https://doi.org/10.1016/J.NEURON.2020.02.004

Dunsmoor, J. E., & Murphy, G. L. (2015). Categories, concepts, and conditioning: how humans generalize fear. *Trends in Cognitive Sciences*, *19*(2), 73–77. https://doi.org/10.1016/j.tics.2014.12.003

FENG, Y., ZHOU, Z., HE, X., WANG, H., GUO, X., HAO, C., GUO, Y., ZHEN, X., & LI, W. (2008). Dysbindin deficiency in sandy mice causes reduction of snapin and displays behaviors related to schizophrenia. *Schizophrenia Research*, *106*(2–3), 218–228. https://doi.org/10.1016/j.schres.2008.07.018

Glen, W. B., Horowitz, B., Carlson, G. C., Cannon, T. D., Talbot, K., Jentsch, J. D., & Lavin, A. (2014). Dysbindin-1 loss compromises NMDAR-dependent synaptic plasticity and contextual fear conditioning. *Hippocampus*, *24*(2), 204–213. https://doi.org/10.1002/hipo.22215

Glimcher, P. W. (2011). Understanding dopamine and reinforcement learning: the dopamine reward prediction error hypothesis. *Proceedings of the National Academy of Sciences of the United States of America*, *108 Suppl 3*(Suppl 3), 15647–15654. https://doi.org/10.1073/pnas.1014269108

Harris, J. A., Mihalas, S., Hirokawa, K. E., Whitesell, J. D., Choi, H., Bernard, A., Bohn, P., Caldejon, S., Casal, L., Cho, A., Feiner, A., Feng, D., Gaudreault, N., Gerfen, C. R., Graddis, N., Groblewski, P. A., Henry, A. M., Ho, A., Howard, R., … Zeng, H. (2019). Hierarchical organization of cortical and thalamic connectivity. *Nature*, *575*(7781), 195–202. https://doi.org/10.1038/s41586-019-1716-z

Hattori, S., Murotani, T., Matsuzaki, S., Ishizuka, T., Kumamoto, N., Takeda, M., Tohyama, M., Yamatodani, A., Kunugi, H., & Hashimoto, R. (2008). Behavioral abnormalities and dopamine reductions in sdy mutant mice with a deletion in Dtnbp1, a susceptibility gene for schizophrenia. *Biochemical and Biophysical Research Communications*, *373*(2), 298–302. https://doi.org/10.1016/j.bbrc.2008.06.016

Houk, J., Adams, J., & Barto, A. (1995). A Model of How the Basal Ganglia Generate and Use Neural Signals that Predict Reinforcement. *Models of Information Processing in the Basal Ganglia*, *Vol. 13*.

Joel, D., Niv, Y., & Ruppin, E. (2002). Actor-critic models of the basal ganglia: new anatomical and computational perspectives. *Neural Networks : The Official Journal of the International Neural Network Society*, *15*(4–6), 535–547. https://doi.org/10.1016/s0893-6080(02)00047-3

Larson, J., Kim, D., Patel, R. C., & Floreani, C. (2008). Olfactory discrimination learning in mice lacking the fragile X mental retardation protein. *Neurobiology of Learning and Memory*, *90*(1), 90–102. https://doi.org/10.1016/j.nlm.2008.01.002

Lau, B., & Glimcher, P. W. (2007). Action and outcome encoding in the primate caudate nucleus. *The Journal of Neuroscience : The Official Journal of the Society for Neuroscience*, *27*(52), 14502–14514. https://doi.org/10.1523/JNEUROSCI.3060-07.2007

Lau, B., & Glimcher, P. W. (2008). Value representations in the primate striatum during matching behavior. *Neuron*, *58*(3), 451–463. https://doi.org/10.1016/j.neuron.2008.02.021

Makino, H., Ren, C., Liu, H., Kim, A. N., Kondapaneni, N., Liu, X., Kuzum, D., & Komiyama, T. (2017). Transformation of Cortex-wide Emergent Properties during Motor Learning. *Neuron*, *94*(4), 880-890.e8. https://doi.org/10.1016/j.neuron.2017.04.015

Marsh, B. T., Tarigoppula, V. S. A., Chen, C., & Francis, J. T. (2015). Toward an Autonomous Brain Machine Interface: Integrating Sensorimotor Reward Modulation and Reinforcement Learning. *The Journal of Neuroscience*, *35*(19), 7374–7387. https://doi.org/10.1523/JNEUROSCI.1802-14.2015

McBurney-Lin, J., Vargova, G., Garad, M., Zagha, E., & Yang, H. (2022). The locus coeruleus mediates behavioral flexibility. *Cell Reports*, *41*(4), 111534. https://doi.org/10.1016/j.celrep.2022.111534

McNiel, D. B., Choi, J. S., Hessburg, J. P., & Francis, J. T. (2016). Reward value is encoded in primary somatosensory cortex and can be decoded from neural activity during performance of a psychophysical task. *2016 38th Annual International Conference of the IEEE Engineering in Medicine and Biology Society (EMBC)*, 3064–3067. https://doi.org/10.1109/EMBC.2016.7591376

McNiel, D., Bataineh, M., Choi, J., Hessburg, J., & Francis, J. (2016). Classifier Performance in Primary Somatosensory Cortex Towards Implementation of a Reinforcement Learning Based Brain Machine Interface. *2016 32nd Southern Biomedical Engineering Conference (SBEC)*, 17–18. https://doi.org/10.1109/SBEC.2016.19

Mine, C., & Saiki, J. (2018). Pavlovian reward learning elicits attentional capture by reward-associated stimuli. *Attention, Perception & Psychophysics*, *80*(5), 1083–1095. https://doi.org/10.3758/s13414-018-1502-2

Ramakrishnan, A., Byun, Y. W., Rand, K., Pedersen, C. E., Lebedev, M. A., & Nicolelis, M. A. L. (2017). Cortical neurons multiplex reward-related signals along with sensory and motor information. *Proceedings of the National Academy of Sciences of the United States of America*, *114*(24), E4841–E4850. https://doi.org/10.1073/pnas.1703668114

Rossi-Pool, R., Zainos, A., Alvarez, M., Diaz-deLeon, G., & Romo, R. (2021). A continuum of invariant sensory and behavioral-context perceptual coding in secondary somatosensory cortex. *Nature Communications*, *12*(1), 2000. https://doi.org/10.1038/s41467-021-22321-x

Samejima, K., Ueda, Y., Doya, K., & Kimura, M. (2005). Representation of action-specific reward values in the striatum. *Science (New York, N.Y.)*, *310*(5752), 1337–1340. https://doi.org/10.1126/science.1115270

Schultz, W. (2016). Dopamine reward prediction error coding. *Dialogues in Clinical Neuroscience*, *18*(1), 23–32. https://doi.org/10.31887/DCNS.2016.18.1/wschultz

Takao, K., Toyama, K., Nakanishi, K., Hattori, S., Takamura, H., Takeda, M., Miyakawa, T., & Hashimoto, R. (2008). Impaired long-term memory retention and working memory in sdy mutant mice with a deletion in Dtnbp1, a susceptibility gene for schizophrenia. *Molecular Brain*, *1*, 11. https://doi.org/10.1186/1756-6606-1-11

Watson, P., Pearson, D., Wiers, R. W., & Le Pelley, M. E. (2019). Prioritizing pleasure and pain: attentional capture by reward-related and punishment-related stimuli. *Current Opinion in Behavioral Sciences*, *26*, 107–113. https://doi.org/10.1016/J.COBEHA.2018.12.002

Wickens, J., & Kötter, R. (1995). Cellular models of reinforcement. In *Models of information processing in the basal ganglia.* (pp. 187–214). The MIT Press.